Universidade de Aveiro
2015

Departamento de Engenharia de Materiais e Cerâmica

Frederico Calheiros Maia

Micro/nanoreservatórios para libertação controlada de espécies ativas em revestimentos funcionais

Micro/nanoreservoirs for controlled release of active species in smart functional coatings

Universidade de Aveiro
2015

Departamento de Engenharia de Materiais e Cerâmica

Frederico Calheiros Maia

Micro/nanoreservatórios para libertação controlada de espécies ativas em revestimentos funcionais

Micro/nanoreservoirs for controlled release of active species in smart functional coatings

Tese apresentada à Universidade de Aveiro para cumprimento dos requisitos necessários à obtenção do grau de Doutor em Ciência e Engenharia de Materiais, realizada sob a orientação científica do Professor Doutor Mikhail L. Zheludkevich, Professor Associado Convidado, e do Professor Doutor Mário G.S. Ferreira, Professor Catedrático, ambos do Departamento de Engenharia de Materiais e Cerâmica da Universidade de Aveiro

Apoio financeiro da FCT e do POPH/FSE no âmbito do III Quadro Comunitário de Apoio através da bolsa SFRH/BD/72663/2010.

Dedico este trabalho aos meus pais e irmão.

E à memória da minha avó.

o júri

presidente

Prof. Doutor José Carlos da Silva Neves
Professor Catedrático da Universidade de Aveiro

Prof. Doutor Albano Augusto Cavaleiro Rodrigues de Carvalho
Professor Catedrático da Faculdade de Ciências e Tecnologia da Universidade de Coimbra

Prof. Doutor Fernando Jorge Mendes Monteiro
Professor Catedrático da Faculdade de Engenharia da Universidade do Porto

Prof. Doutor Jorge Ribeiro Frade
Professor Catedrático da Universidade de Aveiro

Prof. Doutor Mikhail Larionovich Zheludkevich
Professor Associado Convidado da Universidade de Aveiro

Prof. Doutora Maria de Fátima Costa Montemor
Professora Auxiliar do Instituto Superior Técnico da Universidade de Lisboa

agradecimentos

Agradeço ao Professor Doutor Mikhail L. Zheludkevich e ao Professor Doutor Mário G.S. Ferreira, do Departamento de Engenharia de Materiais e Cerâmica por me terem aceitado como aluno de doutoramento no seu grupo de investigação, pela orientação científica, discussões científicas e partilha de conhecimentos.

Agradeço ao Doutor João Tedim, por toda a orientação, partilha de conhecimentos, conselhos e ajuda nos momentos mais críticos, e pela constante motivação e amizade.

Agradeço, também, a todos aqueles que de forma direta ou indireta contribuíram para a realização deste trabalho, nomeadamente ao Doutor Alexandre Bastos, Doutor Andrei Salak, Doutor Kiryl Yasakau, Doutor Silvar Kallip, Doutora Isabel Sousa, Alena Kuznetsova, Aleksey Lisenkov, Olga Karavai, Stanley Ofoegbu, Jorge Carneiro, Ana Caetano, Maksim Starykevich e André Oliveira. Em particular aos que partilharam o laboratório comigo nas nossas maratonas experimentais pela noite dentro, por todos os momentos de discussão de resultados, partilhas de conhecimento, amizade e bons momentos.

Agradeço à Fundação para a Ciência e Tecnologia (FCT) pelo financiamento através da bolsa de doutoramento SFRH/BD/72663/2010.

Agradeço de igual forma às entidades financiadoras e participantes nos projetos em que participei nos últimos anos, em particular os projetos MUST (NMP3/LA/2008/ 214261), NATAL (Ref. 11474-Adi/QREN/FEDER), SARISTU (FP7-AAT-2011-RTD-1) e NANOMAR (MC-IRSES-295145).

E por fim, aos meus familiares e amigos pelo apoio e motivação para concluir este trabalho.

palavras-chave

corrosão, antivegetativo, sensores, revestimentos funcionais, encapsulação, inibidores de corrosão, biocidas, micro e nanocápsulas, reservatórios.

resumo

Este trabalho reporta uma possível abordagem para o desenvolvimento de novos revestimentos funcionais utilizados para prolongar o tempo de vida de estruturas metálicas. As funcionalidades selecionadas e atribuídas a revestimentos, no âmbito deste trabalho, foram a proteção à corrosão, auto-sensora e prevenção da bioincrustação (antivegetativa). O modo usado para conferir essas funcionalidades aos revestimentos modelo teve como base a encapsulação de compostos ativos (inibidores de corrosão, indicadores de pH e biocidas) em micro e nanocontentores seguido da sua incorporação nas matrizes dos revestimentos.

Para conferir proteção ativa contra a corrosão, um inibidor de corrosão (2-mercaptobenzotiazola, MBT) foi encapsulado em dois diferentes contentores, em nanocápsulas de sílica (SiNC) e em microcápsulas poliureia (PU-MC). A incorporação dos dois contentores em dois revestimentos modelo mostram uma melhoria significativa na proteção à corrosão da liga de alumínio 2024 (AA2024). Seguindo a mesma abordagem, SiNC e PU-MC também foram utilizados na encapsulação de fenolftaleína (um indicador de pH muito conhecido) para introduzir propriedades sensoras em revestimentos poliméricos. SiNC e PU-MC contendo fenolftaleína atuaram como sensores de corrosão, demonstrando uma coloração rosa devido ao início da reação catódica, resultado num aumento de pH identificado por essas cápsulas. O desempenho como sensor foi comprovado em suspensão e quando integrados em revestimentos para a liga de alumínio 2024 e de magnésio AZ31.

De forma similar, a atividade biocida (antivegetativa) foi conferida a duas matrizes poliméricas usando SiNC para encapsulação de um biocida (dicloro-2-octil-2*H*-isotiazol-3-ona, DCOIT). As SiNC-MBT também foram testadas como biocida. A atividade antivegetativa desses dois compostos encapsulados foi avaliada através da inibição e consequente diminuição da bioluminescência da *E. coli* modificada. Esse efeito foi verificado em suspensão e quando incorporado em revestimentos para a liga de aço carbono AISI 1008.

Os micro e nanocontentores desenvolvidos demonstraram o desempenho desejado, permitindo a introdução de novas funcionalidades a revestimentos modelo, mostrando potencial para serem usados como aditivos funcionais para a próxima geração de revestimentos multifuncionais.

keywords

corrosion, antifouling, sensors, functional coatings, encapsulation, corrosion inhibitors, biocides, micro and nanocapsules, reservoirs.

abstract

This work reports one possible way to develop new functional coatings used to increase the life time of metallic structures. The functionalities selected and attributed to model coatings in the frame of this work were corrosion protection, self-sensing and prevention of fouling (antifouling). The way used to confer those functionalities to coatings was based on the encapsulation of active compounds (corrosion inhibitors, pH indicators and biocides) in micro and nanocontainers followed by their incorporation into the coating matrices.

To confer active corrosion protection, one corrosion inhibitor (2-mercaptobenzothiazole, MBT) was encapsulated in two different containers, firstly in silica nanocapsules (SiNC) and in polyurea microcapsules (PU-MC). The incorporation of both containers in different models coatings shows a significant improvement in the corrosion protection of aluminum alloy 2024 (AA2024). Following the same approach, SiNC and PU-MC were also used for the encapsulation of phenolphthalein (one well known pH indicator) to introduce sensing properties in polymeric coatings. SiNC and PU-MC containing phenolphthalein acted as corrosion sensor, showing a pink coloration due to the beginning of cathodic reaction, resulting in a pH increase identified by those capsules. Their sensing performance was proved in suspension and when integrated in coatings for aluminium alloy 2024 and magnesium alloy AZ31.

In a similar way, the biocide activity (antifouling) was assigned to two polymeric matrices using SiNC for encapsulation of one biocide (Dichloro-2-octyl-2*H*-isothiazol-3-one, DCOIT) and also SiNC-MBT was tested as biocide. The antifouling activity of those two encapsulated compounds was assessed through inhibition and consequent decrease in the bioluminescence of modified *E. coli*. That effect was verified in suspension and when incorporated in coatings for AISI 1008 carbon steel.

The developed micro and nanocontainers presented the desired performance, allowing the introduction of new functionalities to model coatings, showing potential to be used as functional additives in the next generation of multifunctional coatings.

Table of Contents

List of Figures

List of Tables

Introduction

The main objective of this work is the development of micro and nanoreservoirs for immobilization of active compounds, namely corrosion inhibitors, indicators and biocides, which can be incorporated in smart functional coatings. The idea is to confer new functionalities through the incorporation of active compounds in coatings, without the drawbacks typically attributed to the direct addition of such species to coating formulations. These drawbacks can be overcome by encapsulation, which protects the active compound from surroundings avoiding their deactivation, the negative interaction with coating matrix and allowing the controlled release of the encapsulated compounds.

This PhD thesis reports part of the work developed in the last four years, where several attempts to create new micro and nanocontainers were performed, some of them did not result according to our expectations and some of them were successful.

The most important results obtained are presented in the following chapters, divided by system, active compound (functionality) and application.

The work is divided into several chapters, where the first one report the state of art related to subject of this thesis and provide useful information related to the thesis topic. The second chapter summarizes the details on the performed experimental work and contains general information about the characterization techniques. More detailed information about techniques and procedures used during this work is reported in the next individual chapters which are composed by complementary published papers.

The most important results obtained are presented in subsequent chapters, divided by hosting structure system, active/guest compound (functionality) and application. Chapters 3 and 4 report the encapsulation of 2-mercaptobenzothiazole (MBT), a well-known corrosion inhibitor, using two different types of reservoirs: silica nanocapsules and polyurea microcapsules, respectively, and their incorporation in model formulations for corrosion protection of aluminium alloy 2024 (AA2024). Chapters 5 and 6 describe the encapsulation of phenolphthalein, a pH indicator, in silica nanocapsules and polyurea microcapsules, and consequent application of coatings for early detection of corrosion process for AZ31 magnesium alloy and for AA2024. The encapsulation of biocide 4,5-Dichloro-2-octyl-4-isothiazolin-3-one (DCOIT) in silica nanocapsules is reported together with the encapsulation of MBT in chapter 7. The application of these encapsulated systems

in antifouling coatings for carbon steel substrates is discussed. Text and data reported in chapters 3 to 7 were already submitted and/or published in peer reviewed journals specialized in corresponding fields.

The last chapter – chapter 8 – reports general conclusions of all the work developed and points out future activities in the field of multifunctional coatings.

CHAPTER 1

State of the Art

1. State of the art

Nowadays, most of the objects and structures present in our daily life are coated materials. Coatings play an important role conferring specific functionalities, from protection to decorative purposes. The activities on development of new coatings with novel features have drastically increased in recent times [1] in order to expand the market offer and the lifetime of coated substrates, preventing their early degradation.

1.1. Corrosion

One of the most common types of material degradation (in particular for metals) is corrosion. Every day in our routines is possible to observe the effects of corrosion in simple consumer goods and/or in important infra-structures, such as bridges, electrical towers, highways and pieces of transportation vehicles [2]. The economic impact of corrosion was estimated to be 4.2% of gross national product (GNP), equivalent to $100 billion in USA and around €200 billion in Europe [3, 4]. The global energy lost each year associated with this problem is approximately 1/5. [4].

Corrosion can be defined by "the physic-chemical interaction between a metal and its environment, which results in changes in the properties of the metal and which may often lead to impairment of the function of the metal, the environment, or the technical system of which these form a part" (ISO 8044-1986).

In a very simple way, corrosion is typically characterized by two half-reactions, one anodic (oxidation of the metal) and another cathodic (reduction of oxygen), as represented in the following equations [2, 5]:

Anodic reaction: $M \rightarrow ne^- + M^{n+}$ (Eq. 1)

Cathodic reaction in neutral/alkaline conditions: $O_2 + 2H_2O + 4e^- \rightarrow 4HO^-$ (Eq. 2)

Cathodic reaction in acidic conditions: $O_2 + 4H^+ + 4e^- \rightarrow 2H_2O$ (Eq. 3)

Hydrogen evolution: $2H^+ + 2e^- \rightarrow H_2\,(g)$ (Eq. 4).

The type of material and the properties of the environments affect significantly the way how material is degraded and how the corrosive process will occur. Thus, the assessment of corrosion is very complex and depends upon several parameters including temperature,

pH, the type of materials involved and the atmosphere/environment where they are exposed.

In this work three different metallic alloys were used: aluminum alloy 2024-T3 (AA2024-T3), magnesium alloy AZ31 and carbon steel AISI 1008. According to the specific composition (Table 1, Table 2 and Table 3 [6-8]) and intrinsic properties of each alloy, the way how they corrode is also completely different. AA2024-T3 and magnesium alloy AZ31 are light alloys very used in aeronautic industry while carbon steel AISI 1008 is used in maritime industry.

Table 1: Chemical composition of AA2024-T3 [6].

Chemical composition (wt %)								
Cu	Fe	Mg	Mn	Si	Zn	Ni	V	Zr
4.45	0.28	1.34	0.54	0.065	0.14	15 ppm	120 ppm	20 ppm

Table 2: Chemical composition of magnesium alloy AZ31 [7].

Chemical composition (wt %)								
Al	Zn	Mn	Si	Cu	Fe	Ni	Ca	Zr
3.1	0.73	0.25	0.02	<0.001	0.005	<0.001	<0.01	<0.001

Table 3: Chemical composition of carbon steel AISI 1008 [8].

Chemical composition (wt %)													
C	Mn	P	S	Si	Cu	Ni	Cr	Mo	Sn	Al	Ti	Ca	N
0.04	0.28	0.007	0.006	0.003	0.05	0.03	0.04	0.03	0.008	0.041	0.001	0.0001	0.0015

AA2024-T3 is characterized by the presence of high content of copper and magnesium elements in its composition, which can lead to a formation of micro-galvanic couples with intermetallic particles and consequent localized corrosion (pitting), as explained in Figure 1, one of the most dangerous types of corrosion. On the other side, magnesium alloy AZ31 is characterized by the presence of a significant amount of aluminum in its composition which results in a beneficial effect on the corrosion behavior in chloride media [7] and carbon steel AISI 1008 is characterized by the low amount of carbon on their composition making it more malleable and ductile. Both magnesium and steel alloys present a uniform

corrosion which is less problematic, from the point of view of its detection, since it is easily observed as shown in Figure 2.

The most common type of corrosion is uniform or general corrosion (Figure 2), which results in the uniform dissolution and reduction of metal thickness over the exposed surface. General corrosion is responsible for most of the corrosion induced consumption, nevertheless it's easily detected and quantified which facilitate its prediction and control. Another important type of corrosion is pitting (Figure 1 and Figure 2), which is a localized and self-propagated form of corrosion characterized by the formation of extensive holes in the metal. Pitting occurs when a spot in the surface becomes anodic or cathodic while the rest of the exposed surface is cathodic or anodic, respectively. This is one of the most dangerous type of corrosion due to the small size of pits and their difficult localization. The autocatalytic behavior of pitting leads to severe damages in the metallic substrates through the creation of huge and internal cavities, making this form of corrosion very common in metal alloys like AA2024-T3 [6].

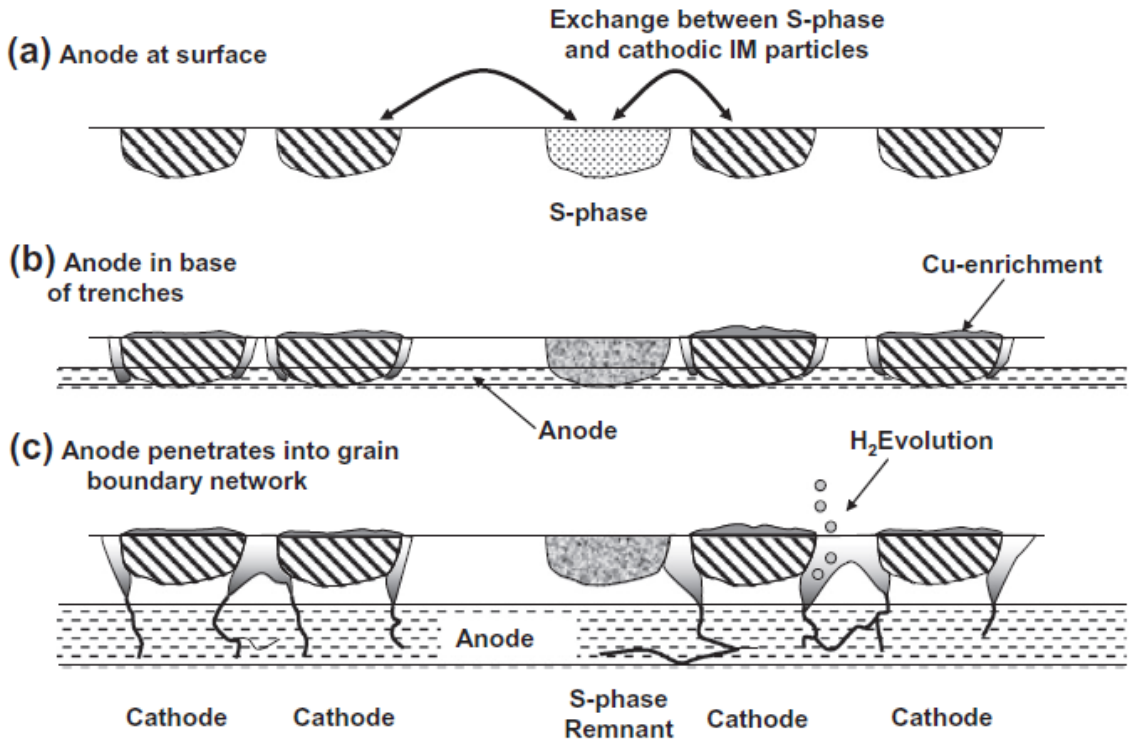

Figure 1: Model of co-operative corrosion. (a) Represents initiation through coupling of IM anodes and matrix with cathodes at the surface, (b) the formation trenching around the cathodic particles driving the active anode into the base of trenches where an acidic anolyte solution develops, initial copper-enrichment occurs during this period and (c) as the corrosion proceeds, the anode is driven into the grain boundary network. (Reprinted from [6], Copyright © 2011 with permission from Elsevier).

Figure 2: Differences between uniform and localized (pitting) corrosion.

There are a few primary methods to prevent and mitigate corrosion. The first one is related to the selection and design of materials. Each material has an intrinsic corrosion rate, some are more resistant then others. Combining the materials nature and some design principles is possible to increase the life time of materials and reduce the maintenance costs. One of the main strategies used to control corrosion is based upon coating application, which according to their chemical nature can be divided in metallic and nonmetallic. The metallic coating can be used to improve the corrosion resistance by application of a noble metal (taken the advantage of their intrinsic characteristics) or using one metal more active, working as a sacrificial coating (the one where corrosion is preferential) and protecting the main substrate. In the case of nonmetallic coating, the idea is to protect the substrate, through the creation of a barrier between substrate and the external environment, avoiding the contact with aggressive species in the corrosive media [2]. One important way to control corrosion is the use of corrosion inhibitors, which is "a substance which retards corrosion when added to an environment in small concentrations" (NACE). Corrosion inhibitors act by one or more of these mechanisms:

i) adsorption on the surface of a corroding material as a thin film,
ii) inducing formation of a thick corrosion product,
iii) forming a passive film on the metal surface,
iv) changing characteristics of the environment either by producing protective precipitates or by removing or inactivating an aggressive constituent.

Regarding the way they act, corrosion inhibitors can be classified by different classes, such as passivating, cathodic, organic, precipitate-inducing and vapor-phase corrosion inhibitors [9]. These inhibitors can be introduced in protective coatings and/or in primers, being

leached in coating defects decreasing the corrosion process. The combination of two or more primary methods previously described and the synergic effect achieved by them are the best way to avoid and mitigate corrosion.

There are some methods to control and protect structures from corrosion, however it is always very complex and there are several variables to consider and adjust. Corrosion is an electrochemical process and sometimes other natural processes, can influence the typical corrosive process. One common process is the formation of biofilm, especially in wet environments, which changes completely the electrochemical process and the interactions in the interface metal-solution. This modification (also a type of corrosion) is called microbiologically influenced corrosion, or microbial corrosion or biological corrosion (MIC) and reflects how biofilm formation affect the corrosive process [10-12].

The presence or absence of living organisms has a significant role in the life time of structures and also affects their degradation. The adhesion and accumulation of microorganisms in wet surfaces has very often a synergetic effect with corrosion in the degradation processes. That phenomenon is denominated biofouling.

1.2 Biofouling

The formation of biofilm, as a result of bacterial activity, in wet conditions is a very complex process and involves the medium, the type of surface and the presence and type of bacteria. In a very simple way the biofilm formation begins with the accumulation (physical adhesion or adsorption) of organic matter and minerals. This initial film is formed in seconds. The following step is the settlement and growth of pioneer bacteria forming the biofilm matrix (primary colony). The presence of such film allows the retention of nutrients (food), which are essential for the fixation of multicellular species (e.g., spores of macroalgae). This step is called microfouling and can be formed in hours to a few days. The growth and maturation of biofilm leads in the capture of other organisms and particles, such as larvae of marine macroorganisms, resulting in very complex colonies with a high diversity of fouling organisms [13, 14], as represented in Figure 3.

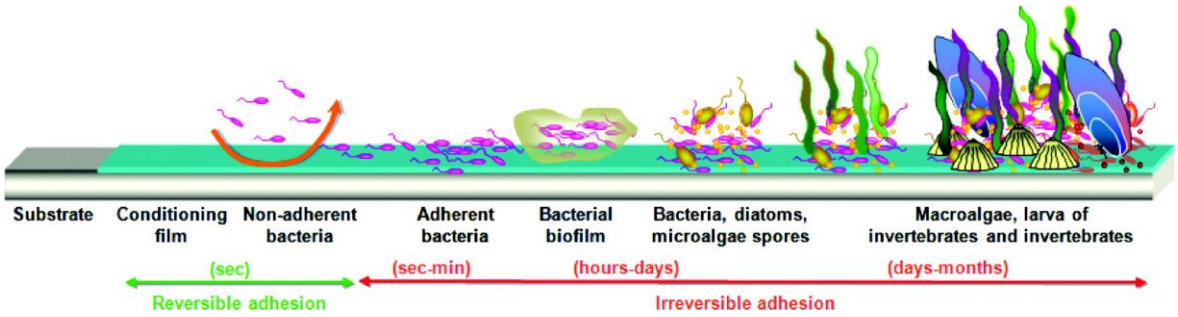

Figure 3: Development processes of marine biofouling. (Reprinted with permission from [13, 15], Copyright © 2012, American Chemical Society).

Biofouling and corrosion processes are intimately related. The presence of living organisms attached to the metal substrate surfaces generates a set of specific conditions that weaken that surface, causing the appearance of cracks and pores, and contributing for the progress of corrosion. The economic impact of these processes is considerable. It includes costs associated with regular maintenance operations, replacement of offshore structures, or expenditure of extra fuel because of the increase of drag forces in ships [16]. The effects and consequences of biofouling and their influence in corrosion are observed in different fields, not only in maritime environments. Coetser and Cloete report the influence of biofouling and biocorrosion in industrial water systems [17] on the surface of different pieces of industrial equipment and the damages caused by the biofilm formation, namely the contamination of pharmaceutical or microelectronic products, unexpected corrosion of stainless steel, the reduction on the heat exchanger efficiency and the premature destruction of mineral materials [17]. In a similar way, industrial equipment failures were found to be caused by MIC [18], where three technical equipments made with different metallic alloys (carbon steel heat exchanger, floating roofs made of magnesium–aluminum alloy and engine cooling system made of cast aluminum alloy) failed due to the presence of microorganisms [18].

Although the effect of biofilm formation on metallic surfaces is mainly negative, there are some examples where the formation of biofilm reduces the corrosion rate of some metallic alloys as reported in the Mansfeld´s review article [19]. The author shows the corrosion inhibition in some metallic alloys in the presence of specific bacteria, contributing to the increase of the open-circuit potential (E_{corr}) due to the formation of a biofilm. In the same direction the pitting process of AA2024-T3 in artificial seawater was controlled by the formation of a regenerative biofilm, decreasing the oxygen concentration in the surface of

AA2024 and the corrosion potential became nobler in the presence of bacteria *Bacillus subtilis* [20]. The protective effect is proved when antibiotics were added to artificial seawater, killing the bacteria in the biofilm. Within a few hours pitting occurred and the decrease in the E_{corr} was also observed [21]. The mechanism of biofilm protection is very complex and still unknown, for that reason there is some controversy on the real benefits of protective biofilm when compared to damages resulted from their formation on metallic surfaces.

1.3. Coatings

The most used and efficient way to control and prevent the degradation of metallic structures from corrosion and biofouling is the application of protective coatings with anticorrosive and antifouling functionalities [22, 23].

Coating, in a very simple way, is defined as a material which is applied onto a surface and appears as either a continuous or discontinuous film. It can also be described as a physical separation between one substrate and their surrounding environment. The most common coating applications are for protective, decorative and functional purposes, or a combination of these three. Depending on the application, it can be constituted by several layers, where each layer plays a specific function. A typical example of a coating system used in aeronautical industry is shown in Figure 4 [24]. The first layer is the result of the substrate pretreatment and is normally called conversion coating. This layer provides corrosion protection and improves the adhesion between the substrate and the primer. It is characterized by a very thin inorganic layer, typical between a few nanometers to few micrometers. The second layer (primer) is composed by a pigmented organic matrix and affords additional functions to the conversion film. Primer is thicker then conversion film and can reach dozens of micrometers. Its main function is corrosion protection, by barrier and inhibitor reservoir. The last layer is named topcoat and has the function to act as a main barrier against aggressive species that are present in the environment. It can also be used for decorative purposes. This is thicker layer of full coating system and can attain 2-3 hundreds of micrometers. Full coating system, as presented in Figure 4, is composed by pretreatment, primer and topcoat [24].

Figure 4: Schematic of components that make up an aircraft coating system, adapted from [24].

'Functional coatings' is a recent term used to describe any extra functionality with respect to the classic coating properties (barrier effect and decoration) [1]. The additional functionality (e.g. hydrophobicity, anticorrosive, antifouling, photochromic, self-sensing, etc.) is normally provided by additives incorporated within the coating or intrinsically by matrix functionalization. In the last decade the search and development of new coatings with new functionalities, namely self-healing, anticorrosive, self-sensing and antifouling, is reflected by the significant number of publications in the field, as depicted in Table 4.

Table 4: Number of hits obtained using specific keywords in a basic search in Web of Science database.

Keyword(s)	Number of hits
Self-healing	12738
Self-healing coatings	959
Anticorrosive coatings	6113
Self-healing coatings + corrosion	376
Self-sensing coatings	33
Antifouling coatings	3767

1.3.1. Feedback active coatings for anticorrosion and antifouling applications

In terms of materials degradation, there are some environments which are particularly aggressive for metal substrates due to humidity, different oxygen concentrations, salinity (high concentrations of NaCl) and presence of microorganisms, algae and plants, that lead to corrosion and biofouling of metallic substrates [22, 23].

In terms of corrosion, chromium (VI) based coatings were the most used solution due to their great anticorrosive performance. Chromium compounds were used both in pretreatments (chromium (III) and (VI) conversion coatings) and in primers containing chromate-based pigments. In a general way, coating matrix acts as protective barrier,

preventing the direct contact of metal with external environment (passive protection), whereas the anticorrosive pigments inhibits and suppress corrosion activity (active protection) when the coating barrier effect fails. Due to high toxicity and carcinogenic effects of Cr(VI) compounds, these were banned from the market and the scientific community have been working hard in order to find solutions with similar performance in terms of corrosion protection but with less health and environmentally-related problems [24].

In the last years different alternatives to chromium conversion coatings were reported. One possible approach is based on chromium-free conversion coatings using other inorganic species (which can also be used as corrosion inhibitors) like rare-earth elements (REE) [25-28], phosphates, permanganate and vanadate, [28, 29], to create a thick and passivating layer to improve the corrosion resistance of this film. Another reported solution is based on the application of sol-gel films [30-34] which confer some passive protection and improves the adhesion between metallic substrate and the top layers of the coating. Sol-gel layer also allows the incorporation of corrosion inhibitors, combining passive and active protection [31, 35, 36]. The formation of regular nanostructured inorganic layers on the metallic substrates surfaces results on the metal passivation combined with active protection, due to the possibility to entrap corrosion inhibitors in the structure formed [37-39].

Regarding polymeric coatings containing anticorrosive pigments (primers), different types of organic and inorganic compounds, like azole derivatives [40-42], inorganic salts such as vanadate, molybdate and cerium [31, 43-45] and combinations between organic and inorganic compounds [46, 47] have been considered as alternatives to chromates but many issues still remain and needs to be solved. Despite the incorporation of inhibitors confer active protection to polymeric matrices, the direct addition of active compounds to coating formulations can often promote negative effects on the final applications, namely deactivation of the active compound due to interaction with coating matrix, promoting degradation of the latter and spontaneous leaching of the former [48, 49]. One way to overcome these problems is the encapsulation of active compounds in ‘smart’ micro and nanocontainers that release the encapsulated compounds in response to specific stimuli.

1.3.1.1. Self-healing coatings for corrosion protection

A new generation of functional coatings has recently appeared the so-called *self-healing coatings*. The recovery of the coating protective action in an autonomous way has attracted

many material scientists. Some of them have focused their research on the recovery of the coating integrity through encapsulation of a healing agent in a polymeric microcapsule, dispersing it together with a specific catalyst in the coating matrix as showed in Figure 5. When the coating cracks, microcapsules embedded in the matrix also ruptures. The healing agent is released and reacts with the catalyst, polymerizing and repairing the crack and recovering the coating initial characteristics [50]. Another possibility using the same methodology is by catalyst encapsulation and dispersing the healing agent droplets in a matrix together with the microcapsules, as reported by Braun [51].

In the same direction there is a range of organic molecules (or polymers) which forms dynamic covalent bonds and exhibit interesting properties such as self-healing, shape memory and environmental adaptation without the presence of any catalyst. A specific example was reported by Ying where the hindered urea bond was rationally designed by a chemical modification, resulting in polymers (polyureas and poly(urethane-urea)s) able to change and autonomous repairing at low temperature in a dynamic and catalyst-free way [52]. This type of modifications can be used for broaden the scope of applications of these type of materials [52].

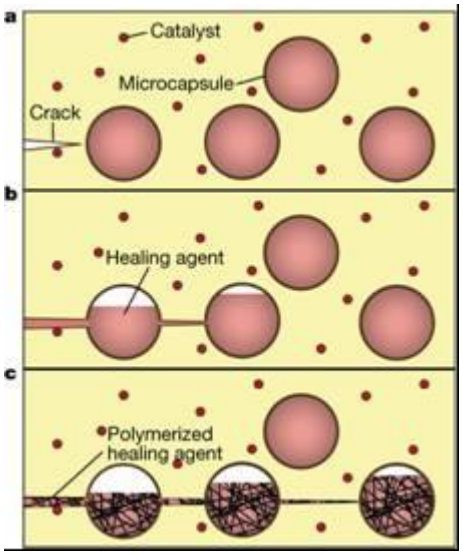

Figure 5: A microencapsulated healing agent is embedded in a structural composite matrix containing a catalyst capable of polymerizing the healing agent. (a) Cracks form in the matrix wherever damage occurs; (b) the crack ruptures the microcapsules, releasing the healing agent into the crack plane through capillary action; (c) the healing agent contacts the catalyst, triggering polymerization that bonds the crack faces closed. (Reprinted from [50], Copyright © 2001, Rights Managed by Nature Publishing Group).

Materials with self-healing properties are still in their early stage, but this type of mechanism was already known and is present in the human body when a bone or our skin form example heals and recover their initial properties. One more time, as in many other fields, materials scientists and engineers are trying to mimic Nature to obtain high-performance material. In this context, Fischer explains how this phenomenon occurs in Nature and gives some examples where it is already applied in some materials [53]. The difference between active and passive mechanisms is explained, detailed triggers for different fields are specified and suggestions for a new generation of self-healing systems are presented [53].

One example where the self-healing ability can be applied is the prevention of corrosion propagation. The suppression of corrosion activity in a coating defect by the coating autonomously can be also classified as self-healing, due to the recovery of its main function (corrosion protection), after being damaged. The huge number of works and reviews that have been published showing the importance of self-healing coatings and 'smart' coatings as potential alternative for chromate based coatings [54-62].

In the last decade, many scientists directed their research on the recovery of the corrosion protection, by encapsulation or immobilization of corrosion inhibitors in 'smart nanoreservoirs or nanocontainers' which releases the inhibitors in a controlled way and, normally, after an external stimulus. In this way the corrosion inhibitors' reservoirs can be introduced in the coating formulation without compromising adhesion and barrier properties as reported in the literature [47, 60, 63, 64].

A significant number of nanocontainers for corrosion inhibitors with different properties were developed in the last years. These nanocontainers can be divided according their release mechanisms or by strategies for inhibitors immobilization. Since this work is focused on the development of new nanocontainers for corrosion inhibitors, i.e. ways to immobilize them in host structures, nanocontainers will be described regarding the way how corrosion inhibitors were immobilized.

One of the first systems developed for immobilization of corrosion inhibitors is based on the intercalation of inhibitor in polyelectrolytes using layer-by-layer (LbL) assembly in silica nanoparticles [48, 65, 66] or in halloysites [66, 67], as represented in Figure 6. These polyelectrolytes are pH-sensitive and allow the inhibitor release when some pH perturbation occurs. Other approach using halloysites nanotubes with stoppers to entrap the

inhibitor inside the tubular structure of halloysite and control the inhibitor release from the loaded structure was reported by Abdullayev [68].

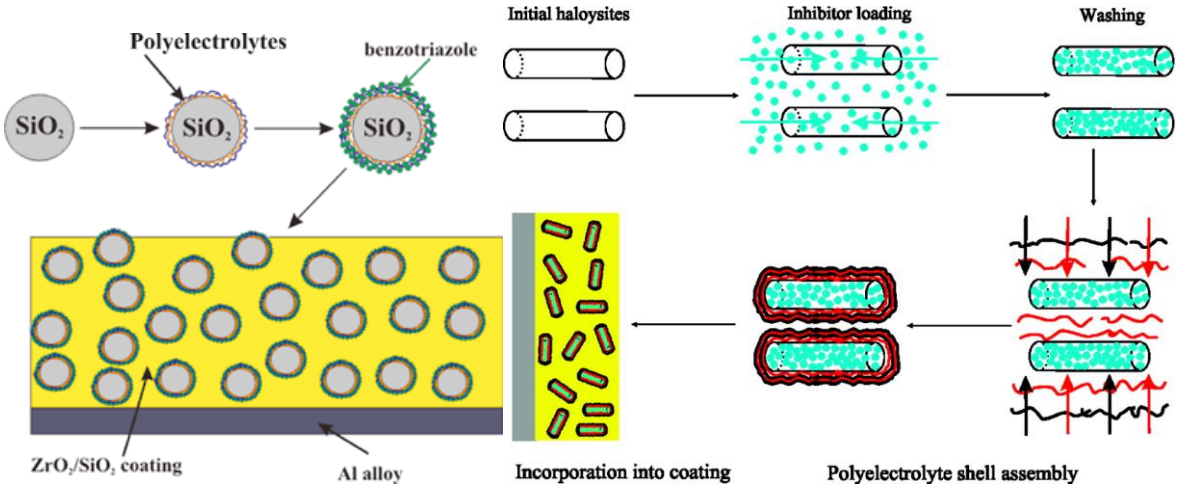

Figure 6: Left: Schematic representation of the fabrication of a composite ZrO2/SiO2 coating loaded with benzotriazole nanoreservoirs. (Reprinted from [48], Copyright © 2006, John Wiley & Sons, Inc). Right: Schematic illustration of the fabrication of 2-mercaptobenzothiazole-loaded halloysite/polyelectrolyte nanocontainers. (Reprinted with permission from [67], Copyright © 2008, American Chemical Society).

More recently, mesoporous silica was used to immobilize corrosion inhibitor into their pores, allowing higher loading content, being the inhibitor released by pH variation, when those mesoporous particles are covered with polyelectrolytes [64], or by diffusion as reported by Borisova [69]. Borisova, using the same nanocontainers also have demonstrated the importance of coating design, namely the concentration and position of nanocontainers into the coating layers to maximize the corrosion protection [70, 71]. A similar methodology was reported by Fu and coworkers [72], where hollow mesoporous silica (HMS) nanoparticles were used for corrosion entrapment. The surface of HMS was modified with supramolecular nanovalves in the form of bistabe pseudorotaxanes allowing the controlled release of corrosion inhibitor as a double response of pH variations, for acidic and alkaline conditions [72].

Many other materials were reported as reservoirs for corrosion inhibitors to be used in 'smart' coatings with other entrapment methodologies. TiO_2 and cerium molybdate containers were prepared using polystyrene nanospheres as template, being coated by sol-gel method with the desired composition, calcined, resulting in a crystalline hollow

particles. These particles were loaded with inhibitors using saturated solutions under vacuum conditions [73, 74]. A different structure (nanowires) for cerium molybdate complex was reported, but these structure is amorphous and has higher solubility when compared to crystalline structures. The structure dissolves and releases cerium and molybdate ions which are themselves corrosion inhibitors [75]. Snihirova and colleagues reported the encapsulation of 8-hydroxyquinoline in Eudragit pH-sensitive particles [76]. The encapsulation was obtained via emulsion-solvent preparation, resulting in spherical particles which dissolves at acidic pH values, releasing the stored inhibitor [76]. Another form of encapsulation of inhibitors was reported based on the preparation of polyurethane microcapsules by interfacial polymerization in an oil-in-water emulsion [77]. Other common way to immobilize corrosion inhibitors is by simple adsorption in porous structures, such as cellulose nanofibers [78] or in hydroxyapatite particles [79]. Hydroxyapatite particles also has the ability to store corrosion inhibitors by cationic-exchange method. In this case calcium is replaced by Ce^{3+} or La^{3+}. These inhibitors are released by dissolution of hydroxyapatite particles in acidic conditions [79].

Another class of materials well known for its exchange capabilities used for entrapment of ionic compounds are zeolites. These materials allow the intercalation of corrosion inhibitors in their cationic form [80-82]. In the proper conditions it is possible to promote the immobilization of more than one compound in the same particle combining cationic-exchange and adsorption mechanisms [82], as explained in Figure 7.

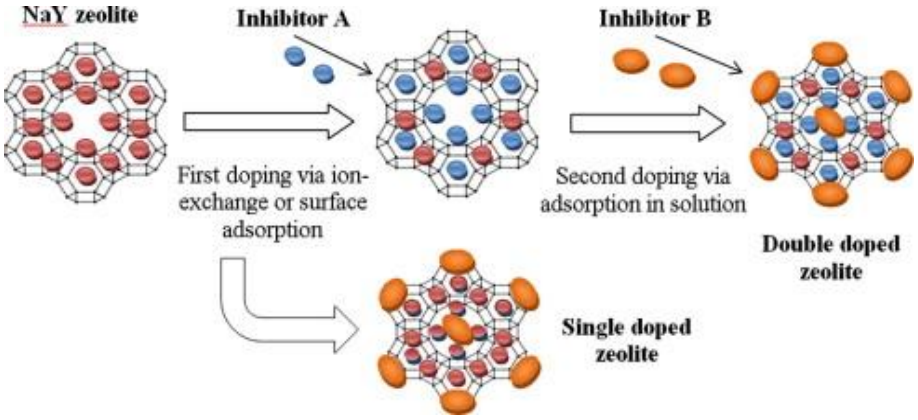

Figure 7: Schematic of single and double inhibitor doping concepts in NaY zeolite. (Reprinted from [82], Copyright © 2014 with permission from Elsevier).

Layered double hydroxides (LDHs) are also materials where the incorporation of corrosion inhibitors is performed by ionic-exchange, but contrastingly to zeolites, LDHs are anionic-

exchange materials and allows the entrapment of anionic species. The intercalation of different compounds in their anionic form are exchange by anions present in the LDHs structure [63, 83-85]. These materials showed high efficiency due to their multiple role: the corrosion inhibitors are released by anion exchange, while chloride ions are trapped using the same mechanism used for inhibitors intercalation, and LDHs can also act as a buffer for the surroundings media, preventing the propagation of corrosion [63, 83-85], as depicted in Figure 8.

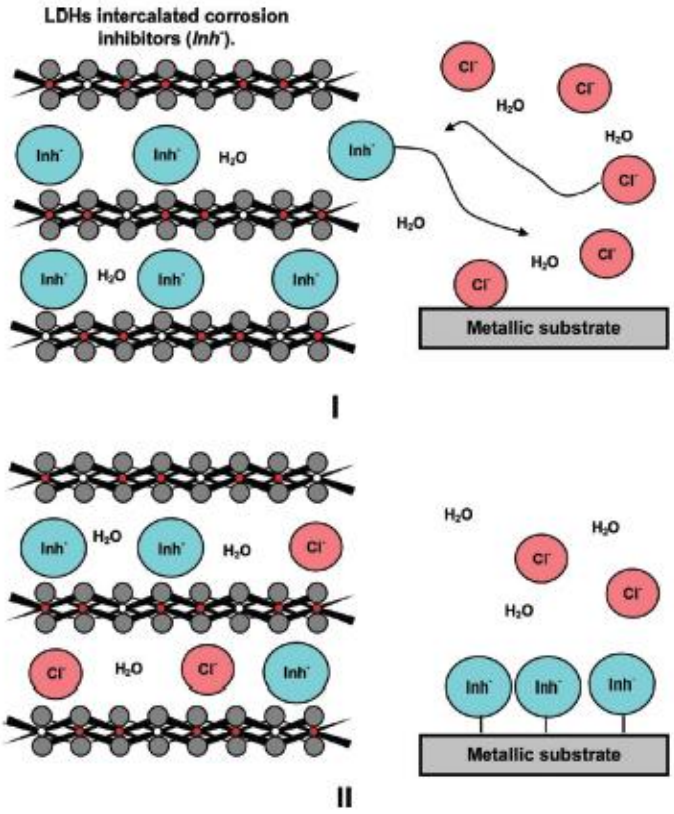

Figure 8: Schematic View of the LDHs Action in Corrosion Protection. (I) The release of inhibitors (Inh^-) is triggered by the presence of anions in solution (Cl^-). (II) LDHs play a double-role, providing inhibitors to protect the metallic substrates and entrapping aggressive species from the environment. (Reprinted with permission from [85], Copyright © 2010, American Chemical Society).

The combination of two immobilization strategies was reported by Carneiro and colleagues using LDHs for incorporation of mercaptobenzothiazole, followed by polyelectrolytes assembly on LDH surface, allowing the intercalation of cerium ions in the polyelectrolytes layers [86]. This approach allows the immobilization of two different inhibitors resulting in an improved corrosion protection due to the synergic effect of inhibitors [46, 86].

The combination of different strategies for immobilization of corrosion inhibitors and the synergy between different classes of nanocontainers was studied in a large European project – MUST [87].

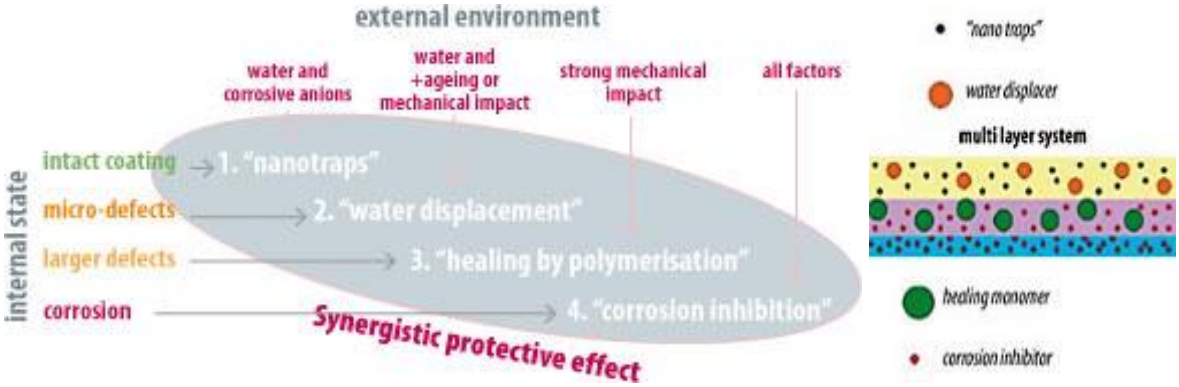

Figure 9: Scheme of the active multi-level protective system developed in MUST project [87].

In this project one new concept of multifunctional coatings was created, combining different levels of protection against adverse effects from the environment. Each layer can be constituted by specific containers with a well-defined function or by different containers with several functionalities resulting in multifunctional layers, as shown in Figure 9.

Following the approach developed in MUST project for corrosion protection, the combination of different nanocontainers was reported [88, 89] which can be incorporated in different layers of the coating for multiple purposes, resulting in multifunctional coatings. In the external layers, nanocontainers were incorporated for water and chlorine trapping [89, 90] while in the inner layers, for controlled release of corrosion inhibitors [88, 89], as represented in Figure 10.

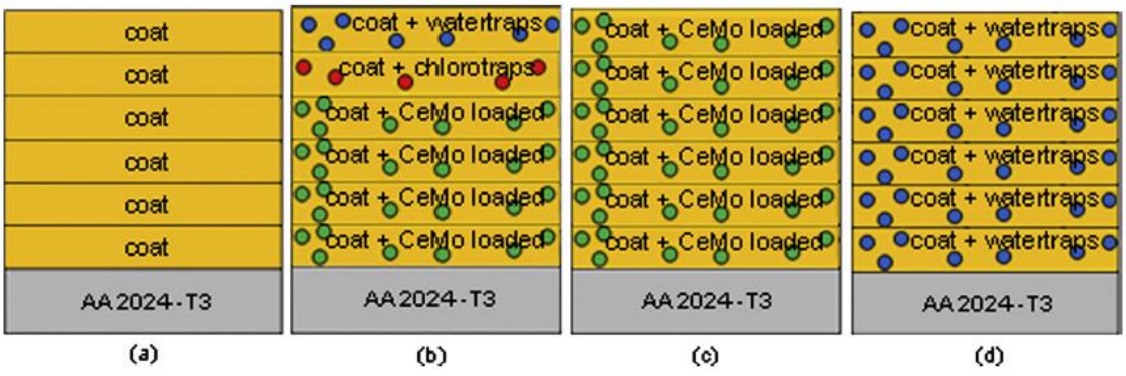

Figure 10: Schematic representation of: (a) reference coating, (b) multifunctional coating, (c) inhibitor loaded nanocontainers coating and (d) water traps coating. (Reprinted from [89] Copyright © 2014 with permission from Elsevier.

1.3.1.2 Self-diagnosis/sensing coatings

Another important feature in the field of 'smart' coatings that should be applied together with the capacity to recover from damage in an autonomous way is the ability to detect the coating failure (or the corrosion onset, in the specific case of corrosion). The damage detection (identification and location) is fundamental for the understanding and implementation of self-healing systems [53]. The mechanism used for damage sensing (detection) can be used as trigger for active compounds release and healing process.

In the field of corrosion, the early detection of corrosion onset and coating damage can avoid catastrophic accidents and trigger simpler and less onerous maintenance actions. Using the products of the corrosive process to help in the selection of compounds with sensing properties, pH indicators seem to be a good option.

As explained in the beginning of this chapter, the corrosive process can be divided in two half reactions: (i) anodic (oxidation of the metal) and (ii) cathodic (reduction of oxygen or water molecules from the environment), where the most significant resulting products are metal cations and hydroxide anions. With the formation of hydroxide ions, local pH increases in the cathode and decreases in the anode as a result of hydrolysis reactions. These pH variations can be detected using pH indicators.

Methods to sense corrosion like the one reported by Buchheit [83] based on the crystal structure modification when inhibitor anions are released and with chloride ion uptake, can be applied but are very complex. This method in particular is not practical and requires X-ray diffraction [83]. Colour development seems to be a simple and easy way to assess the corrosion onset and in the recent years a few developments have been reported using this approach. The direct addition of phenolphthalein (a very well-known pH indicator) to acrylic based paint [91, 92] and to a sol-gel matrix [93] results in corrosion sensing coatings, determined by passing cathodic current and determining the charge at which color changes and for monitoring acid-base reactions, respectively. Other examples of phenolphthalein were reported using it encapsulated in dextran derivatives [94] and pH sensitive polymeric microcapsules [95-98]. The polymer used in these pH sensitive capsules is based on urea-formaldehyde and melamine-formaldehyde, combined with a cross-linking agent that has one or more ester and mercapto groups such as pentaerythritol tetrakis (3-mercaptopropionate), which breaks down under alkaline conditions, releasing the pH indicator as result of corrosion activity [97].

The great advantage of adding sensing ability to self-healing coatings is the possibility to identify damages or failures in coatings, even if they were then repaired autonomously, but it is important to know that damaged-healed structure is now more fragile, although repaired. It is one way to have extra precaution and increase the level of accidents prevention. One good example of that combination is shown in Figure 11 and was reported by Calle [97], where the pH sensitive capsules loaded with corrosion inhibitor and with pH indicators are triggered by pH variation, resulting in the release of the encapsulated agents, allowing the identification of damaged areas and at the same time the healing process of those damaged areas (combination of self-healing and sensing properties).

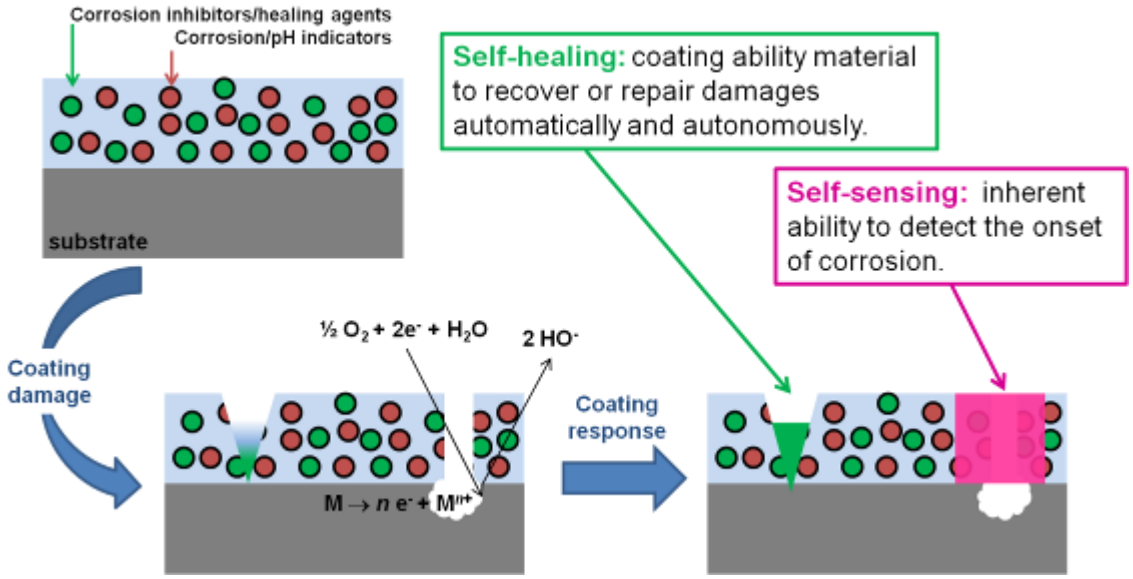

Figure 11: Schematic illustration of one multifunctional coating with self-healing and self-sensing properties. Adapted from [97].

1.3.1.3 Antifouling coatings

Although reported strategies to protect metallic structures against corrosion look very promising for application in onshore structures and vehicles, the occurrence of biofouling in offshore structures and ships requires additional functionalities to protect the metallic substrates in these conditions. The improvement of coatings used for marine applications has included both the optimization of formulations, to obtain coatings with higher barrier properties, hydrophobicity and smoothness [22], and the incorporation of AF agents [23]. The most used AF agent in the past was tributyltin (TBT) but in 2003 the International Maritime Organization banned it because of its high toxicity and bioaccumulation [23]. Since then, paint companies have the challenge to produced tin-free paints to prevent

biofouling. The most common alternatives in use, contains high amounts of copper(Cu)-based compounds, since it is about ten times less toxic than TBT.

In the last years different strategies have been developed to tackles biofouling in order to keep the surfaces free of micro and macroorganisms. There are two main types of coating to prevent biofouling, one is biocide based and the other is non-biocide based.

Biocidal AF coatings contain biocides or compounds biologically-active that are released into the surrounding waters from the paint surface to prevent fouling. The leaching rate determines the amount of biocide released and must be kept high enough to prevent fouling during the lifetime of the paint before recoating is required. There are different ways of releasing the biocide, being the three main types based on a soluble matrix (oldest one), insoluble matrix with soluble biocides and self-polishing paint [13, 99]. Paint based in a soluble matrix, dissolves with time and needs constant maintenance, was used in the fifties but now is not very used. Paint with insoluble matrix, keeps the matrix intact while the biocide itself dissolves slowly to be eventually depleted, leaving an exhausted matrix of paint that must be removed before the surface is re-coated and finally the self-polishing paint, where the paint erodes or is "self-polishing" or ablative, gradually releasing the biocide and copolymers, as shown in Table 5 [23, 99].

Booster biocides, used to enhance the AF performance of copper-based coatings, can be broadly grouped into inorganic and organic types. The application of organic biocides and their effect was reported [13, 91-94], where specific compounds such as Irgarol, Diuron, Sea-nine (or Kathon), Dichlofluanid and chlorothalonil [100-103] was studied. Another class of compounds also used as biocides for AF coatings is based on organic compounds complexed with metals, being the most used based in copper and zinc [100, 101, 103]. However, these biocide alternatives also show high level of toxicity and in some cases a severe degree of bioaccumulation. A monitoring program shows the presence of some of these biocides in enclosed seawater from Spanish Mediterranean Coast [102] from AF paints. It is an indication that greener and safer alternatives need to be found.

An interesting alternative was suggested by Olsen [104] where inorganic based peroxides were added to paint formulations; they react with seawater and hydrogen peroxide is release acting as biocide [104]. This approach shows some potential, but requires further studies to assess the stability and AF efficiency of these pigments as additives for AF coatings. Another alternative is based on the encapsulation of these active compounds to

control their release and preliminary works have been already reported using different strategies [105, 106]. DCOIT (4,5-dichloro-2-n-octyl-4-isothiazoline-3-one) was encapsulated in two different systems. The first one, Sea-nine (the active compound is DCOIT) was encapsulated in poly(methyl methacrylate-co-butyl acrylate using a two-stage miniemulsion process [105]. The release studies performed showed that limited amount of DCOIT released is sufficient to impart AF properties. The other system used for DCOIT encapsulation is based in chitosan/xanthan gum microcontainers and when these microcontainers where incorporated in a polymer coating, they have shown an antimicrobial activity more sustained than DCOIT in its non-encapsulated form [106].

Table 5: Main types of antifouling paint used on steel hulls in the second half of the 20th century. (Adapted from [99] Copyright © 2007 with permission from Elsevier).

Type of paint	Proposed mechanisms	Toxicant release in time
Soluble matrix	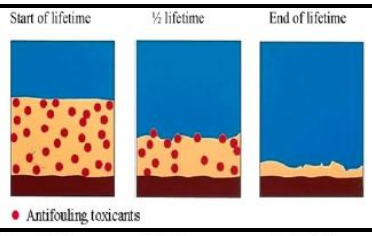	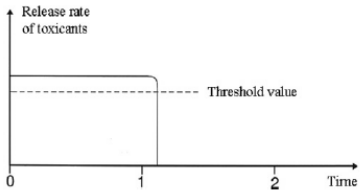
Insoluble matrix or contact paint	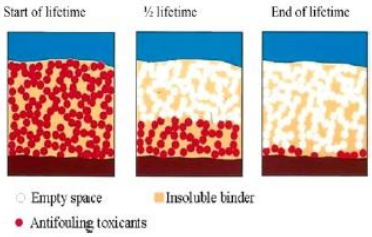	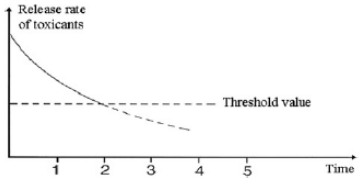
Self-polishing paint	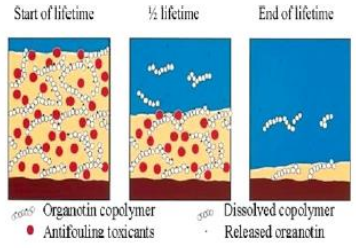	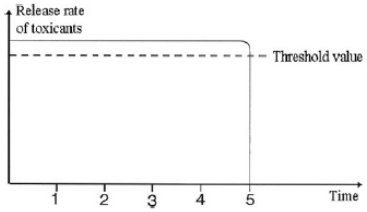

The use of biocide based AF with booster biocides provides a provisory alternative to TBT based coatings, however due to their toxicity, other approaches without biocides have been developed and their application is growing.

Foul Release Coatings (FRCs) are based in the surface modification of exposed surfaces, decreasing their surface energy and consequently the adhesion and the organism's

possibility to generate interfacial bonds with the surface [13, 107]. This "non-stick" approach also facilitates the fouling removal by shear and tensile stresses. There are several possibilities to create hydrophobic and non-stick surfaces, being fluoropolymer and silicone based polymer coatings [13, 99, 107-111] the most used ways and already available in the market. Oligo- and poly(ethylene glycol) polymer blends [112, 113] and biodegradable polyester binders [114] have been also studied in the polymeric surface functionalization of FRCs.

Other interesting approach in fabrication of FRCs is modification of surface chemistry and topography in order to change the natural mechanism of microorganism adhesion to those surfaces [115-119]. Those developed structures are normally inspired by Nature, where one more time, scientists are trying to design and mimic natural surfaces, such as shark and whale's skin, echinoderms and molluscs [115, 118, 119], as shown in Figure 12. The morphology and topography of the structures play an important role in the adhesion or repellence of microorganisms onto those surfaces. The way how the interaction between organisms and surface is established depends on size, type, scale and geometry of the structures "build on" the surfaces [117]. Due to the higher number of marine organisms is very difficult to find one structure able to avoid the adhesion of all type of fouling. Macro topographies are favourable for fouling and are not suitable for AF applications. On the other hand, micro topographies show some success limiting the fouling for a wide range of microorganisms [117].

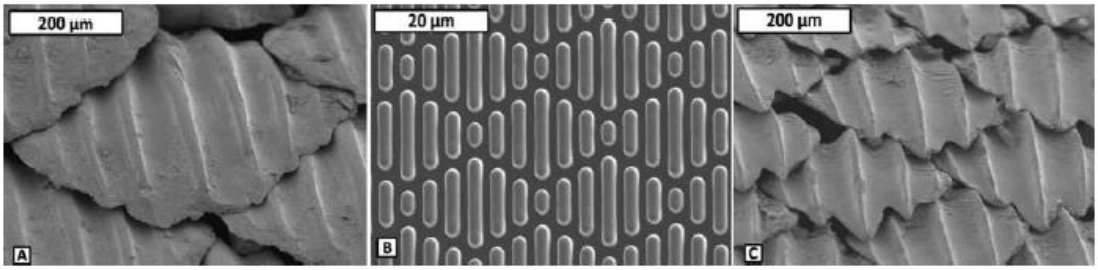

Figure 12: Riblets of sharkskin scales of (a) the spinner shark (*Carcharhinus brevipinna*), (c) the Galapogos shark (*Carcharhinus galapagensis*) and (b) the bio-inspired SharkletTM film fabricated in polydimethylsiloxane (c). (Reprinted from [118] Copyright © 2011 Taylor & Francis).

Virtually, any artificial structure immersed in sea water is fouled in short periods of time due to the natural marine flora and fauna. At the same time, some marine microorganisms have the ability to produce chemical compounds that can limit the settlement and growth of

other fouling organisms [120, 121]. In the last years several compounds were extracted and isolated from marine microorganisms showing multiple bioactivities, namely high AF potential [121]. A range of compounds with AF properties was obtained from marine microorganism. Those compounds were studied taking in consideration their ecological role and potential industrial application. The compounds studied with the desired properties were terpenoids, steroids and saponins, fatty acid-related compounds, bromotyrosine derivatives and heterocyclic compounds [120]. Due to the promising results obtained in the realizes test, some compounds derivatives were synthesized and incorporated into polymers and tested in the field, resulting in the inhibition on the settlement and growth of fouling organisms [120]. Other approaches using enzymes [116, 121, 122] for biofilm disruption and heterotrophic bacteria with antialgal and antilarval activity [116, 121] shows the huge potential of using natural and less toxic compounds with AF properties in AF coatings. Nevertheless, the study of all those complex mechanisms and a better comprehension of the biofouling settlement and inhibition are needed to find the best alternative for TBT based coatings.

In conclusion, the rapid change enforced by the prohibition of organotin paints, combined with the current low carbon revolution, rising fuel prices and heightened environmental awareness, have stimulated massive research efforts in the last decade or so in the area of antifouling technology. This research effort is ongoing and much is still at an early stage. There is potential for developments in several areas, namely on development of new and safer biocides, creation of new surfaces such as amphiphilic and zwitterionic, and nanostructures, low surface energy coatings and controlled release of biocides. Probably the best solution will be the result of the combination of some of these approaches due to the complexity of the biofouling process settlement.

1.3.1.4. Synergy between anticorrosive and AF coatings

As already discussed in this chapter, corrosion and biofouling are intrinsically connected, and both phenomena present very complex mechanisms, contributing to degradation of materials, in particular for metals. In the same way, the efforts to increase the durability of those materials must be combining anticorrosive and antifouling strategies.

For an efficient and effective protection (from corrosion and biofouling) a three layered coating can be applied, where the primer contains the self-healing system (anticorrosive) with the suitable corrosion inhibitor for the substrate, followed by a tie-coat with high level

of solids (fillers) to increase barrier properties of the coating, and the last layer (top-coat) contains an efficient and less toxic AF system, as represented in Figure 13.

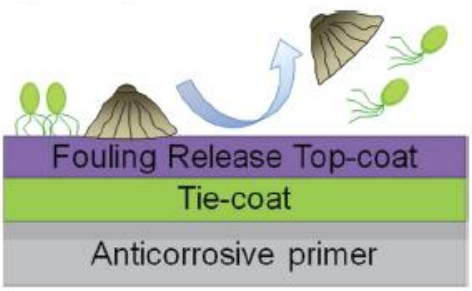

Figure 13: Schematic representation of a coating composed by three layers: primer, tie-coat and top-coat, combining anticorrosive and AF properties. (Reprinted with permission from [13], Copyright © 2012, American Chemical Society).

Szabó et al. [123] reported the combination of self-healing (film-forming materials + corrosion inhibitors) and AF agent, using all components encapsulated in polymeric microcapsules and in natural polymer microspheres, respectively. These containers were incorporated in different layers of the coating and after curing an artificial scratch was made. The resulted scratch was filled by the healing agent and the corrosion decreased by a self-healing mechanism. The antifouling tests show the reduction in the adhesion of micro- and macroorganisms [123]. In a similar way, Zheng and coworkers [124] reported the use of mesoporous silica nanoparticles as delivery tools for incorporation of benzotriazole (corrosion inhibitor) and benzalkonium chloride (biocide) in multifunctional coatings. The hybrid coating containing the responsive release system demonstrates self-healing properties and antifouling effect as result of the controlled release of benxotriazole and benzalkonium chloride as response of pH variation and presence of sulfide ions [124].
These two works shows the potential synergetic effect resulted from the combination of anticorrosive and antifouling systems in the protection of metallic substrates, increasing this way their life time and avoiding early maintenance and replacement of metallic parts in bigger structures, especially when exposed to maritime environment.

In this work new materials for encapsulation of active compounds were developed, i.e. silica nanocapsules and polyurea microcapsules. The developed capsules within the active compounds storage were obtained in a single-step. These capsules were prepared using oil-in-water emulsions, allowing the encapsulation of lipophilic compounds (previously

dissolved in the dispersed phase). This approach allows the incorporation of new functionalities, by introduction of active compounds, into model coating formulations, showing a significant improvement of their performance (anticorrosive, self-sensing and antifouling).

Thesis objectives

The main goal of this work was the development of new multifunctional coatings based on active containers. The new functionalities were introduced in model coatings using micro and nanoreservoirs with the ability to immobilize active compounds with intrinsic anticorrosive, antifouling and sensing properties. The synthesized materials release the active species to the surrounding environment on demand, under the action a predefined stimulus, in order to ensure the desirable active functionality, overcoming the typical drawbacks of direct introduction of active compounds. These materials were incorporated in various protective coatings to prevent biofouling and corrosion in metallic structures or to detect and sense coating damages.

More specifically, the main objectives were:

1) Synthesis of micro and nanoreservoirs and encapsulation of corrosion inhibitors, biocides and indicators.

2) Physico-chemical characterization of the synthesized materials.

3) Studies of controlled release of encapsulated species at different pH and salinity conditions.

4) Correlation between the release profiles and extent antifouling or anticorrosion action with respect to bare metal substrates.

5) Functionalization of the carriers for tuning of the release responses.

6) Development of reservoirs with multiple release mechanisms.

7) Incorporation of reservoirs loaded with active species into simplified commercial formulations and study of the coating performance.

8) Combination of different hosting/inert materials loaded with different active compounds in order to obtain multifunctional coatings.

9) Construction of a prototype and application of the best formulations in offshore structures/maritime conditions in order to study their antifouling and anticorrosive properties in real conditions (sea/ocean environment).

References

1. S.K. Ghosh, "Functional Coatings and Microencapsulation: A General Perspective in Functional Coatings", 2006, Wiley-VCH (Weinheim, Germany), pp. 1-3.

2. J.R. Davis, "Corrosion: Understanding the Basics", 2000, ASM International (Ohio, USA), pp 1-20.

3. H. Wei, Y. Wang, J. Guo, N.Z. Shen, D. Jiang, X. Zhang, X. Yan, J. Zhu, Q. Wang, L. Shao, H. Lin, S. Wei and Z. Guo, "Advanced micro/nanocapsules for self-healing smart anticorrosion coatings", J. Mater. Chem. A, 2015, 3, 469-480.

4. D. Wang and G.P. Bierwagen, "Sol–gel coatings on metals for corrosion protection", Progress in Organic Coatings, 2009, 64, 327-338.

5. E. Ghali, V.S. Sastri and M. Elboujdaini, in Corrosion Prevention and Protection: Practical Solutions, John Wiley & Sons Ltd, Chichester, 2007.

6. A.E. Hughes, A. Boag, A.M. Glenn, D. McCulloch, T.H. Muster, C. Ryan, C. Luo, X. Zhou, G.E. Thompson, "Corrosion of AA2024-T3 Part II: Co-operative corrosion", Corrosion Science, 2011, 53, 27–39.

7. A. Pardo, M.C. Merino, A.E. Coy, R. Arrabal, F. Viejo and E. Matykina, "Corrosion behaviour of magnesium/aluminium alloys in 3.5 wt.% NaCl", Corrosion Science, 2008, 50, 823–834.

8. M.I. Khan and T. Yasmin, "Erosion–Corrosion of Low Carbon (AISI 1008 Steel) Ring Gasket Under Dynamic High Pressure CO2 Environment", J Fail. Anal. and Preven., 2014, 14, 537–548.

9. S. Papavinasam, Chapter 59, "Corrosion Inhibitors" Uhlig's Corrosion Handbook, Ed. R.W. Revie, ISBN0-471-15777-5, John Wiley & Sons, Inc, N.Y. 2000, p.1089-1105.

10. H.A. Videla and L.K. Herrera, "Microbiologically influenced corrosion: looking to the future", Int. Microbiol., 2005, 8, 169-180.

11. H.A. Videla and L.K. Herrera, "Understanding microbial inhibition of corrosion. A comprehensive overview", International Biodeterioration & Biodegradation 63 (2009) 896–900.

12. D. Enning and J. Garrelfs, "Corrosion of Iron by Sulfate-Reducing Bacteria: New Views of an Old Problem", Applied and Environmental Microbiology, 2014, 80, 1226–1236.

13. M. Lejars, A. Margaillan and C. Bressy, "Fouling Release Coatings: A Nontoxic Alternative to Biocidal Antifouling Coatings", Chem. Rev. 2012, 112, 4347−4390.

14 P.-Y. Qian, S.C.K. Lau, H.-U. Dahms, S. Dobretsov, T. Harder, "Marine Biofilms as Mediators of Colonization by Marine Macroorganisms: Implications for Antifouling and Aquaculture", Mar. Biotechnol. 2007, 9, 399-410.

15. D. Haras, "Biofilms et altérations des matériaux : de l'analyse du phénomène aux stratégies de prévention", 2005, Matériaux & Techniques 93, 27-41.

16. M.P. Schultz, J.A. Bendick, E.R. Holm and W.M. Hertel, "Economic impact of biofouling on a naval surface ship", Biofouling, 2011, 27, 87-98.

17. S.E. Coetser and T.E. Cloete, "Biofouling and Biocorrosion in Industrial Water Systems", Crit Rev Microbiol., 2005, 31, 213-232.

18. J. Starosvetsky, D. Starosvetsky, R. Armon, "Identification of microbiologically influenced corrosion (MIC) in industrial equipment failures", Engineering Failure Analysis, 2007, 14, 1500–1511.

19. F. Mansfeld, "The interaction of bacteria and metal surfaces", Electrochimica Acta, 2007, 52, 7670–7680.

20. D. Örnek, A. Jayaraman, T.K. Wood, Z. Sun, C.H. Hsu, F. Mansfeld, "Pitting corrosion control using regenerative biofilms on aluminium 2024 in artificial seawater", Corrosion Science, 2001, 43, 2121–2133.

21. R. Zuo, E. Kus, F. Mansfeld, T.K. Wood, "The importance of live biofilms in corrosion protection", Corrosion Science, 2005, 47, 279–287.

22. P. A. Sørensen, S. Kiil, K. Dam-Johansen and C. E. Weinell, "Anticorrosive coatings: a review", J. Coat. Technol. Res., 2009, 6, 135–176.

23. D. M. Yebra, S. Kiil and K. Dam-Johansen, "Antifouling technology—past, present and future steps towards efficient and environmentally friendly antifouling coatings", Prog. Org. Coat., 2004, 50, 75-104.

24. R.L. Twite, G.P. Bierwagen, "Review of alternatives to chromate for corrosion protection of aluminum aerospace alloys", Progress in Organic Coatings, 1998, 33, 91–100.

25. M. Dabalà, L. Armelao, A. Buchberger, I. Calliari, "Cerium-based conversion layers on aluminum alloys", Applied Surface Science, 2001, 172, 312-322.

26. A. Decroly and J.-P. Petitjean, “Study of the deposition of cerium oxide by conversion on to aluminium alloys”, Surface & Coatings Technology, 2005, 194, 1-9.

27. M.F. Montemor, A.M. Simões and M.J. Carmezim, “Characterization of rare-earth conversion films formed on the AZ31 magnesium alloy and its relation with corrosion protection”, Applied Surface Science, 2007, 253, 6922–6931.

28. S. Pommiers, J. Frayret, A. Castetbon, M. Potin-Gautier, “Alternative conversion coatings to chromate for the protection of magnesium alloys”, Corrosion Science, 2014, 84, 135-146.

29. A.S. Hamdy, I. Doench, H. Möhwald, “Intelligent self-healing corrosion resistant vanadia coating for AA2024”, Thin Solid Films, 2011, 520, 1668–1678.

30. T.L. Metroke, R.L. Parkhill, Edward T. Knobbe, “Passivation of metal alloys using sol–gel-derived materials - a review”, Progress in Organic Coatings, 2001, 41, 233–238.

31. N.N. Voevodin, N.T. Grebasch, W.S. Soto, F.E. Arnold, M.S. Donley, “Potentiodynamic evaluation of sol-gel coatings with inorganic inhibitors”, Surface and Coatings Technology, 2001, 140, 24-28.

32. V. Palanivel, D. Zhu, W.J. van Ooij, “Nanoparticle-filled silane films as chromate replacements for aluminum alloys”, Progress in Organic Coatings, 2003, 47, 384-392.

33. M.L. Zheludkevich, I.M. Salvado and M.G.S. Ferreira, “Sol–gel coatings for corrosion protection of metals”, J. Mater. Chem., 2005, 15, 5099-5111.

34. V. Dalmoro, J.H.Z. dos Santos, E. Armelin, C. Alemán, D.S. Azambuja, “Sol–gel hybrid films based on organosilane and montmorillonite for corrosion inhibition of AA2024”, Journal of Colloid and Interface Science, 2014, 426, 308–313.

35. M.L. Zheludkevich, R. Serra, M.F. Montemor, K.A. Yasakau, I.M. Miranda Salvado, M.G.S. Ferreira, “Nanostructured sol–gel coatings doped with cerium nitrate as pre-treatments for AA2024-T3 Corrosion protection performance”, Electrochimica Acta, 2005, 51, 208–217.

36. A.N. Khramov, N.N. Voevodin, V.N. Balbyshev, R.A. Mantz, “Sol–gel-derived corrosion-protective coatings with controllable release of incorporated organic corrosion inhibitors”, Thin Solid Films, 2005, 483, 191– 196.

37. R.G. Buchheit, S.B. Mamidipally, P. Schmutz and H. Guan, “Active Corrosion Protection in Ce-Modified Hydrotalcite Conversion Coatings”, Corrosion, 2002, 58, 3-14.

38. J. Tedim, M.L. Zheludkevich, A.N. Salak, A. Lisenkov and M.G.S. Ferreira, "Nanostructured LDH-container layer with active protection functionality", J. Mater. Chem., 2011, 21, 15464–15470.

39. J. Tedim, M.L. Zheludkevich, A.C. Bastos, A.N. Salak, J. Carneiro, F. Maia, A.D. Lisenkov, A.B. Oliveira and M.G.S. Ferreira, "Effect of Surface Treatment on the Performance of LDH Conversion Films", ECS Electrochem. Lett., 2014, 3, C4-C8.

40. N.C. Subramanyam and S.M. Mayanna, "Azoles as corrosion inhibitors for mild steel in alkaline mine water", Corros. Sci., 1985, 25, 163-169.

41. R. Subramanian and V. Lakshminarayanan, "Effect of adsorption of some azoles on copper passivation in alkaline medium", Corros. Sci., 2002, 44, 535-554.

42. J. Carneiro, J. Tedim, S.C.M. Fernandes, C.S.R. Freire, A. Gandini, M.G.S. Ferreira, and M.L. Zheludkevich, "Chitosan as a Smart Coating for Controlled Release of Corrosion Inhibitor 2-Mercaptobenzothiazole", ECS Electrochemistry Letters, 2013, 2, C19-C22.

43. V. Moutarlier, B. Neveu and M.P. Gigandet, "Evolution of corrosion protection for sol–gel coatings doped with inorganic inhibitors", Surf. Coat. Technol., 2008, 202, 2052-2058.

44. M.L. Zheludkevich, J. Tedim, C.S.R. Freire, S.C.M. Fernandes, S. Kallip, A. Lisenkov, A. Gandini and M.G.S. Ferreira, "Self-healing protective coatings with "green" chitosan based pre-layer reservoir of corrosion inhibitor", J. Mater. Chem., 2011, 21, 4805-4812.

45. J. Carneiro, J. Tedim, S.C.M. Fernandes, C.S.R. Freire, A.J.D. Silvestre, A. Gandini, M.G.S. Ferreira, M.L. Zheludkevich, "Chitosan-based self-healing protective coatings doped with cerium nitrate for corrosion protection of aluminum alloy 2024", Progress in Organic Coatings, 2012, 75, 8–13.

46. S. Kallip, A.C. Bastos, K.A. Yasakau, M.L. Zheludkevich and M.G.S. Ferreira, "Synergistic corrosion inhibition on galvanically coupled metallic materials", Electrochem. Comm., 2012, 20, 101-104.

47. M. Serdechnova, S. Kallip, M.G.S. Ferreira, M.L. Zheludkevich, "Active self-healing coating for galvanically coupled multi-material assemblies", Electrochemistry Communications, 2014, 41, 51–54.

48. D. G. Shchukin, M. Zheludkevich, K. Yasakau, S. Lamaka, M. G. S. Ferreira and H. Mohwald, "Layer-by-Layer Assembled Nanocontainers for Self-Healing Corrosion Protection", Adv. Mater., 2006, 18, 1672-1678.

49. D. Raps, T. Hack, J. Wehr, M.L. Zheludkevich, A.C. Bastos, M.G.S. Ferreira and O. Nuyken, "Electrochemical study of inhibitor-containing organic–inorganic hybrid coatings on AA2024", Corros. Sci., 2009, 51, 1012–1021.

50. S.R. White, N.R. Sottos, P.H. Geubelle, J.S. Moore, M.R. Kessler, S.R. Sriram, E.N. Brown and S. Viswanathan, "Autonomic healing of polymer composites", Nature, 2001, 409, 794-797.

51. S.H. Cho, S.R. White and P.V. Braun, "Self-Healing Polymer Coatings", Adv. Mater., 2009, 21, 645-649.

52. H. Ying, Y. Zhang, J. Cheng, "Dynamic urea bond for the design of reversible and self-healing polymers", NATURE COMMUNICATIONS, 2014, 5, 3218.

53. H. Fischer, "Self-repairing material systems-a dream or a reality?", Natural Science, 2010, 2, 873-901.

54. V. Sauvant-Moynot, S. Gonzalez, J. Kittel, "Self-healing coatings: An alternative route for anticorrosion protection", Progress in Organic Coatings, 2008, 63, 307–315.

55. M. Samadzadeh, S. Hatami Boura, M. Peikari, S.M. Kasiriha, A. Ashrafi, "A review on self-healing coatings based on micro/nanocapsules", Progress in Organic Coatings, 2010, 68, 159–164.

56. A.E. Hughes, I.S. Cole, T.H. Muster and R.J. Varley, "Designing green, self-healing coatings for metal protection", NPG Asia Mater., 2010, 2 143–151.

57. M.L. Zheludkevich, J. Tedim, M.G.S. Ferreira, "'Smart' coatings for active corrosion protection based on multi-functional micro and nanocontainers", Electrochimica Acta, 2012, 82, 314– 323.

58. A. Stankiewicz, I. Szczygieł, B. Szczygieł, "Self-healing coatings in anti-corrosion applications", J Mater Sci, 2013, 48, 8041–8051.

59. D. Shchukin and H. Möhwald, "A Coat of Many Functions", SCIENCE, 2013, 341, 1458-1459.

60. D.G. Shchukin, M. Zheludkevich and H. Mohwald, "Feedback active coatings based on incorporated nanocontainers", J. Mater. Chem., 2006, 16, 4561-4566.

61. M.F. Montemor, "Functional and smart coatings for corrosion protection: A review of recent advances", Surface & Coatings Technology, 2014, 258, 17–37.

62. H. Wei, Y. Wang, J. Guo, N.Z. Shen, D. Jiang, X. Zhang, X. Yan, J. Zhu, Q. Wang, L. Shao, H. Lin, S. Wei and Z. Guo, "Advanced micro/nanocapsules for self-healing smart anticorrosion coatings", J. Mater. Chem. A 3, 2015, 469–480.

63. M.L. Zheludkevich, S.K. Poznyak, L.M. Rodrigues, D. Raps, T. Hack, L.F. Dick, T. Nunes and M.G.S. Ferreira, "Active protection coatings with layered double hydroxide nanocontainers of corrosion inhibitor", Corros. Sci., 2010, 52, 602–611.

64. E.V. Skorb, D. Fix, D.V. Andreeva, H. Möhwald and D.G. Shchukin, "Surface-Modified Mesoporous SiO2 Containers for Corrosion Protection", Adv. Funt. Mater., 2009, 19, 2373-2379.

65. M.L. Zheludkevich, D.G. Shchukin, K.A. Yasakau, H. Möhwald, and M.G.S. Ferreira, "Anticorrosion coatings with self-healing effect based on nanocontainers impregnated with corrosion inhibitor", Chem. Mater.,2007, 19, 402–411.

66. D. G. Shchukin and H. Möhwald, "Surface-Engineered Nanocontainers for Entrapment of Corrosion Inhibitors", Adv. Funct. Mater., 2007, 17, 1451-1458.

67. D.G. Shchukin, S.V. Lamaka, K.A. Yasakau, M.L. Zheludkevich, M.G.S. Ferreira, and H. Möhwald, "Active Anticorrosion Coatings with Halloysite Nanocontainers", J. Phys. Chem. C, 2008, 112, 958–964.

68. E. Abdullayev, R. Price, D. Shchukin and Y. Lvov, "Halloysite Tubes as Nanocontainers for Anticorrosion Coating with Benzotriazole", ACS Appl. Mater. Interfaces, 2009, 1, 1437–1443.

69. D. Borisova, H. Möhwald and D.G. Shchukin, "Mesoporous Silica Nanoparticles for Active Corrosion Protection", ACS Nano, 2011, 5, 1939–1946.

70. D. Borisova, H. Möhwald and D.G. Shchukin, "Influence of Embedded Nanocontainers on the Efficiency of Active Anticorrosive Coatings for Aluminum Alloys Part I: Influence of Nanocontainer Concentration", ACS Appl. Mater. Interfaces, 2012, 4, 2931–2939.

71. D. Borisova, H. Möhwald and D.G. Shchukin, "Influence of Embedded Nanocontainers on the Efficiency of Active Anticorrosive Coatings for Aluminum Alloys Part II: Influence of Nanocontainer Position", ACS Appl. Mater. Interfaces, 2013, 5, 80–87.

72. J.J. Fu, T. Chen, M.D. Wang, N.W. Yang, S.N. Li, Y. Wang, and X.D. Liu, "Acid and Alkaline Dual Stimuli-Responsive Mechanized Hollow Mesoporous Silica Nanoparticles

as Smart Nanocontainers for Intelligent Anticorrosion Coatings", ACS Nano, 2013, 7, 11397–11408.

73. I.A. Kartsonakis, A.C. Balaskas, G.C. Kordas, "Influence of cerium molybdate containers on the corrosion performance of epoxy coated aluminium alloys 2024-T3", Corrosion Science, 2011, 53, 3771–3779.

74. E.D. Mekeridis, I.A. Kartsonakis, G.C. Kordas, "Multilayer organic–inorganic coating incorporating TiO2 nanocontainers loaded with inhibitors for corrosion protection of AA2024-T3", Progress in Organic Coatings, 2012, 73, 142– 148.

75. K.A. Yasakau, J. Tedim, M.L. Zheludkevich, R. Drumm, M. Shem, M. Wittmar, M. Veith, M.G.S. Ferreira, "Cerium molybdate nanowires for active corrosion protection of aluminium alloys", Corrosion Science, 2012, 58, 41–51.

76. D. Snihirova, S.V. Lamaka, M.Margarida Cardoso, J.A.D. Condeço, H.E.C.S. Ferreira, M.F. Montemor, "pH-sensitive polymeric particles with increased inhibitor-loading capacity as smart additives for corrosion protective coatings for AA2024", Electrochimica Acta, 2014, 145, 123–131.

77. E. Koh, S.-Y. Baek, N.-K. Kim, S. Lee, J. Shin and Y.-W. Kim, "Microencapsulation of the triazole derivative for self-healing anticorrosion coatings", New J. Chem., 2014, 38, 4409-4419.

78. A. Yabuki, A. Kawashima, I.W. Fathona, "Self-healing polymer coatings with cellulose nanofibers served as pathways for the release of a corrosion inhibitor", Corrosion Science, 2014, 85, 141–146.

79. D. Snihirova, S.V. Lamaka, M. Taryba, A.N. Salak, S. Kallip, M.L. Zheludkevich, M.G.S. Ferreira, and M.F. Montemor, "Hydroxyapatite Microparticles as Feedback-Active Reservoirs of Corrosion Inhibitors", ACS Appl. Mater. Interfaces, 2010, 2, 3011–3022.

80. S.A.S. Dias, S.V. Lamaka, C.A. Nogueira, T.C. Diamantino, M.G.S. Ferreira, "Sol–gel coatings modified with zeolite fillers for active corrosion protection of AA2024", Corrosion Science, 2012, 62, 153–162.

81. S. Roselli, N. Bellotti, C. Deyá, M. Revuelta, B. del Amo, R. Romagnoli, "Lanthanum-exchanged zeolite and clay as anticorrosive pigments for galvanized steel", J. Rare Earths, 2014, 32, 352-359.

82. E.L. Ferrer, A.P. Rollon, H.D. Mendoza, U. Lafont, S.J. Garcia, "Double-doped zeolites for corrosion protection of aluminium alloys", Microporous and Mesoporous Materials, 2014, 188, 8–15.

83. R.G. Buchheit, H. Guan, S. Mahajanam, F. Wong, "Active corrosion protection and corrosion sensing in chromate-free organic coatings", Progress in Organic Coatings, 2003, 47, 174–182.

84. S.K. Poznyak, J. Tedim, L.M. Rodrigues, A.N. Salak, M.L. Zheludkevich, L.F.P. Dick and M.G.S. Ferreira, "Novel Inorganic Host Layered Double Hydroxides Intercalated with Guest Organic Inhibitors for Anticorrosion Applications", ACS Appl. Mater. Interfaces, 2009, 1, 2353–2362.

85. J. Tedim, S.K. Poznyak, A. Kuznetsova, D. Raps, T. Hack, M.L. Zheludkevich and M.G.S. Ferreira, "Enhancement of Active Corrosion Protection via Combination of Inhibitor-Loaded Nanocontainers", ACS Appl. Mater. Interfaces, 2010, 2, 1528-1535.

86. J. Carneiro, A.F. Caetano, A. Kuznetsova, F. Maia, A.N. Salak, J. Tedim, N. Scharnagl, M.L. Zheludkevich and M.G.S. Ferreira, "Polyelectrolyte-modified layered double hydroxide nanocontainers as vehicles for combined inhibitors", RSC Adv., 2015, 5, 39916-39929.

87. http://www.sintef.no/projectweb/must/

88. M.F. Montemor, D.V. Snihirova, M.G. Taryba, S.V. Lamaka, I.A. Kartsonakis, A.C. Balaskas, G.C. Kordas, J. Tedim, A. Kuznetsova, M.L. Zheludkevich, M.G.S. Ferreira, "Evaluation of self-healing ability in protective coatings modified with combinations of layered double hydroxides and cerium molibdate nanocontainers filled with corrosion inhibitors", Electrochimica Acta, 2012, 60, 31– 40.

89. I.A. Kartsonakis, E. Athanasopoulou, D. Snihirova, B. Martins, M.A. Koklioti, M.F. Montemor, G. Kordas, C.A. Charitidis, "Multifunctional epoxy coatings combining a mixture of traps and inhibitor loaded nanocontainers for corrosion protection of AA2024-T3", Corrosion Science, 2014, 85, 147–159.

90. J. Tedim, A. Kuznetsova, A.N. Salak, F. Montemor, D. Snihirova, M. Pilz, M.L. Zheludkevich, M.G.S. Ferreira, "Zn–Al layered double hydroxides as chloride nanotraps in active protective coatings", Corrosion Science, 2012 55, 1–4.

91. J. Zhang and G.S. Frankel, "Corrosion-Sensing Behavior of an Acrylic-Based Coating System", Corrosion, 1999, 55, 957-967.

92. W. Feng, S.H. Patel, M-Y. Young, J. L. Zunino III and M. Xanthos, "Smart Polymeric Coatings-Recent Advances", Advances in Polymer Technology, 2007, 26, 1–13.

93. I.M. El-Nahhal, S.M. Zourab and N.M. El-Ashgar, "Encapsulation of Phenolphthalein pH-Indicator into a Sol-Gel Matrix", J. Dispersion Sci. Technol., 2001, 22, 583–590.

94. G. Engelmann, M. Jobmann and G. Rafler, "Dextran carbamates-materials for microencapsulation", Ind. Crop. Prod., 2004, 20, 37–48.

95. W. Li and L.M. Calle, Controlled Release Microcapsules for Smart Coatings, NACE Corrosion 2007, Paper 07228, Nashville, TN, March 2007.

96. W. Li and L. M. Calle, A smart coating for the Early Detection and Inhibition of Corrosion, Proceeding of the Sman Coatings 2007, p.191, Orlando, Florida, February 2007.

97. L.M. Calle and W. Li, "Coatings and Methods for Corrosion Detection and/or Reduction" U.S. Patent No. 7,790,225, U.S. Patent and Trademark Office, 2010.

98. L.M. Calle, J.W. Buhrow, W.Li, S.T. Jolley, "A Multifunctional Coating for Autonomous Corrosion Control", downloaded from http://ntrs.nasa.gov/archive/nasa/casi.ntrs.nasa.gov/20110014507.pdf

99. E. Almeida, T.C. Diamantino and O. Sousa, "Marine paints: The particular case of antifouling paints", Prog. Org. Coat., 2007, 59, 2–20.

100. N. Voulvoulis, M.D. Scrimshaw and J.N. Lester, "Review Alternative Antifouling Biocides", Appl. Organometal. Chem., 1999, 13, 135–143.

101. I.K. Konstantinou, T.A. Albanis, "Worldwide occurrence and effects of antifouling paint booster biocides in the aquatic environment: a review", Environment International, 2004, 30, 235– 248.

102. K. Martínez, I. Ferrer, M.D. Hernando, A.R. Fernández-Alba, R.M. Marcé, F. Borrull and D. Barceló, "Occurrence of Antifouling Biocides in the Spanish Mediterranean Marine Environment", Environmental Technology, 2001, 22, 543-552.

103. K.V. Thomas, "The Environmental Fate and Behaviour of Antifouling Paint Booster Biocides: a Review", Biofouling, 2001, 17, 73-86.

104. S.M. Olsen, L.T. Pedersen, M.H. Hermann, S. Kiil, K. Dam-Johansen, "Inorganic precursor peroxides for antifouling coatings", J. Coat. Technol. Res., 2009, 6, 187–199.

105. M. Zhang, E. Cabane, J. Claverie, "Transparent Antifouling Coatings Via Nanoencapsulation of a Biocide", Journal of Applied Polymer Science, 2007, 105, 3824–3833.

106. T.N. Borodina, D.O. Grigoriev, M.A. Carillo, J. Hartmann, H. Moehwald, D.G Shchukin, "Preparation of Multifunctional Polysaccharide Microcontainers for Lipophilic Bioactive Agents", ACS Appl Mater Interfaces, 2014, 6, 6570-6578.

107. L.D. Chambers, K.R. Stokes, F.C. Walsh, R.J.K. Wood, "Modern approaches to marine antifouling coatings", Surface & Coatings Technology, 2006, 201, 3642–3652.

108. S.A. Kumar, A. Sasikumar, "Studies on novel silicone/phosphorus/sulphur containing nano-hybrid epoxy anticorrosive and antifouling coatings", Progress in Organic Coatings, 2010, 68, 189–200.

109. M.R. Detty, R. Ciriminna, F.V. Bright and M. Pagliaro, "Environmentally Benign Sol–Gel Antifouling and Foul-Releasing Coatings", Acc. Chem. Res., 2014, 47, 678–687.

110. R.F. Brady Jr., "A fracture mechanical analysis of fouling release from nontoxic antifouling coatings", Progress in Organic Coatings, 2001, 43 188–192.

111. S. Krishnan, C.J. Weinman and C.K. Ober, "Advances in polymers for anti-biofouling surfaces", J. Mater. Chem., 2008, 18, 3405-3413.

112. A. Rosenhahn, S. Schilp, H.J. Kreuzer and M. Grunze, "The role of ''inert'' surface chemistry in marine biofouling prevention", Phys. Chem. Chem. Phys., 2010, 12, 4275–4286.

113. I. Banerjee, R.C. Pangule, and R.S. Kane, "Antifouling Coatings: Recent Developments in the Design of Surfaces That Prevent Fouling by Proteins, Bacteria, and Marine Organisms", Adv. Mater., 2011, 23, 690–718.

114. D. Carteau, K. Vallée-Réhel, I. Linossier, F. Quiniou, R. Davy, C. Compère, M. Delbury, F. Faÿ, "Development of environmentally friendly antifouling paints using biodegradable polymer and lower toxic substances", Progress in Organic Coatings, 2014, 77, 485– 493.

115. J.A. Callow and M.E. Callow, "Trends in the development of environmentally friendly fouling-resistant marine coatings", Nature Communications, 2011, 2, 244.

116. J.E. Gittens, T.J. Smith, Rami Suleiman, Robert Akid, "Current and emerging environmentally-friendly systems for fouling control in the marine environment", Biotechnology Advances, 2013, 31, 1738–1753.

117. F.W.Y. Myan, J. Walker and O. Paramor, "The interaction of marine fouling organisms with topography of varied scale and geometry: a review", Biointerphases, 2013, 8:30.

118. A.J. Scardino and R. de Nys, "Mini review: Biomimetic models and bioinspired surfaces for fouling control", Biofouling, 2011, 27, 73–86.

119. C.M. Magin, S.P. Cooper and A.B. Brennan, "Non-toxic antifouling strategies", Materials Today, 2010, 13, 36-44.

120. N. Fusetani, "Biofouling and antifouling", Nat. Prod. Rep., 2004, 21, 94–104.

121. S. Dobretsov, R.M.M. Abed and M. Teplitski, "Mini-review: Inhibition of biofouling by marine microorganisms", Biofouling, 2013, 29, 423–441.

122. J.B. Kristensen, R.L. Meyer, C.H. Poulsen, K.M. Kragh, F. Besenbachera, and B.S. Laursen, "Biomimetic silica encapsulation of enzymes for replacement of biocides in antifouling coatings", Green Chem., 2010, 12, 387–394.

123. T. Szabó, L. Molnár-Nagy, J. Bognár, L. Nyikos, J. Telegdi, "Self-healing microcapsules and slow release microspheres in paints", Progress in Organic Coatings, 2011, 72, 52–57.

124. Z. Zheng, X. Huang, M. Schenderlein, D. Borisova, R. Cao, H. Möhwald and D. Shchukin, "Self-Healing and Antifouling Multifunctional Coatings Based on pH and Sulfide Ion Sensitive Nanocontainers", Adv. Funct. Mater., 2013, 23, 3307–3314.

CHAPTER 2

Experimental Section Summary

Experimental Section Summary

This chapter aims at summarizing all the experimental work performed during this thesis. The main objective of this work was the development of nanocontainers for incorporation in multifunctional coatings. In order to achieve it, different synthesis and encapsulation methodologies were employed, followed by characterization of the resulting nanocontainers. The developed capsules were then incorporated into different coating formulations and their anticorrosive/sensing/antifouling performance was assessed.

In more detail, this work was divided in three stages, as depicted in Figure 14: 1) material preparation, 2) tests in solution and 3) tests in coating.

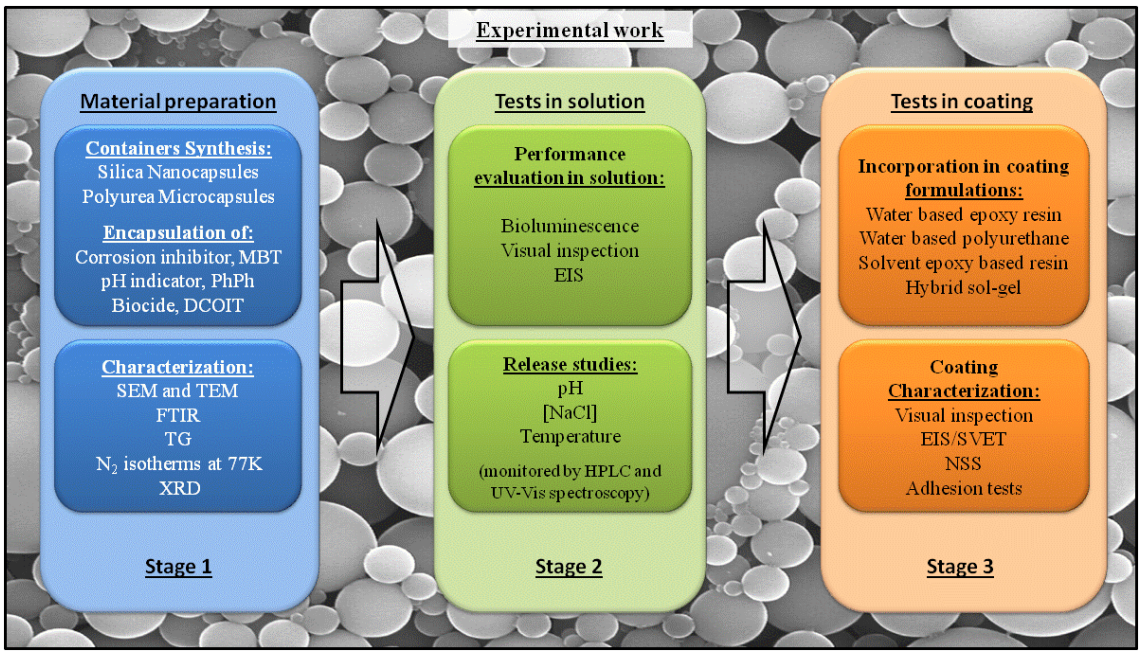

Figure 14: Summary of experimental work realized in the frame of this thesis.

Since this work focused primarily on the development of micro and nanocontainers and their application, the theoretical principles of the several characterization techniques used will not be described in this chapter. Nonetheless, the following paragraphs explain how the work was done and what was expected using those techniques and the type of information obtained from them. Further experimental details will be presented in each chapter of results.

The first stage of this work was centered in the development and optimization of synthesis parameters to produce silica nanocapsules (SiNCs) and polyurea microcapsules (PU-MCs)

and the encapsulation of active compounds into those capsules. As corrosion inhibitor, 2-mercaptobenzothiazole (MBT) was the selected compound due to its proved inhibition effect on copper rich aluminum alloys, like aluminum alloy 2024 (AA2024), one of the most used alloys in aeronautical industry, and also used in this work. To be used as corrosion sensor, phenolphthalein (PhPh) was selected due to its intrinsic characteristics, in particular the pH range when it turns from colorless to pink (~8.5) which is suitable for identification of cathodic areas, as a result of the beginning of corrosive process. The compound 4,5-dichloro-2-octyl-4-isothiazolin-3-one (DCOIT) was the biocide selected due to their well-known performance and also because it has a rapid biodegradation and minimal bioaccumulation. This compound is used commercially with the following names: Sea-Nine™ 211N, Parmetol® S15 and Kathon™ 910 SB.

The capsule preparation and the encapsulation of different compounds were always made in a single step. The methodology adopted for the encapsulation of compounds was based on an oil-in-water (o/w) emulsion, where the continuous phase was hydrophilic (water based) and the dispersed phase lipophilic (solvent based). All the compounds used for encapsulation are soluble in organic solvents, thus they were dissolved in the adequate solvents and added to the disperse phase of the o/w emulsion. The synthesis of SiNCs was performed using tetraethyl orthosilicate (TEOS) as silicon precursor and cetyl trimethylammonium bromide (CTAB) as emulsion stabilizer and template for condensation (polymerization) of TEOS. In the case of PU-MCs, the polymerization of polyurea occurs at the interface between aqueous and organic phases, where both monomers (diisocyanate and amine) react through an interfacial polycondensation, promoting the encapsulation of the organic (dispersed) phase, resulting in microcapsules loaded with the lipophilic compound.

After the preparation of our materials (SiNCs and PU-MCs), they were fully characterized. The morphological properties (size and shape) were assessed using microscopic techniques such as scanning electron microscopy (SEM) and transmission electron microscopy (TEM), which allow to confirm the success of the capsules preparation, their dimensions and uniformity, and in some cases porosity and shell thickness. In terms of structural characterization, x-ray diffraction (XRD) was used to confirm the absence of crystallinity in SiNCs. Another important property, based on the chemistry of the materials, was studied by Fourier transform infrared spectroscopy (FTIR). In FTIR spectra, the main typical

vibrational modes of silica and polyurea were identified. This technique was also used to confirm the presence of the encapsulated compounds, although in most of the cases it was difficult to achieve, due to the overlapping of those bands by other intense bands from the capsules. As SiNCs are porous materials, isotherms of N_2 at 77K was performed and Brunauer-Emmett-Teller (BET) model was applied for determination of surface area and Barrett-Joyner-Halenda (BJH) model was used for measurement of pore size distribution. Thermogravimetric assays were realized to assess the thermal stability of the produced capsules and also to quantify the amount of active compound encapsulated in percentage of the total mass of capsules.

The following stage was focus on the assessment of the developed containers performance in solution and incorporated in coatings, in terms of anticorrosive pigment, sensor and AF agent.

In solution, SiNCs containing MBT were tested in the corrosion protection of AA2024, using sodium chloride solution as electrolyte, where the capsules were dispersed. The monitoring of corrosion protection of SiNC-MBT was done using electrochemical impedance spectroscopy (EIS). Regarding corrosion sensing, suspensions of capsules containing PhPh were prepared and pH of those suspension was gradually increased to verify the coloration of the suspension (or the capsules) as result of pH variation. This test was done in order to simulate the conditions in corroding defects. Concerning AF tests, modified *E.coli* with a bioluminescent gene was used to monitor the biocide effect of SiNCs with DCOIT and MBT. The optimum conditions for bacteria growth was settled and a suspension of biocide material was added to bacteria medium and the biocide effect was assessed as a result of the bioluminescence decrease.

In parallel to those experiments, release studies of the encapsulated compounds were performed varying the most important parameters relevant for the selected application, such as pH, temperature and sodium chloride concentration. The release of the encapsulated compound was monitored by high-performance liquid chromatography (HPLC) or by UV-Vis spectroscopy.

The third stage of this work was based on the incorporation of developed capsules in different coating formulations (epoxy, polyurethane and sol-gel), selected according to the desired functionality under study and substrate used, and the assessment of the performance of the developed coating.

The corrosion protection properties of new coatings (primers) were assessed using electrochemical techniques, like EIS and scanning vibrating electrode technique (SVET). In one of the last coatings developed using sol-gel, electrochemical data was corroborate by industrial standard tests performed in collaboration with a company, where neutral salt spray (NSS) and adhesion tests were done.

Developed sensing coatings were characterized by visual inspection. Coated aluminum and magnesium alloys were immersed in a sodium chloride solution to promote corrosion and pictures were taken at defined times to capture the beginning of corrosive process, by color modification of the coating due to the incorporation of sensor based in capsules containing PhPh.

The evaluation of antifouling properties was performed by immersion of the coated carbon steel with two modified formulations in a phosphate-buffered saline (PBS) solution. This medium was selected because is suitable for bacteria growth and we took aliquots of these solutions (where coated samples were immersed) and they were added to fresh modified *E.coli* cultures to test the effect of biocide released from coating on their bioluminescence. The correlation of bioluminescence with biocides release was also performed to assess the most adequate type of formulation form this functionality.

In conclusion, all developed containers were fully characterized and their performance, according to the functionality desired, were assessed firstly in solution and then incorporated in specific coating models in similar conditions to the real applications.

CHAPTER 3

"Silica nanocontainers for active corrosion protection"

Nanoscale

Dynamic Article Links

Cite this: *Nanoscale*, 2012, **4**, 1287

www.rsc.org/nanoscale

PAPER

Silica nanocontainers for active corrosion protection

Frederico Maia, João Tedim, Aleksey D. Lisenkov, Andrei N. Salak, Mikhail L. Zheludkevich* and Mário G. S. Ferreira

Received 18th October 2011, Accepted 5th December 2011
DOI: 10.1039/c2nr11536k

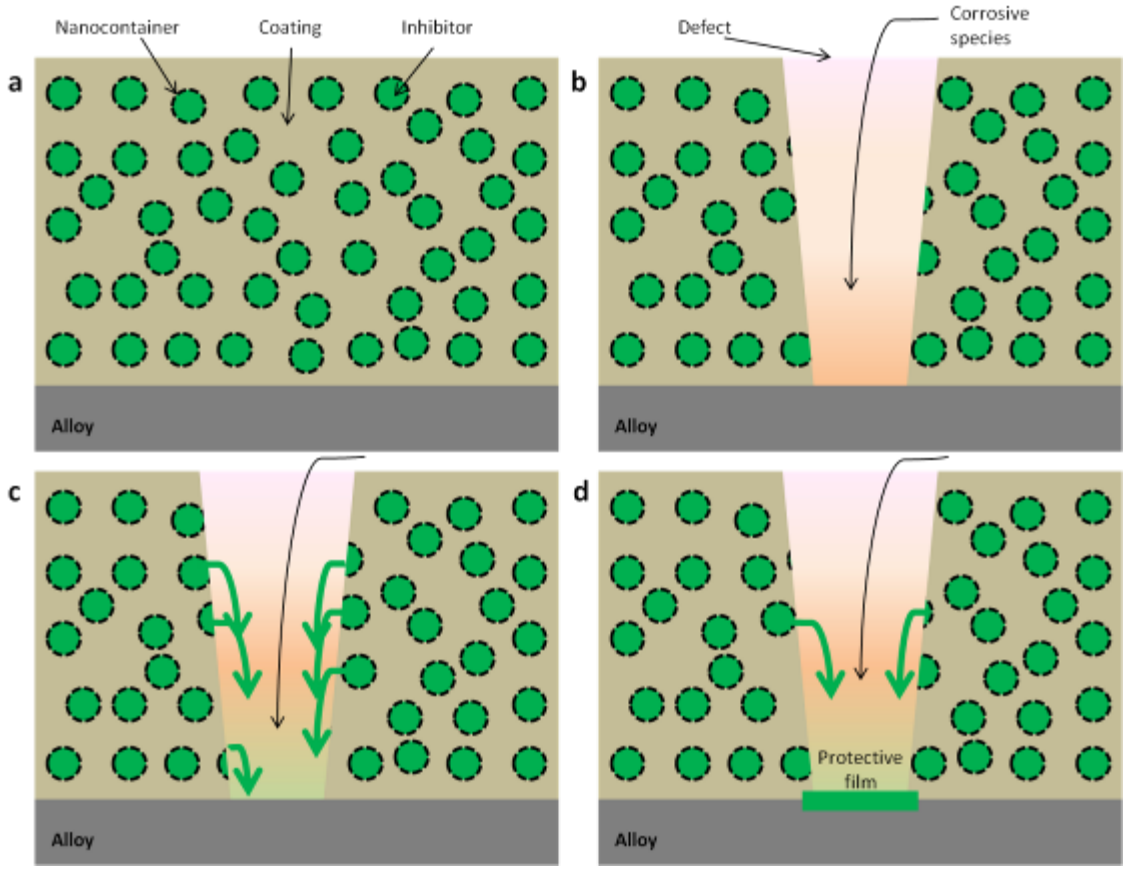

Abstract

Novel self-healing protective coatings with nanocontainers of corrosion inhibitors open new opportunities for long-term anticorrosion protection of different metallic materials. In this paper a new type of functional nanoreservoir based on silica nanocapsules (SiNC) synthesized and loaded with corrosion inhibitor 2-mercaptobenzothiazole (MBT) in a one-stage process is reported for the first time. Unlike conventional mesoporous silica nanoparticles, SiNC possess an empty core and shell with gradual mesoporosity, arising from the particular conditions of the synthetic route adopted, which confers significant loading capacity and allows prolonged and stimuli-triggered release of the inhibiting species. The kinetics of inhibitor release was studied at different pH values and concentrations of NaCl. The results show a clear dependence of the release profiles on corrosion relevant triggers such as pH and Cl^- concentration. When SiNC loaded with MBT are dispersed in NaCl solution, there is a significant decrease of the corrosion activity on aluminium alloy 2024. More importantly, when SiNC–MBT is added to a conventional water-based coating formulation, the modified coating hampers corrosion activity at the metal interface, better than in the case of direct addition of corrosion inhibitor. Furthermore, self-healing is observed before and after artificially inflicting defects in the modified coatings. As a result, the developed nanocontainers show high potential to be used in new generation of active protective coatings.

Introduction

The development of novel materials for prolonged or even controllable release of targeted active substances is a challenge with a major impact in different areas, from pharmaceuticals to the aerospace industry. Quite often, control over the release of species is achieved by immobilization or encapsulation of the active species in inert carriers such as micrometre and nanometre-sized hollow particles, which can be modified to release the species in response to certain triggers and, ideally, on demand.

There has been a lot of work and debate concerning the development of ‘‘smart’’ functional coatings showing self-healing ability. Some authors have been focusing on the recovery of coating integrity after defects being formed (recovery at the structural level) [1], whereas others suggest that the recovery of coating properties for the specific applications to which they were initially designed may be equally classified as self-healing

(recovery at the functional level). In the latter category one may include the restoration of anticorrosion action arising from the presence of smart nanoreservoirs loaded with corrosion inhibitors [2–5].

In corrosion, the direct addition of corrosion inhibitors to coating formulations has been a strategy commonly adopted to protect metallic substrates against corrosion. The coating matrix works as a physical barrier, preventing direct contact between the metal surface and aggressive species (e.g., chlorides) - passive protection - while the dispersed corrosion inhibitors are responsible for damping corrosion activity at the metal surface when the coating matrix is degraded (by development of pores, cracks, delamination zones and blisters) and the barrier effect no longer works - active protection. However, there are several issues related to the direct addition of corrosion inhibitors to coating formulations. The inhibitor often interacts with the coating formulation, thereby resulting in deactivation of the inhibitor and/or fast degradation of coating (adhesion, barrier properties) as reported by Raps [6] and Shchukin [7]. In addition, the constant leaching of inhibitors from the coating to environment, even when it is not necessary for the protection of metal, can pose real threats to the ecosystems, especially when toxic or carcinogenic compounds, such as chromates, are used. One way of overcoming these problems is by encapsulation of the corrosion inhibitors in inert nanomaterials that are consequently dispersed in the coating formulation (here, ‘‘inertness’’ does not mean lack of functionality, but tendency to not interact detrimentally with the coating matrix).

There are reports of MBT immobilization in cyclodextrins [8, 9], halloysite nanotubes [10], ion-exchange clay nano-pigments [11, 12] and polymer capsules [13]. However the encapsulation of MBT in robust inorganic nanocontainers is still a very new topic. In fact, this approach would allow the achievement of high loading capacity together with mechanical stability, which is not only important during coating preparation if high shear forces and application by roll-coaters is necessary to properly disperse the nanocontainers, but also to impart additional stability to the coatings during the service life of structures.

In this work corrosion inhibitor 2-mercaptobenzothiazole (MBT) was encapsulated in silica nanocapsules (SiNC) with mesoporous shells via microemulsion oil-in-water in a single stage polymerization process, with dynamic interaction at the water–oil interfaces [14]. This method was selected among others because it is a one-step process involving both synthesis of SiNC and encapsulation of MBT with high loading content, hence being a

simpler and easier process when compared to more traditional routes for the preparation of mesoporous silica nanoparticles [5]. This is a feature of paramount importance for scaling up of the process at the industrial level. 2-Mercaptobenzothiazole was selected because of its superior corrosion inhibiting properties [8, 10, 15, 16]. The obtained SiNC were characterized using different techniques, giving particular attention to the factors triggering the release of MBT from these nanostructures and to the anticorrosion efficiency of these nanomaterials towards aluminium alloy 2024-T3 (AA2024-T3) both in solution and when incorporated into protective coatings.

Experimental section

Materials

Ammonia solution (NH4OH) (25–28%), sodium chloride (NaCl), ethyl ether (99.5%) and buffer solutions were obtained from Riedel-de-Haën. Cetyltrimethylammonium bromide (CTAB) (99%), tetraethoxysilane (TEOS) (99.9%) and 2-mercaptobenzothiazole (MBT) (97%) were purchased from Sigma-Aldrich. Ethanol was supplied by Panreac (Spain) and acetonitrile (HPLC grade) from ROMIL. All chemicals were analytic grade and were used without further purification.

Synthesis of silica nanocapsules (SiNC)

SiNC were prepared as described in the literature [14], by using CTAB as cationic surfactant, ethyl ether as co-solvent and ammonia solution as catalyst (Scheme 3.1). Firstly, a CTAB solution was prepared (0.25 g in 35 mL of water) and 0.25 mL of ammonia solution (25–28%) was subsequently added (solution 1). Afterwards, 0.1 g of MBT dissolved in 25 mL of ethyl ether (solution 2) was added to solution 1, and an oil-in-water microemulsion was obtained. Then, 2.0 mL of TEOS was added to the microemulsion under vigorous stirring and kept in a closed vessel for 24 h. The obtained precipitate was filtered, washed with pure water and dried at 60 ºC. A small portion of these nanocapsules were calcined at 550 ºC during 5 hours, with a heating rate of 10 $^{o}C.min^{-1}$, in order to facilitate the determination of MBT loading content.

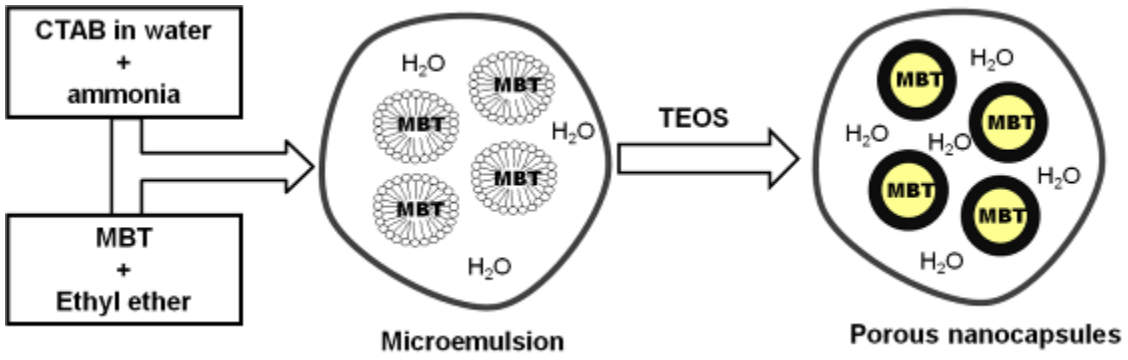

Scheme 3.1: Synthesis of SiNC and encapsulation of MBT.

Characterization

Particle morphology was characterized by scanning electron microscopy (SEM) coupled with energy dispersive spectroscopy (EDS) (Hitachi S-4100 system with electron beam energy of 25 keV) and by transmission electron microscopy (TEM) (Hitachi H9000 TEM system with an electron beam energy of 300 keV). FTIR experiments were carried out on a Bruker IF55 spectrometer equipped with the ATR system (Golden Gate—SPECAC) and X-ray diffraction (XRD) study of the powders was performed using a Philips X'Pert MPD diffractometer (Cu Ka radiation, tube power 40 kV, 50 mA) at room temperature. A PW1711 proportional detector and an X'celerator detector were used for the XRD data collection over the angular ranges $1 < 2\theta < 6^{o}$ and $4 < 2\theta < 65^{o}$, respectively.

A Malvern Zetasizer 4 instrument was used to perform dynamic light scattering (DLS) and zeta potential measurements. Thermogravimetric analysis (TG/DTA) was carried out in a Sataram-Labsys system under air atmosphere, with a heating rate of 10 $^{o}C.min^{-1}$ from room temperature up to 800 ^{o}C.

The textural properties of samples were evaluated based on the adsorption–desorption isotherms of N_2 at -196 ^{o}C, performed on the equipment Quantachrome NOVA 4200e. Samples were previously degassed at 180 ^{o}C for 6 h. The specific area (S_{BET}) was calculated by the BET method (Brunauer, Emmett and Teller), the volume of micropores (V_{micro}) was determined from the method-t, and the total pore volume ($V_{P p/p^{o}=0.98}$) was obtained from the total volume of N2 adsorbed to p/p^{o} = 0.98 [17]. The most frequent diameter of pores (mode of pore diameter distribution) was calculated by two different methods: the BJH method (Barrett–Joyner–Halenda) [17, 18], applied to the desorption branch of isotherm, and the DFT method (density functional theory) using a routine

available in the software of Quantachrome equipment that was developed for the adsorption of N_2 on porous materials based on silicon, assuming a cylindrical pore model.

Release studies of MBT from SiNC

The release profiles of MBT were monitored by high performance liquid chromatography (HPLC) using a Shimadzu chromatograph equipped with a SPP-M20A diode array detector, using a C18 column as the stationary phase and acetonitrile/pure water (90:10, v/v) as the mobile phase with a flow of 1 $mL.min^{-1}$. The correlation coefficient of the calibration curves obtained with 5 MBT standards was higher than 0.999.

100 mg of SiNC–MBT were dispersed in 20 mL of an aqueous solution where NaCl concentration and buffered pH were systematically varied (NaCl concentration: 0.005 M, 0.05 M and 0.5; pH = 4, 7 and 10) and the MBT release profiles were determined by HPLC. 1 mL sample of the mixture was extracted with a syringe and filtered with a specific syringe filter (PTFE membrane with 0.20 mm pore size). In order to determine the total amount of MBT encapsulated, 100 mg of SiNC–MBT were dispersed in 20 mL of ethanol during 24 hours to guarantee the maximum release of MBT. 1 mL of the resulting solution was extracted with a syringe, filtered, and then analyzed by HPLC. The encapsulation efficiency was determined by the expression: $\%E = n_{MBText}/n_{MBTi} \times 100$, where n_{MBText} is the amount of MBT extracted from SiNC and n_{MBTi} is the initial amount of MBT used in the encapsulation.

Anticorrosion efficiency in solution and in coated AA2024

The aluminium alloy 2024 substrates were cleaned and etched according to a standard commercial procedure (alkaline cleaning in Metaclean T2001 at 68 ºC for 25 min, alkaline etching in Turco Liquid Aluminetch N2 at 60 ºC for 45 s, acid etching in Turco Liquid Smutgo NC at 30 ºC for 7 min, each step followed by washing in distilled water).

Dried and cleaned AA2024 substrates were coated with an aqueous-based model film generously provided by Mankiewicz GmbH with fast drying at room temperature. The model film consists of a resin component and a hardener. The resin is a water-based epoxy emulsion and the hardener consists of water-based amine, both without organic solvents. The application was done through the incorporation (2 wt% with respect to the resin) of SiNC–MBT into the resin and stirred until obtaining uniform dispersion (~30 minutes).

Subsequently, the hardener was added to the dispersion and the coating was applied on AA2024 plates using a bar coater (30 μm thickness). After application, samples were dried at room temperature (~25 ºC) for 12 h. The same procedure was followed for the incorporation of empty SiNC and for the direct addition of MBT, using proportions stated previously. In order to verify the active protection of SiNC–MBT in the coated samples, two circular defects (spots) were made with a needle tip in each sample.

Electrochemical impedance spectroscopy (EIS) measurements were carried out on bare and coated aluminium alloy 2024 at room temperature in a three-electrode cell consisting of a saturated calomel reference electrode, a platinum foil counter electrode and an AA2024 plate as the working electrode in the horizontal position (an exposed area of *ca*. 3 cm^2). The cell was placed in a Faraday cage to avoid the interference of external electromagnetic fields. The electrolyte was 0.05MNaCl aqueous solution for the bare AA2024 and 0.5 M NaCl for the coated plates (V = 10 mL), stagnant and in equilibrium with air. The measurements were performed using a Gamry FAS2 Femtostat with a PCI4 Controller. The selected frequency range was typically from 1×10^5 to 1×10^{-2} Hz, with a 10 mV RMS sinusoidal perturbation *vs*. open circuit potential. The impedance plots were fitted using different RC equivalent circuits, where pure capacitances were replaced by constant-phase elements (CPE). The software used for the fittings was Gmary Echem Analyst 5.61, and the χ^2 varied between 10^{-2} and 10^{-4}.

Results and discussion

Synthesis and characterization of SiNC

SiNC were produced in a one-step process through an oil-in water microemulsion polymerization (recall Scheme 3.1), using CTAB as template-surfactant and ethyl ether as co-solvent. A white powder was obtained in the case of empty silica nanocapsules, whereas when the inhibitor was encapsulated the color of the powder was found to be pale yellow due to the presence of MBT. TEOS was the silica precursor used for the preparation of SiNC and for encapsulation of MBT. The polymerization of TEOS is an exothermic process that increases the temperature in the reaction media, causing gasification of the volatile co-solvent from the center to the outside of nanocapsules (ethyl ether has a low vaporization point, ~35 ºC). This creates differentiated porosity from core to shell allowing the entrapment of MBT in the generated pores. The formation of SiNC is the result of a

dynamic cross-coupling of two processes - namely, the dynamic gasification of the template and stabilization process of condensation together with self-assembly controlled by the presence of CTAB [14].

In order to analyze the morphology (size and shape) of synthesized nanoparticles, SiNC and SiNC–MBT samples were observed by SEM (Figure 15). All the particles display a spherical and regular shape, with a diameter between 100 and 150 nm. Moreover, in these images, it is possible to verify that there is some residual polymer attached to the nanocapsules from the synthesis step, contributing to their aggregation. Comparing Figure 15a and b, it is possible to observe that encapsulation of MBT in SiNC did not promote any structural change in terms of size distribution and morphology. However, it appears that a greater amount of polymer is present in the SiNC–MBT sample, probably due to chemical interactions between polymer (polymeric TEOS) and the product to encapsulate, i.e., MBT.

In order to obtain more detailed information about the structure and crystallinity of the samples, TEM images were acquired (Figure 16). The particles have a regular morphology (spherical), as expected after analyzing SEM pictures (Figure 15). Besides, all the particles are porous displaying channels, which confirm that the silica particles under study are capsules because there is a clear distinction between the wall, with a thickness of about 20 nm, and the porous core of the nanocapsules. Mesopores of 20 to 30 nm in diameter in the core and channels connecting the core to the shell wall are visible. Assays of electron diffraction were also performed to estimate crystallinity of the obtained nanoparticles. However, as it can be seen in the inset of Figure 16, the material is completely amorphous.

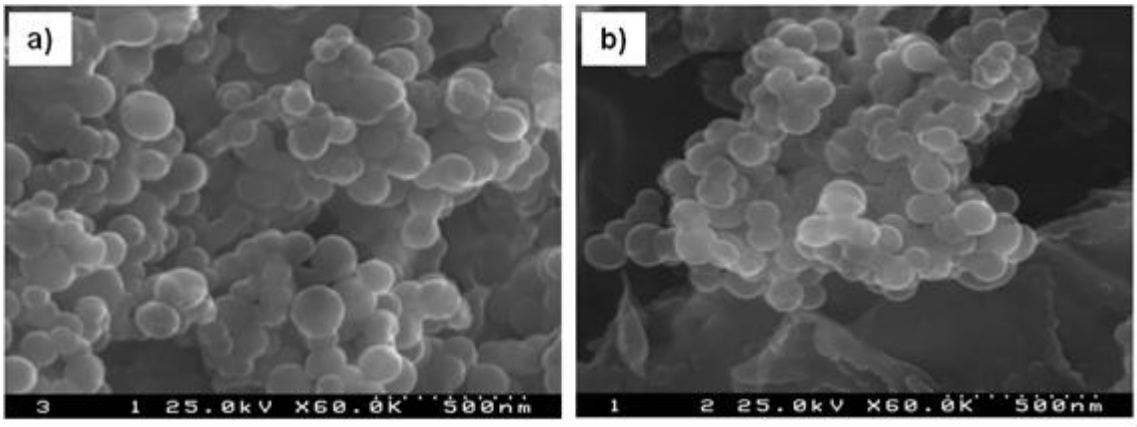

Figure 15: SEM pictures of (a) empty SiNC and (b) SiNC with MBT encapsulated.

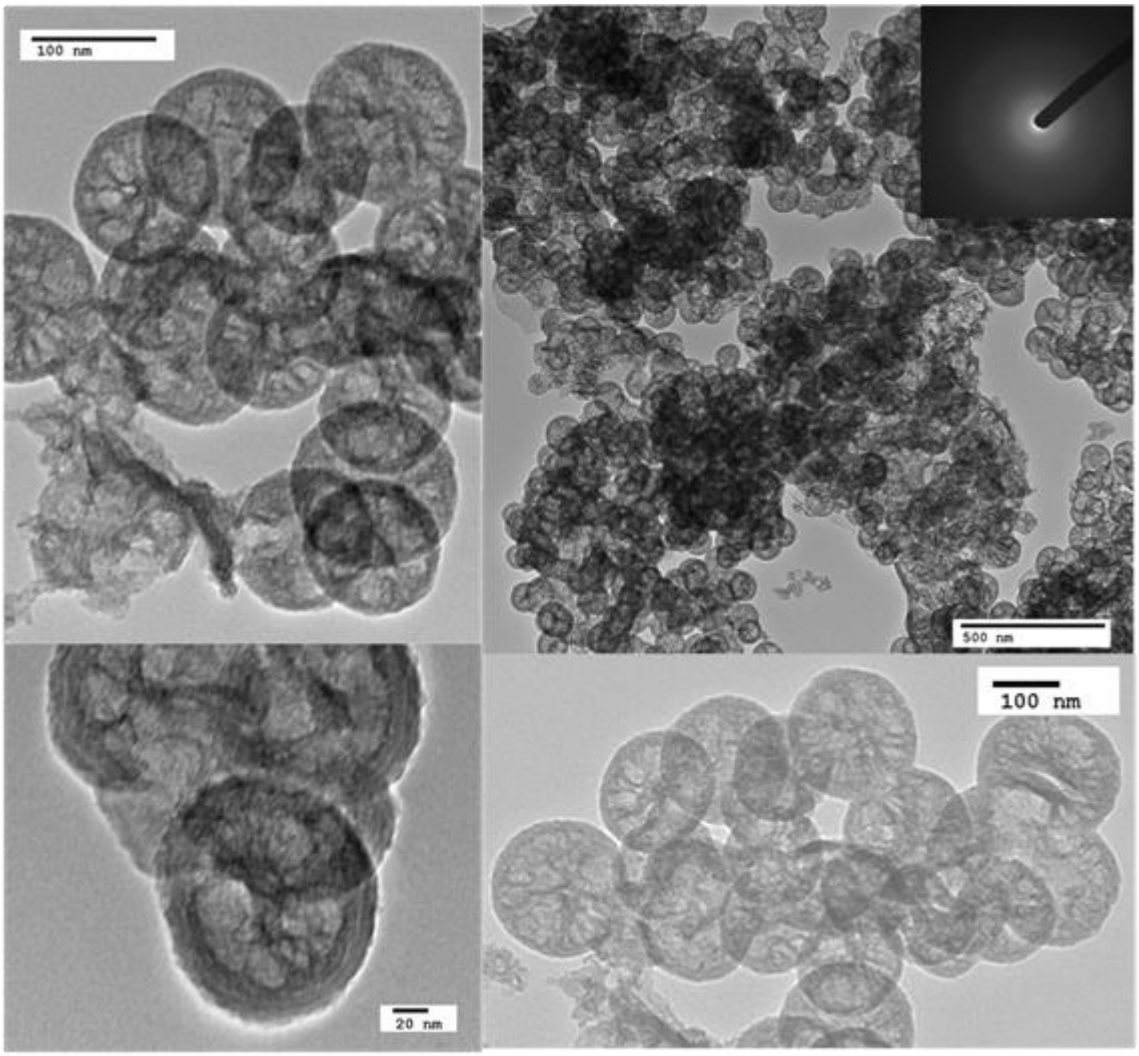

Figure 16: TEM pictures of SiNC with different magnifications; inset: electron diffractogram.

Furthermore, the XRD patterns of SiNC presented in Figure 17 demonstrate a broad band, which indicates the existence of short-range atomic order only. For both the unloaded and MBT loaded nanocapsules this band is centered at $2\theta \approx 21$ º. In terms of *d*-spacing (about 0.4 nm) it corresponds to the average dimension of the SiO_2 unit cell. The low-angle XRD patterns of both SiNC and SiNC–MBT demonstrate a well-marked peak at about 1.3º (see inset in Figure 17). This peak, the same for both types of the samples, can be associated with small-angle scattering by the shells of the nanocapsules. Recalling the TEM images, the shell boundaries are well-defined and the variation of the shell thickness is small. Simulation of the scattering intensity for the given X-ray wavelength using the model of spherical shell was also performed [19]. The observed values of both internal and external shell radii were used and independent normal distribution of the radii is here suggested.

The simulation yields a maximum of intensity at the 2θ ≈ 1.3º. In the SiNC XRD pattern, a diffuse peak centered at about 1.75º is also observed. This peak, which is absent in the XRD pattern of SiNC–MBT, can be attributed to the scattering by the channels of the nanocapsules. These channels with a typical diameter of 5–7 nm are characterized by a weaker contrast in the TEM images and are less regular in shape than the shells. Therefore, the 1.75º peak is rather more diffuse than that at about 1.3º. In SiNC–MBT the channels are filled with MBT. As a difference between the form factors of silica and MBT at such low scattering angles is negligible, the filled channels do not contribute to the correlated scattering.

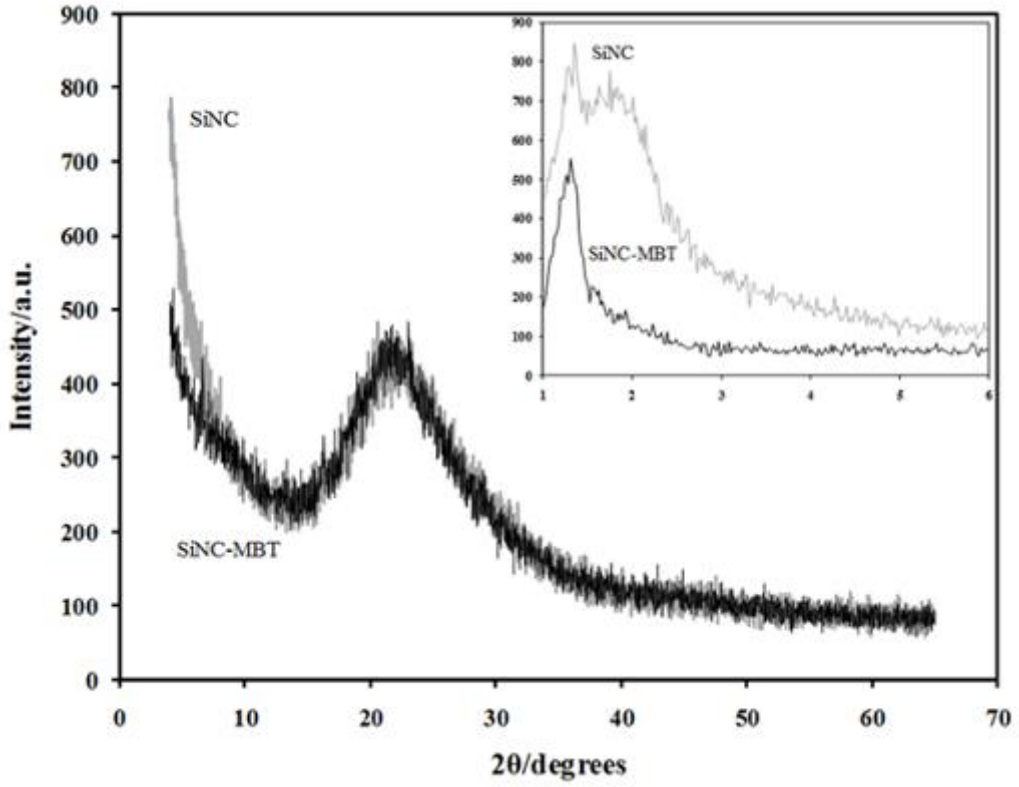

Figure 17: XRD patterns of SiNC and SiNC–MBT nanocapsules for the angular ranges 4/65º and 1/6º (inset).

The textural properties of silica nanocapsules (SiNC and SiNC–MBT) were evaluated based on adsorption–desorption isotherms of N_2 at -196 ºC. Figure 18a shows adsorption–desorption isotherms for both samples. The results are typical of multilayer adsorption in mesoporous materials with a very wide pore size distribution. Table 6 presents the main results of textural characterization of materials which include specific area (S_{BET}), the

volume of micropores (V_{micro}), the total pore volume ($V_{Pp=p^o=0.98}$) and the most frequent diameter of pores (mode of distribution of pore diameter). The samples show a similar BET specific area, with minor variations, which means that encapsulation of MBT did not promote any significant change in the surface area, from 151$m^2.g^{-1}$ (SiNC) to 168$m^2.g^{-1}$ (SiNC–MBT). The method-*t* revealed that the samples do not exhibit microporosity, even the smaller pores presented in the shell of silica nanocapsules are bigger than 2 nm, which means mesoporosity. Figure 18b and c show the pore size distributions in each sample by the two methods applied. For both methods pores were identified with a radius varying between 16 and 450 Å for the BJH method and between 16 and 270 Å for the DFT method. The encapsulation of MBT causes a broadening in the radius distribution curve and a small shift towards higher values, between 30 and 150 Å. Nonetheless, the statistical mode is practically the same in both methods.

The zeta potential and particle size distributions are strongly connected. The low magnitude of the zeta potential can explain the observed aggregation of the nanocapsules (SEM, Figure 15). The low positive value of the zeta potential for empty SiNC (+8.39 mV) is probably due to the presence of some traces of the cationic surfactant CTAB, adsorbed on the nanocapsules surface. The size distribution (Figure 19) of empty nanocapsules exhibits a peak centered at 86 nm, which is in agreement with the size of nanocapsules observed by TEM and SEM. The increase of zeta potential to +34.2 mV, when MBT is encapsulated, could suggest higher stability of the particles in solution, but the appearance of secondary larger particles demonstrated by the particle size distribution (peaks centered at 200 nm and another at 5560 nm) implies that this assumption is not likely. Although SEM and TEM pictures show identical individual silica nanocapsules, the amount of polymer observed together with SiNC–MBT (Figure 15b) may explain the aggregation of nanocapsules into larger particles.

FTIR tests were performed to confirm the encapsulation of MBT. In the FTIR spectra depicted in Figure 20, several characteristic bands associated with empty SiNC can be observed namely, Si–O–Si stretching (1049 cm^{-1}) and Si–O–Si bending (800 cm^{-1}). With respect to MBT, the FTIR spectrum exhibits bands ascribed to C–H stretching (2959, 2889 and 2839 cm^{-1}), C–H and C–N bending (1420 and 1319 cm^{-1}), C–N stretching (1246 and 864 cm^{-1}) and C=S stretching (1080 and 1026 cm^{-1}). In the case of SiNC–MBT, the presence of MBT is confirmed by the presence of bands observed at 1462 and 1408 cm^{-1},

which are associated with the vibrations of the C–N–H group. Another band observed at 1362 cm^{-1} results from the interaction between the N–H bending and C–N stretching vibrations of the C–N–H group. At low wavelengths, two relatively weak bands at 698 and 617 cm^{-1} can be observed, and are due to C–S stretching mode. The presence of these features in the spectrum of SiNC–MBT spectra confirms the successful encapsulation of the corrosion inhibitor.

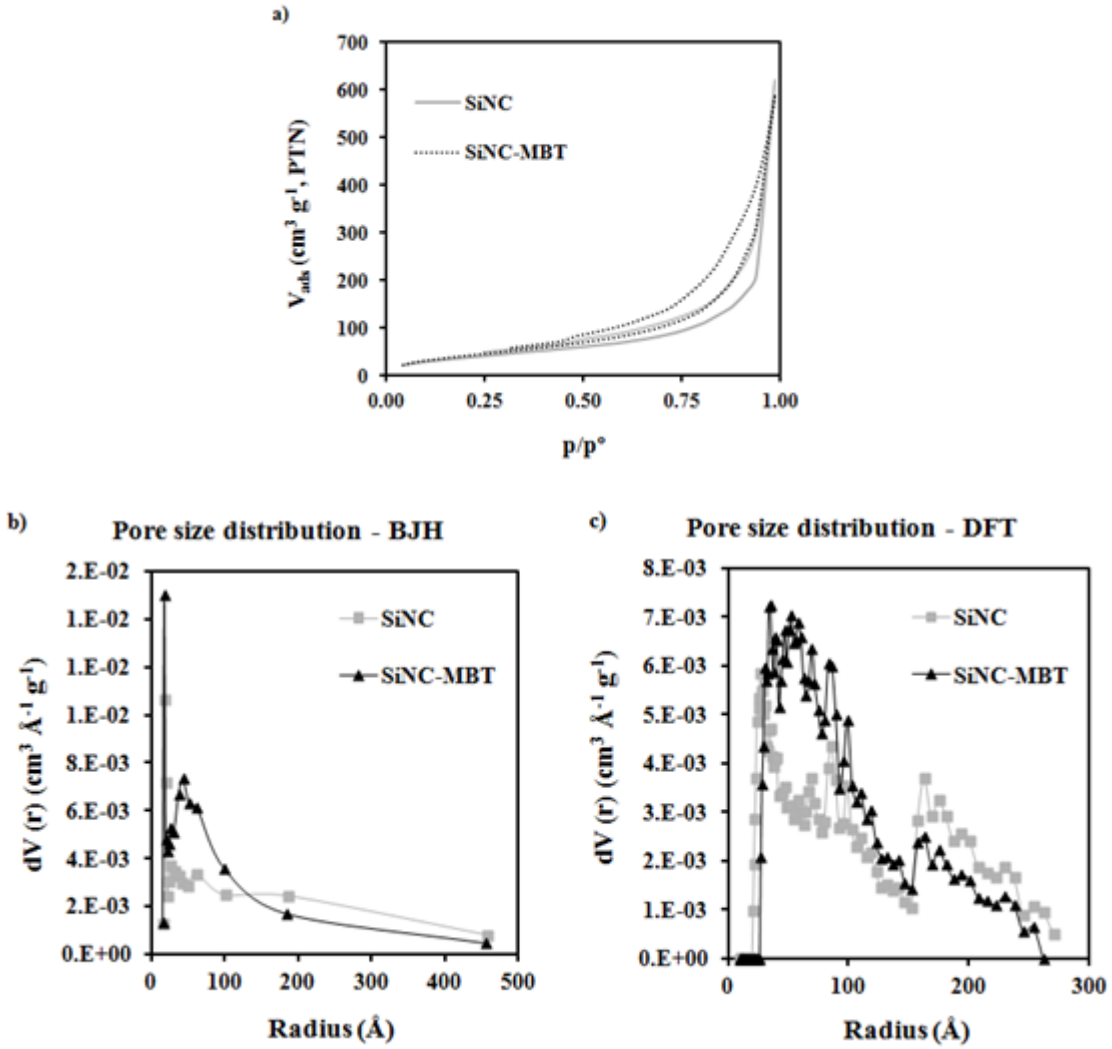

Figure 18: (a) Nitrogen adsorption–desorption isotherms of silica nanocapsules and pore size distribution by two methods: (b) BJH and (c) DFT.

Table 6: Textural properties of the samples determined from the adsorption-desorption isotherms of N_2.

Sample	S_{BET} ($m^2\ g^{-1}$)	V_{micro} (t-method) ($cm^3\ g^{-1}$)	$V_{P\ p/p0=0.98}$ ($cm^3\ g^{-1}$)	ϕ_{poros} BJH [(a)] (nm)	ϕ_{poros} DFT [(a) (b)] (nm)
SiNC	151	0	0.96	3.7	5.5
SiNC-MBT	168	0	0.91	3.7	7.0

(a) The values shown represent the most frequent (mode) value of the distribution of pore diameter. (b) Applying a routine that assumes porous silicon-based cylindrical geometry.

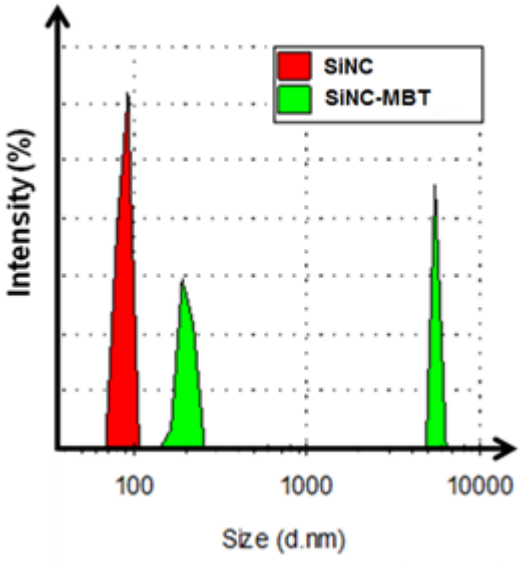

Figure 19: Size distribution of SiNC and SiNC-MBT.

Thermogravimetry experiments were performed in order to verify the thermal stability of silica nanocapsules and to determine the amount of MBT encapsulated. The obtained nanocontainers demonstrate good thermal stability as can be seen in the TG profiles (Figure 21). Moreover, the curve of calcined SiNC shows no significant variation with temperature as expected. The test with the calcined sample was conducted as a reference. From comparison between SiNC and the calcined nanocapsules, one can infer that the mass reduction of approximately 27% is mostly due to degradation of the non-hydrolyzed and non-condensed TEOS and also some residual amount of surfactant. The curve corresponding to SiNC–MBT capsules shows a similar profile, except for the mass reduction between 200 and 300 ºC that is more pronounced and attributed to the presence

of MBT, degraded in this range of temperature [20]. The resulting mass loss is significantly higher in this case and achieves 37%. Therefore, the difference of mass loss for loaded and unloaded nanocontainers can be used to estimate the MBT loading in the capsules, which in this case is 10 wt%. This value is consistent with the result obtained by HPLC after extraction of MBT from the nanocapsules using ethanol, which gives ~8 wt%, corresponding to an encapsulation efficiency of 68%. The value obtained by extraction of MBT with ethanol is lower than the value obtained by TG, probably because the extraction did not remove all MBT that was present in SiNC, leaving a small amount of inhibitor inside. This MBT was consequently released when SiNC were re-dispersed in ethanol. The one-step synthesis of SiNC–MBT leads to an encapsulation of MBT four times more (~340 $mg.L^{-1}$) than in the case of mesoporous silica nanoparticles loaded with one corrosion inhibitor and coated with polyelectrolyte shells after four deposition steps (~90 $mg.L^{-1}$) [5].

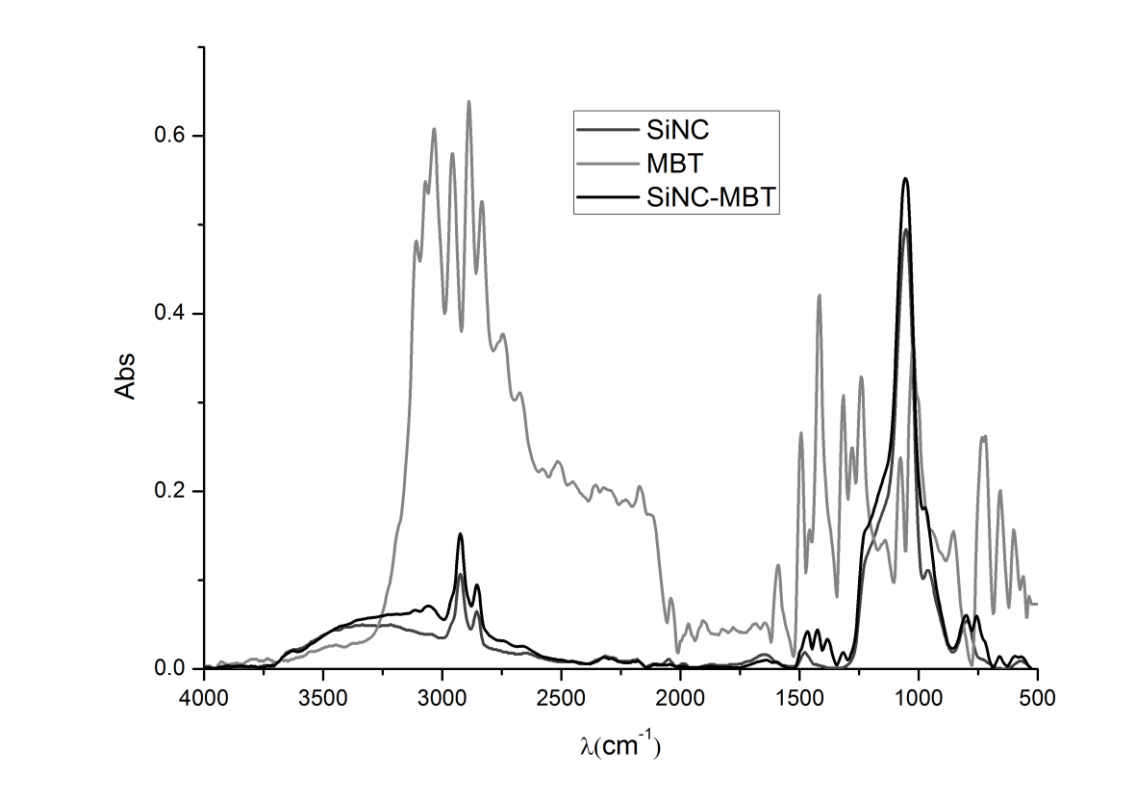

Figure 20: FTIR spectrum of MBT, SiNC and SiNC–MBT.

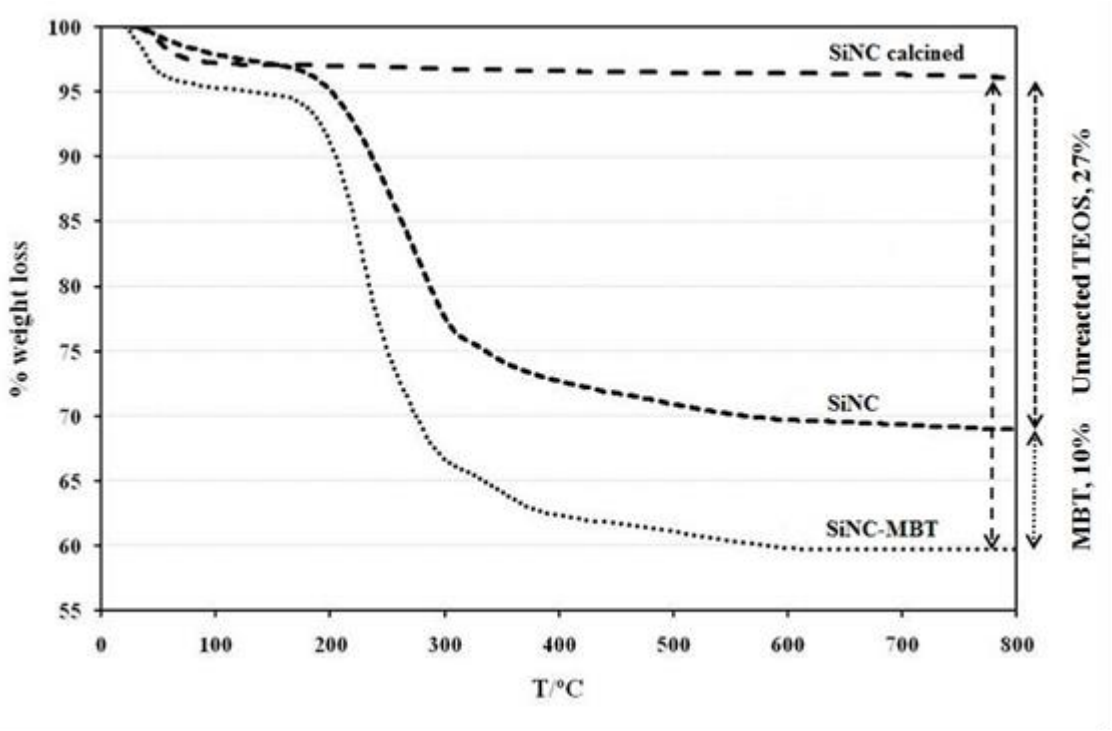

Figure 21: TG profile of SiNC calcined, non-calcined and with MBT encapsulated.

Release studies of MBT

The release of the MBT from SiNC dispersed in aqueous solutions was monitored by HPLC at different pH conditions (4, 7 and 10) and for different NaCl concentrations (0.005, 0.05 and 0.5 M) because chloride concentration and pH are among the most relevant parameters to be considered as corrosion triggers. The profiles obtained at different pH values are similar in shape (Figure 22a) but differ in the amount of MBT released. There are two well-defined stages for inhibitor release. The initial amount of MBT released (first 4 hours) is most likely coming from the outer region of SiNC, i.e., from the shell. In the second stage, between 4 and 48 hours, there is a significant increase of MBT released, coming from the core of the SiNC. After 48 hours, the amount of released MTB begins to stabilize. From the analysis of release profiles it is evident that the MBT is released in greater quantities under alkaline conditions (1.5×10^{-4} M) and acidic conditions (5.7×10^{-4} M), while in neutral conditions the extent of release is relatively low (4.0×10^{-5} M). These differences can be partially explained by the variation of MBT solubility with pH, which is low in the neutral range but relatively higher in alkaline and acidic conditions. In addition, the amount of MBT released in acidic conditions can also be attributed to hydrolysis of non-hydrolyzed TEOS that could have been blocking some

pores in the nanocapsules, thereby facilitating the diffusion of MBT to solution. Hence, the dependence of inhibitor release on pH is shown, confirming the stimuli-responsive triggering of the nanocontainers. For higher times of immersion, the amount of MBT detected in solution tends to stabilize due to the equilibrium between small release of MBT (the solubility of MBT in aqueous solution is low) and degradation of MBT, forming sub-products which are detected in the chromatogram, such as benzothiazole and 2-hydroxybenzothiazole or their dimerization in 2-mercaptobenzothiazole disulfide [21, 22].

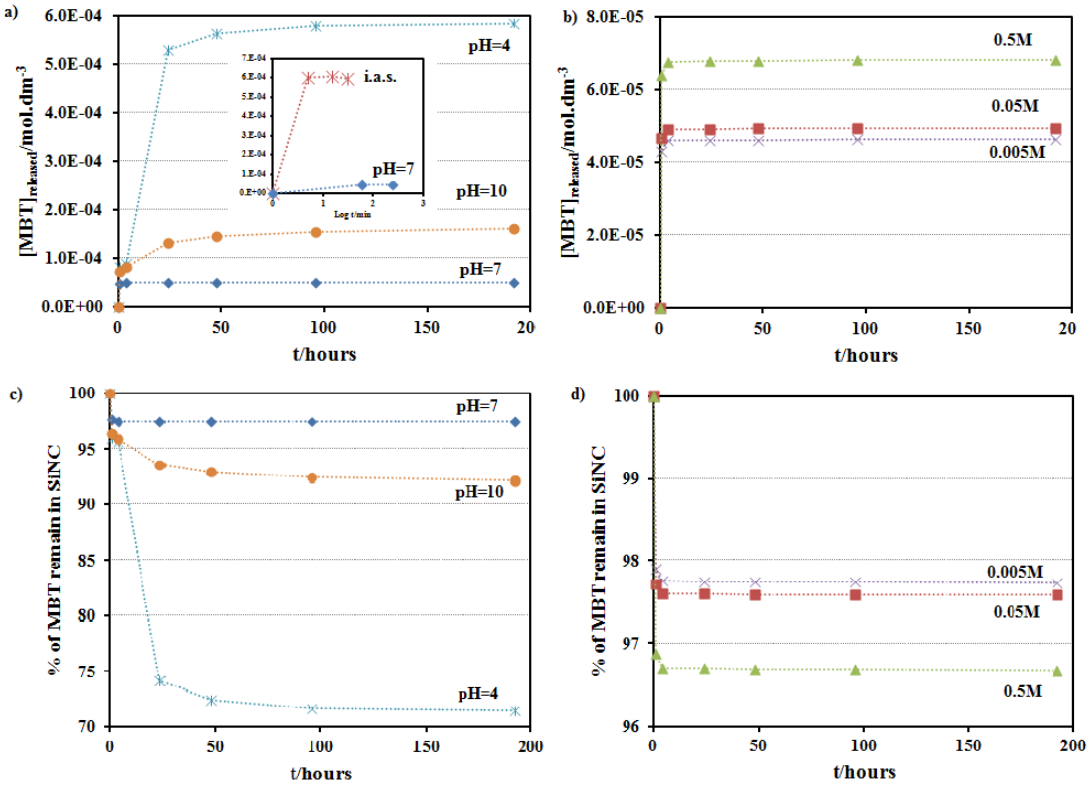

Figure 22: Profiles of release of MBT from SiNC–MBT at (a) different pH's (inset: release of MBT from calcined SiNC with MBT immobilized after synthesis) and (b) different concentrations of NaCl; (c) % of MBT remaining inside SiNC at different pH's and (d) % of MBT remaining inside SiNC at different concentrations of NaCl.

The effect of NaCl concentration (Figure 22b) on the release kinetics, although not so significant as in the pH change, is also evident. The MBT release profiles show that MBT is preferentially released for high NaCl concentration (0.5 M). For lower NaCl concentrations (0.05M and 0.005 M), the amount of MBT released into solution is very similar, yielding values very close to 4.9×10^{-5} M and 4.6×10^{-5} M, respectively. The

increase of MBT release with the concentration of NaCl is most probably related to the interaction of MBT with sodium cations and its ability to form sodium salt (NaMBT) with a solubility much higher than pure MBT [23]. The sensitivity of the silica nanocontainers to the presence of the ions in the electrolyte is also relevant for corrosion related processes since the increase of the ionic strength of the corrosive environment is one of the factors which accelerate the corrosion attack. A very relevant point in this study is the possibility of a prolonged release of MBT. As can be seen in Figure 22c and d, more than 70% of MBT is kept inside the nanocapsules and can be released later in a sustained manner. This observation can be confirmed by the re-dispersion of silica nanocapsules loaded with MBT into a fresh solution and consequent release of MBT as observed in Figure 23.

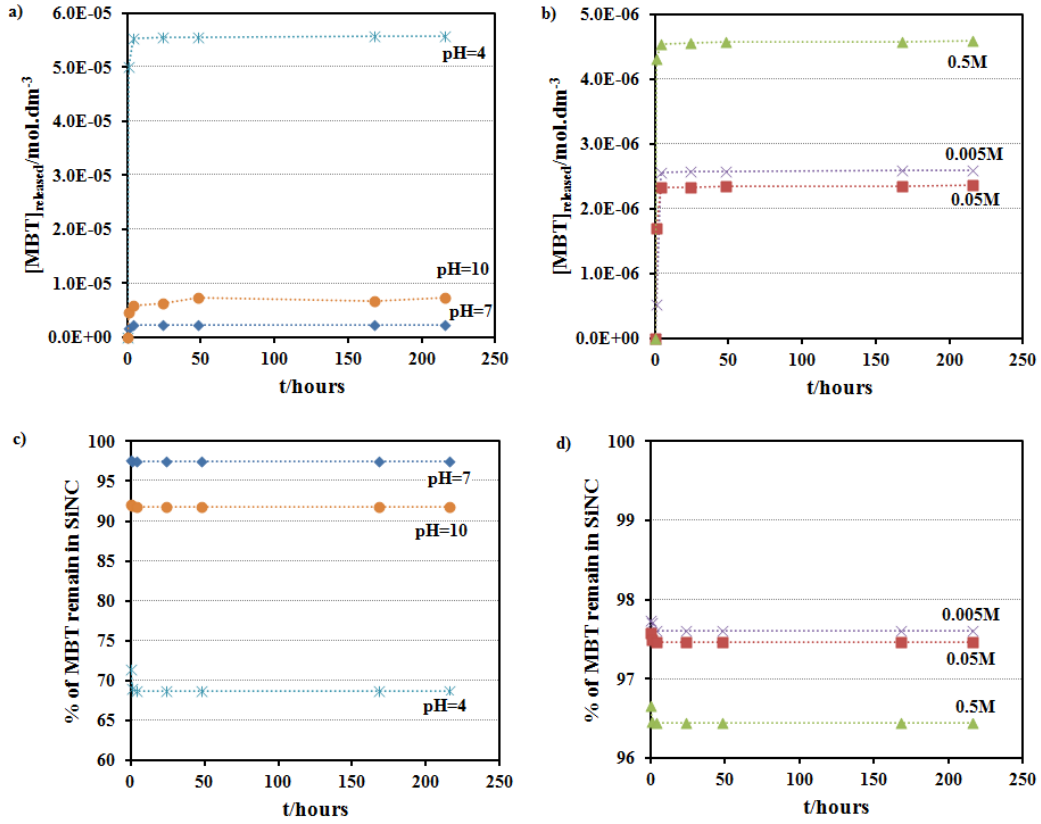

Figure 23: Profiles of released MBT from re-dispersion of SiNC–MBT at (a) different pH's and (b) different concentration of NaCl;% of MBT remaining in SiNC after the second release at (c) different pH's and (d) different concentration of NaCl.

To investigate the region of SiNC where MBT is encapsulated (core vs. shell region), the authors decided to immobilize MBT on calcined SiNC by physical adsorption (sample

i.a.s.), through dispersion of the calcined-SiNC in a concentrated solution of MBT. However, when calcined SiNC were dispersed in the aqueous solutions to perform the release studies, all the MBT was immediately released in less than five minutes (inset in Figure 22a). This result shows that MBT encapsulated by the one step microemulsion polymerization process was mostly allocated in the core of SiNC, which allows a prolonged release of MBT, whereas the post-synthesis immobilization of MBT by physical adsorption resulted in a faster release of the inhibitor.

Anticorrosion efficiency in solution

The main idea of this work is to prove the effectiveness of SiNC as functional elements of active corrosion protective coatings. The first step to understand whether these nanoreservoirs are able to provide any significant inhibition effect is to test them directly in the NaCl solution. The inhibition efficiency of SiNC and SiNC–MBT towards corrosion processes on AA2024 was assessed by EIS. This aluminium alloy is widely used in the aeronautical industry and its corrosion protection is thus very important. The EIS spectra acquired after 1 day and 1 month of immersion in 0.05MNaCl are depicted in Figure 24a-d. In terms of impedance magnitude, the best (highest) results at low frequencies are obtained for the electrolyte with SiNC–MBT, followed by solution with empty SiNC and bare electrolyte. The higher impedance modulus in the low frequency region indicates a lower rate of the corrosion-related electrochemical processes on the alloy surface. Moreover, the phase angle plot only shows one time constant for SiNC–MBT and two time constants for SiNC and bare electrolyte. In the case of SiNC–MBT, the single time constant is assigned to the response of the native aluminium oxide, whilst in the other two cases the time constant at intermediate frequencies is assigned to the aluminium oxide and the time constant occurring at low frequencies is associated to the charge-transfer processes (corrosion activity). After one month of immersion in the presence of SiNC–MBT, the impedance increased and still only one time constant is observed. This means that even after a relatively long period of immersion in the corrosive electrolyte the corrosion activity is minimal, which is consistent with the prolonged release of MBT. Moreover, the low-frequency impedance is even increased after one month in comparison to the initial state. In the case of the other two systems, the impedance magnitude is significantly lower.

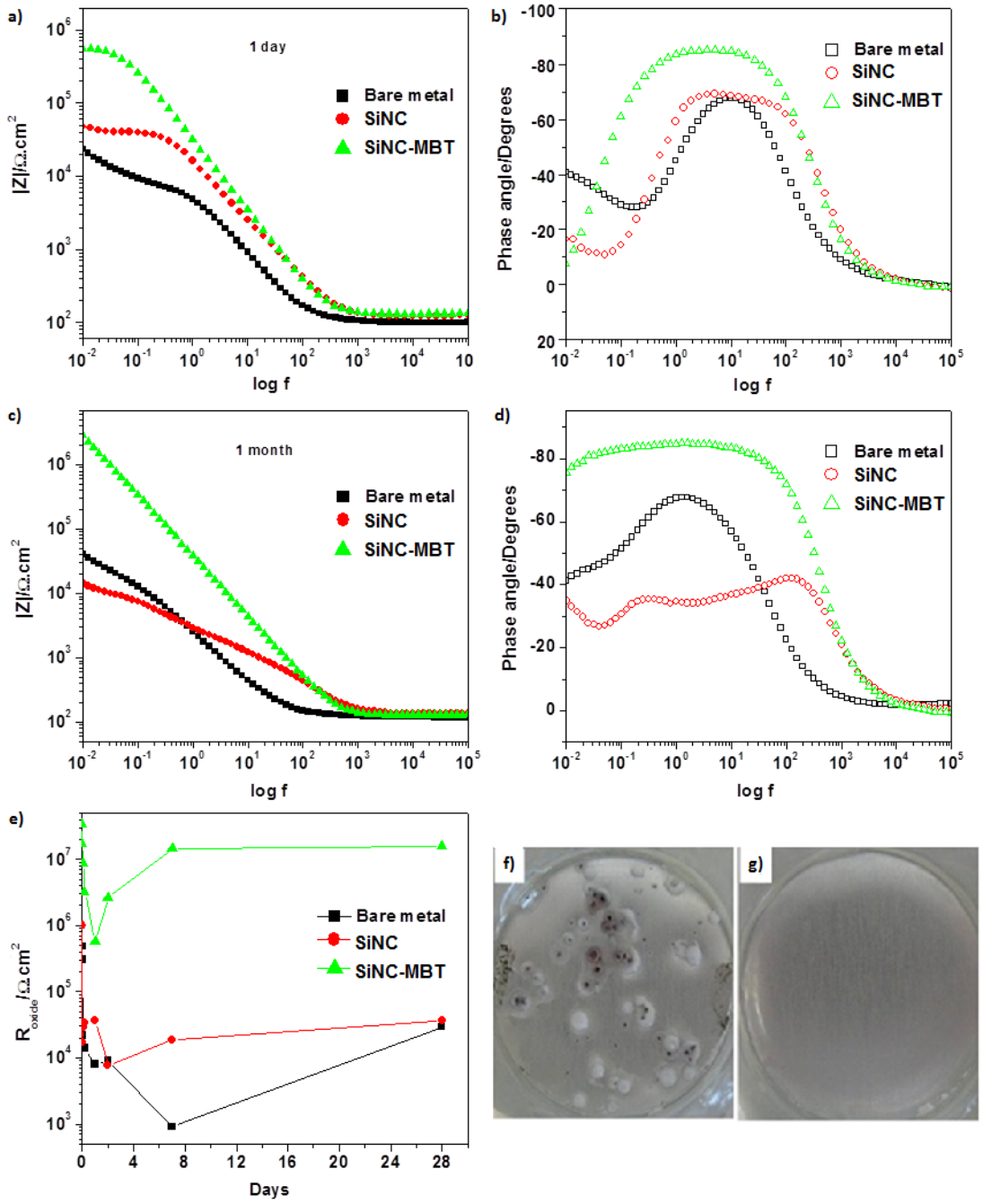

Figure 24: Electrochemical behavior of aluminium alloy 2024 in 0.05 M NaCl solution after (a and b) 1 day and (c and d) 1 month of immersion. (e) Variation of the aluminium oxide resistance (R_{oxide}) as a function of immersion time. Photographs of the AA2024 surface after 1 month of immersion in 0.05 M NaCl in the presence of (f) SiNC and (g) SiNC–MBT.

The undoped electrolyte shows higher values than that of the system with empty SiNC nanocapsules, which may be associated with SiNC being a source of hydroxyl anions that contribute to the lower stability of the aluminium oxide. This is shown by the increase of

pH when the silica capsules are added to solution (pH = 8). The resistance of the aluminium oxide film can be used as a measure of the corrosion resistance since the oxide layer is a last barrier for corrosive species before reaching the metal surface. High oxide film resistance corresponds to low corrosion activity on the alloy surface. The evolution of the oxide resistance obtained from fitting of the EIS spectra is presented in Figure 24e. In the case of SiNC–MBT, after initial decrease during the first 24 hours of immersion the R_{oxide} increases remain constant for long immersion times. The recovery of the oxide stability is attributed to self-healing of defects in the aluminium oxide layer and to the active corrosion protection conferred by the presence of MBT [24]. In contrast, the two other samples show values of R_{oxide} almost 3 orders of magnitude lower than for SiNC–MBT.

The photographs of AA2024 immersed in 0.05 M NaCl for 1 month in the presence of SiNC and SiNC–MBT are shown in Figure 24 (panels f and g, respectively). The differences are remarkable: in the presence of SiNC there is a considerable amount of pits and white deposits ascribed to corrosion products, but the surface of alloy immersed in the SiNC–MBT containing solution is intact without any signs of corrosion.

Anticorrosion efficiency of SiNC–MBT in coated AA2024

The quality of the coating prepared with dispersed particles was investigated by SEM and the cross-section of a coating prepared with SiNC–MBT is depicted in Figure 25. As shown, there are no visible agglomerates of particles, which suggest a good dispersion of the nanomaterials in the coating formulation.

Figure 26 shows the EIS spectra acquired after 1 day and 1 week of immersion in 0.5 M NaCl for coatings loaded with inhibitor only (MBT), empty SiNC and SiNC–MBT. After 1 day of immersion (Figure 26 a and b), the spectra show 3 time constants. The time constant at high frequencies (10^5 Hz) is attributed to the coating response. The identical slope in this frequency region indicates that the three coatings have identical thickness. However, there is a considerable difference in terms of coating resistance (plateau of |Z| between 10^2 and 10^3 Hz): the coating without inhibitor shows better barrier properties than in the presence of MBT. The worst coating in terms of barrier properties is the one with SiNC–MBT. This is probably due to the combination of the detrimental effect of MBT for the coating matrix, together with some degree of disruption of coating barrier properties due to the presence of

the hosting silica structures. The second time constant observed between 10^0 and 10^2 Hz is ascribed to the charge-transfer resistance associated with corrosion processes occurring at the metal/solution interface. This assignment is supported by the presence of black pits in the mm range (Figure 28) and the negative OCP (<-600 mV vs. SCE), which already indicates the destruction of the native aluminium oxide resistance. The low-frequency time constant ($<10^{-2}$ Hz) is ascribed to mass transport-controlled processes.

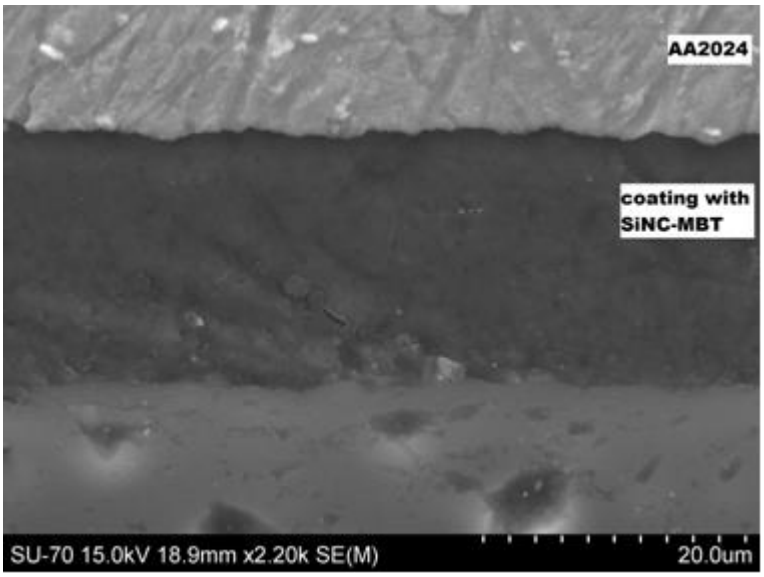

Figure 25: SEM cross-section of a coating modified with SiNC–MBT.

After 1 week of immersion (Figure 26 c and d) the ranking of coating performance changes. In spite of the lowest coating barrier properties, the system with SiNC–MBT shows now the highest values of |Z| in the low frequency range, indicating higher active corrosion protection. Active protection should reflect the hampering of redox reactions as a result of inhibitor action. An important aspect of the coating test is long term protection. To investigate the stability of coating properties in the presence of SiNC–MBT, a coating simulating typical aeronautical system (40 mm thickness) was tested for long immersion times (5 weeks). The EIS spectra show that not only are the barrier properties constant throughout the immersion time, but also the impedance magnitude at low frequencies does not decrease extensively (panels e and f). An important effect can be seen during evolution of the corrosion test. The low frequency impedance modulus increases after two weeks of immersion when compared to one week. This increase of the low frequency impedance can be associated with self-healing ability of the coating [24]. The slight decrease after several

weeks more shows that the reservoirs can be already partially exhausted leading to slight decrease of the active protection. However the values of the impedance modulus are still very high and no defects can be seen on the surface proving efficient long term corrosion protection of the system.

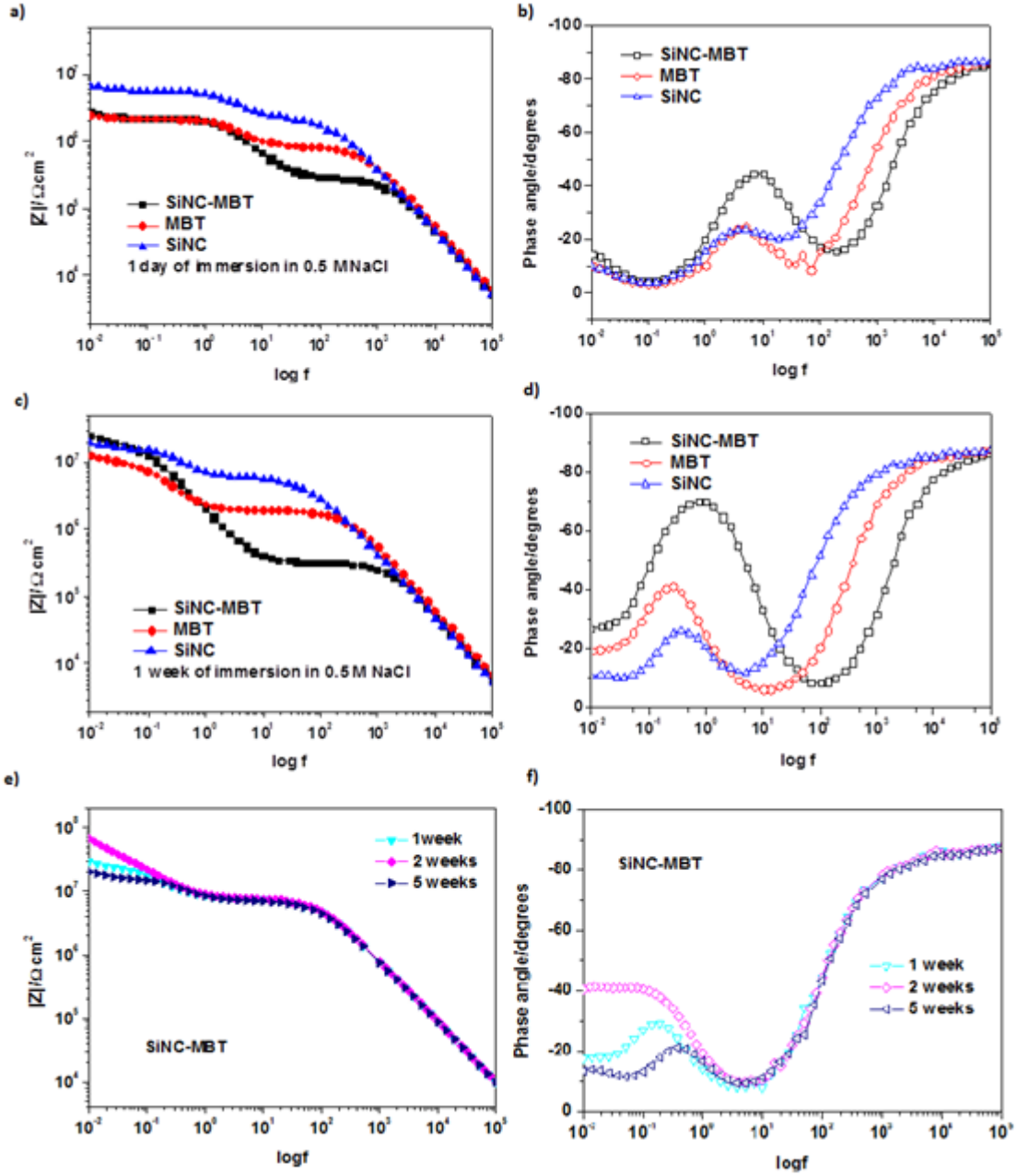

Figure 26: (a–d) EIS spectra of coatings modified with MBT, SiNC and SiNC–MBT. Evolution of EIS spectra (e and f) for a coating (40 mm thick) modified with SiNC–MBT as a function of time.

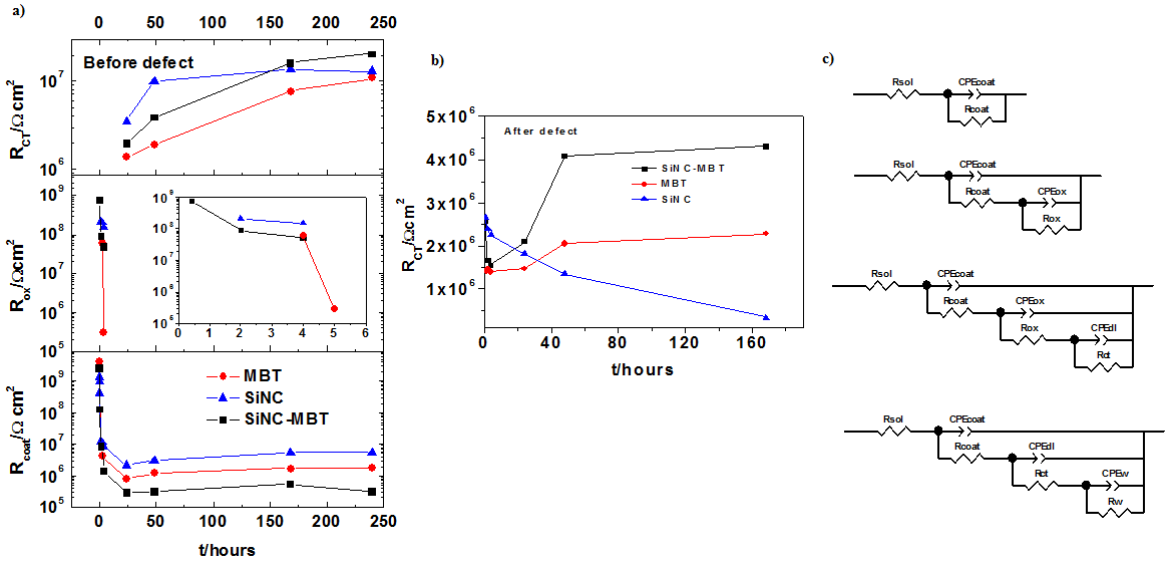

Figure 27: (a and b) Parameters obtained by fitting of EIS spectra using the equivalent circuits presented in (c).

The results of fitting of the impedance spectra are depicted in Figure 27 a and b, using the electrical circuits presented in Figure 27c (see also details in the Experimental section). In the beginning of the immersion tests only one time constant is detected, assigned to the coating response (CPE_{coat} and R_{coat}). As the immersion time progresses additional relaxation processes are observed, which can be associated with the native aluminium oxide (intermediate frequencies, CPE_{ox} and R_{ox}) and the occurrence of corrosion (low frequencies, CPE_{dl} and R_{ct}). For long immersion times, the time constant associated with the oxide layer can no longer be detected due to the extensive degree of corrosion, and the time constant associated with mass transport of species participating in the redox reactions at the metal surface can also be detected (CPE_w and R_w).

The charge-transfer resistance (R_{CT}) is a parameter directly dependent on the active protection provided by corrosion inhibitors (Figure 27a). After 1 day of immersion R_{CT} is the highest for SiNC, due to the high barrier effect provided by the coating and the negative influence of MBT for the coating matrix in the other two systems (MBT and SiNC–MBT). As the time of immersion proceeds, R_{CT} reaches a maximum for the empty SiNC after 1 week of immersion, decreasing afterwards. Conversely, R_{CT} increases continuously for systems with MBT, most notably for SiNC–MBT which is twice as much as for the MBT-loaded coating, demonstrating recovery of the active corrosion protection

in the presence of the inhibitor within SiNC and minimization of MBT interaction with the coating matrix.

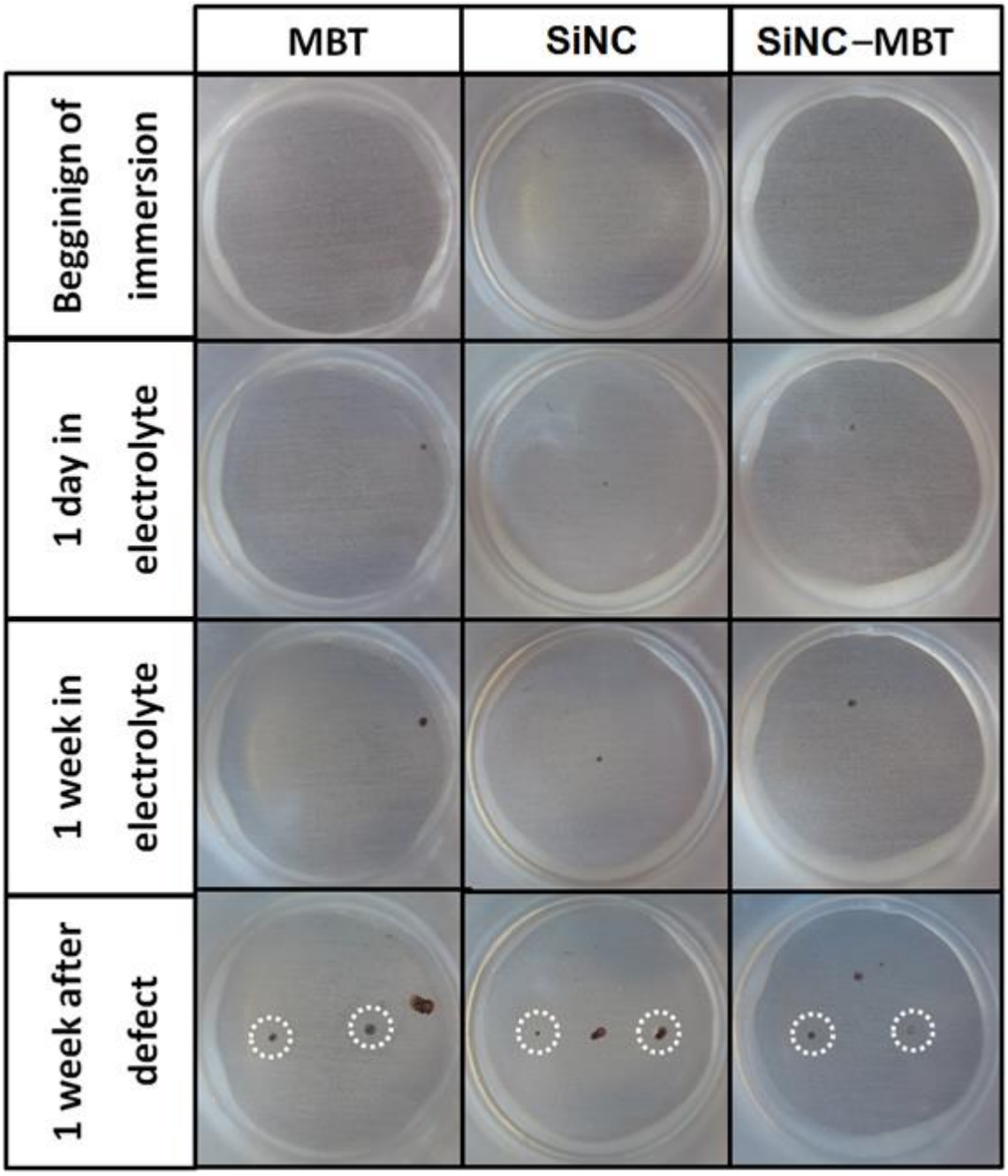

Figure 28: Optical photographs of the coated samples under immersion in 0.5 M NaCl. The dashed circles indicate the areas where artificial defects were made.

To unambiguously prove the self-healing effect in the modified coatings, two defects were inflicted in the samples. The main aim of this procedure was to destroy the coating barrier effect and analyze the evolution of corrosion activity. The variation of R_{CT} is presented in

Figure 27b. As it can be seen, in the MBT-free coating R_{CT} decreases monotonically reaching a value of 0.3 $M\Omega.cm^2$ one week after the defects were made. In the case of MBT loaded coating RCT slightly increases 1.3 times (final value of 2 $M\Omega.cm^2$), but in the case of SiNC–MBT-loaded coating R_{CT} increases after initial decrease, by 2 times with respect to its initial value (final value of $4M\Omega.cm^2$). The order in terms of R_{CT} values can be correlated to the level of corrosion activity inferred from visual inspection of the samples (Figure 28). Overall these results show that, in spite of the loss of a barrier effect due to the insertion of nanomaterials, the active corrosion protection functionality provided to the metal in the long-term, which is the ultimate objective of using a protective coating, is better achieved using SiNC–MBT.

Conclusions

The present paper reports the successful synthesis of silica nanocapsules with a corrosion inhibitor encapsulated. The synthesized nanocapsules are thermally stable, with a regular shape and diameter between 100 and 150 nm and show gradual meso-porosity. The loading content of MBT was found to be 10 wt% and the encapsulation efficiency was 68%.

The release studies showed that SiNC release higher amounts of MBT in acidic pH and at high concentrations of NaCl. The release of MBT is slow and could be used in systems where a prolonged release is required. The active anticorrosion performance of SiNC loaded with MBT is evident from the electrochemical studies and visual inspection. In spite of the decrease in barrier effect, the inclusion of SiNC–MBT in coatings provides active corrosion protection functionality to underlying aluminium alloy, better than when the inhibitor is directly dispersed in the matrix. The self-healing effect was observed for long immersion times in the aggressive electrolyte and when defects were artificially created, thereby demonstrating the prospective applications of SiNC in protective coatings. Besides the self-healing effect demonstrated by the SiNC–MBT, the known biocide effect of MBT makes SiNC–MBT promising systems for application in the maritime industry and offshore structures.

Acknowledgements

This work was funded through European project MUST ref. NMP3-LA-2008-214261 and FCT project PTDC/CTM/65632/2006. FM and JT thank FCT for PhD grant SFRH/BD/72663/ 2010 and post-doc grant SFRH/BPD/64335/2009, respectively.

References

1 S. H. Cho, S. R. White and P. V. Braun, Adv. Mater., 2009, 21, 645–649.

2 D. G. Shchukin,M. Zheludkevich and H. Mohwald, J. Mater. Chem., 2006, 16, 4561–4566.

3 D. G. Shchukin, M. Zheludkevich, K. Yasakau, S. Lamaka, M. G. S. Ferreira and H. Mohwald, Adv. Mater., 2006, 18, 1672–1678.

4 M. L. Zheludkevich, S. K. Poznyak, L. M. Rodrigues, D. Raps, T. Hack, L. F. Dick, T. Nunes and M. G. S. Ferreira, Corros. Sci., 2010, 52, 602–611.

5 E. V. Skorb, D. Fix, D. V. Andreeva, H. Mohwald and D. G. Shchukin, Adv. Funct. Mater., 2009, 19, 2373–2379.

6 D. Raps, T. Hack, J. Wehr, M. L. Zheludkevich, A. C. Bastos, M. G. S. Ferreira and O. Nuyken, Corros. Sci., 2009, 51, 1012–1021.

7 D. G. Shchukin, M. Zheludkevich, K. Yasakau, S. Lamaka, M. G. S. Ferreira and H. Mohwald, Adv. Mater., 2006, 18, 1672–1678.

8 A. N. Khramov, N. N. Voevodin, V. N. Balbyshev and M. S. Donley, Thin Solid Films, 2004, 447, 549–557.

9 A. N. Khramov, N. N. Voevodin, V. N. Balbyshev and R. A. Mantz, Thin Solid Films, 2005, 483, 191–196.

10 D. G. Shchukin, S. V. Lamaka, K. A. Yasakau, M. L. Zheludkevich, M. G. S. Ferreira and H. Mohwald, J. Phys. Chem. C, 2008, 112, 958–964.

11 S. K. Poznyak, J. Tedim, L. M. Rodrigues, A. N. Salak, M. L. Zheludkevich, L. F. P. Dick and M. G. S. Ferreira, ACS Appl. Mater. Interfaces, 2009, 1, 2353–2362.

12 J. Tedim, S. K. Poznyak, A. Kuznetsova, D. Raps, T. Hack, M. L. Zheludkevich and M. G. S. Ferreira, ACS Appl. Mater. Interfaces, 2010, 2, 1528–1535.

13 D. Raps, T. Hack, M. Kolb, M. L. Zheludkevich and O. Nuyken, in Smart Coatings III, Vol. 1050, ed. J. Baghdachi and T. Provder, ACS Symposium Series, Washington DC, USA, 2010, ch. 12, pp. 165–189.

14 H. Chen, J. He, H. Tang and C. Yan, Chem. Mater., 2008, 20, 5894–5900.

15 R. Subramanian and V. Lakshminarayanan, Corros. Sci., 2002, 44, 535–554.

16 M. L. Zheludkevich, K. A. Yasakau, S. K. Poznyak and M. G. S. Ferreira, Corros. Sci., 2005, 47, 3368–3383.

17 K. S. W. Sing, D. H. Everett, R. A. W. Haul, L. Moscou, R. A. Piertti, J. Rouquerol and T. Siemieniewska, Pure Appl. Chem., 1985, 57, 603–619.

18 S. J. Gregg and K. S. W. Sing, Adsorption, Surface Area and Porosity, Academic Press, London, 1982, pp. 209–228.

19 L. A. Feigin and D. I. Svergun, Structure Analysis by Small-Angle XRay and Neutron Scattering, Plenum Press, New York, 1987.

20 D. Pérez-Quintanilla, I. del Hierro, M. Fajardo and I. Sierra, J. Environ. Monit., 2006, 8, 214–222.

21 Z. Zajíčková and C. Párkányi, J. Heterocycl. Chem., 2008, 45, 303–306.

22 M. A. Malouki, C. Richard and A. Zertal, J. Photochem. Photobiol., A, 2004, 167, 121–126.

23 U.S. Environmental Protection Agency, Hazard Characterization Document, June 2010.

24 M. L. Zheludkevich, K. A. Yasakau, A. C. Bastos, O. V. Karavai and M. G. S. Ferreira, Electrochem. Commun., 2007, 9, 2622–2628.

CHAPTER 4

"Corrosion protection of AA2024 by sol-gel coatings modified with MBT-loaded polyurea microcapsules"

Chemical Engineering Journal 283 (2016) 1108–1117

Contents lists available at ScienceDirect

Chemical Engineering Journal

journal homepage: www.elsevier.com/locate/cej

Corrosion protection of AA2024 by sol–gel coatings modified with MBT-loaded polyurea microcapsules

F. Maia [a], K.A. Yasakau [a], J. Carneiro [a], S. Kallip [a], J. Tedim [a,*], T. Henriques [b], A. Cabral [b], J. Venâncio [c], M.L. Zheludkevich [a,d], M.G.S. Ferreira [a]

[a] CICECO – Aveiro Institute of Materials, Department of Materials and Ceramic Engineering, University of Aveiro, 3810-193 Aveiro, Portugal
[b] Instituto de Soldadura e Qualidade, 2740-120 Porto Salvo, Portugal
[c] Aerohélice Lda, Azedia, 2580-552 Alenquer, Portugal
[d] Institute of Materials Research, Helmholtz-Zentrum Geesthacht, Max-Planck-Str. 1, 21502 Geesthacht, Germany

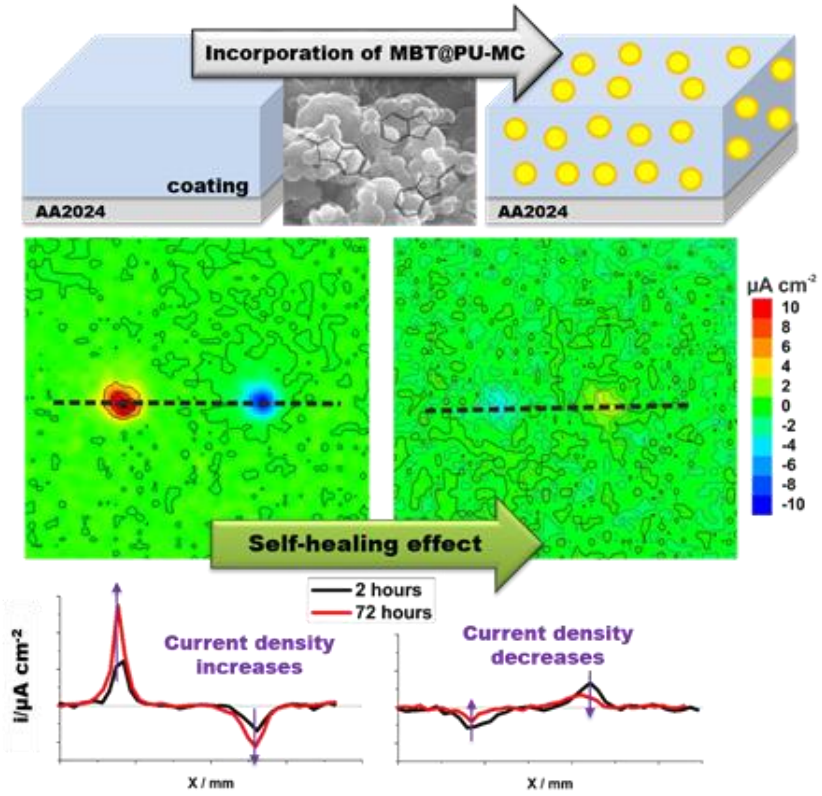

Highlights:

- Successful encapsulation of 2-mercaptobenzothiazole in polyurea microcapsules.
- Encapsulation reduces the detrimental interaction between corrosion inhibitor and sol-gel matrix.
- Loaded microcapsules suppresses corrosion activity and improves the adhesion of sol-gel coatings to the metal substrate.
- Self-healing corrosion protective coatings for AA2024 based on modified sol-gel coating with MBT@PU-MC.

Abstract

In this work we report the synthesis of polyurea microcapsules loaded with corrosion inhibitor 2-mercaptobenzothiazole (MBT) for corrosion protection of 2024 aluminum alloy. The microcapsules were prepared by interfacial polycondensation. The resulting capsules exhibit spherical shape, with diameter ranging between 100 nm and 2 μm. The loading content of MBT was found to be 5 wt% and release studies showed that MBT is preferentially released under acidic and alkaline conditions and follows a Fickian diffusion model. This pH dependency seems suitable for protection of metallic alloys where corrosion processes are accompanied by local pH changes. Furthermore, the microcapsules were added to a hybrid sol-gel coating and its performance assessed by electrochemical and accelerated standard tests. The results obtained indicate that capsules loaded with MBT do not affect negatively the barrier properties of sol-gel coatings, and contribute for the enhancement of adhesion of coatings to the metallic substrate. More relevant, these additives impart active corrosion protection suppressing corrosion activity at defect sites, which opens prospects for application of polyurea microcapsules as additives for high-performance coatings.

Keywords: polyurea microcapsules, corrosion inhibitor, controlled release, corrosion protection, sol-gel coating.

1. Introduction

In the last decade, one of the biggest challenge in the field of corrosion has been the replacement of chromium based pre-treatments and primers by ‘green’ solutions [1].

Several approaches have been reported for aluminum alloys, especially for AA2024, because of its relevance for aeronautical industry [2].

Hybrid sol-gel coatings have been reported as promising systems for protection of aluminum alloys. They are able to establish chemical bonds with the metal surface, which renders good adhesion at the coating/metal interface [3]. Moreover, the fine tuning of properties is possible due to implicit versatility of silane chemistry and wide range of monomers available with different functionalities [4]. Nevertheless, the resulting sol-gel films can exhibit micropores and fissures, allowing the diffusion of aggressive species towards the metal surface [3], which ultimately leads to corrosion attack. Another challenging aspect associated with sol-gel coatings is the lack of active corrosion protection. To overcome this limitation different types of corrosion inhibitors have been incorporated into sol-gel coatings with the aim to confer active protection [5-9].

Generally, the direct addition of corrosion inhibitors to coating formulations is not straightforward due to compatibility issues. Some corrosion inhibitors may cause a decrease in adhesion and coating barrier properties as a result of unwanted, detrimental interactions between these active species and polymeric matrix [5, 8, 9]. To prevent the contact between inhibitors and coating matrix, micro and nanostructured containers have been proposed in the literature. The main role of these containers is the storage of corrosion inhibitors, reducing spontaneous leaching and providing a controlled release of inhibitor.

Several approaches for immobilization of corrosion inhibitors in reservoirs have been reported. These include anion-exchange hydrotalcite loaded with decavanadate [10], organic corrosion inhibitors encapsulated in β-cyclodextrins [11], or SiO_2 nanoparticles and halloysite nanotubes loaded with azole derivatives, covered by polyelectrolyte multilayers [8, 12]. More recently, other carriers for corrosion inhibitors in multifunctional coatings were suggested: TiO_2 nanocontainers loaded with 8-hydroxyquinoline [13], montmorillonite modified with quaternary ammonium salt [14], NaY zeolites loaded with two different inhibitors (cerium and diethyldithiocarbamate) [15] and pH-sensitive polymeric particles loaded with 8-hydroxyquinoline [16]. There are several reviews available describing the latest advances on nano and microcapsules for application in corrosion protective coatings [17, 18], showing the diversity of reservoirs and the respective triggers and mechanisms of action.

Thiazole and triazole derivatives are known to be efficient corrosion inhibitors for AA2024 due to their chemisorption ability in the copper-rich intermetallic particles [8, 11, 12, 19] and have already been encapsulated into different inorganic [20, 21] and polymeric reservoirs [22].

In this work MBT was encapsulated in polyurea microcapsules. The microcapsules obtained were added to hybrid sol-gel pre-treatments for corrosion protection of AA2024. The resulting microcapsules were chemically and morphologically characterized by scanning electron microscopy (SEM), thermogravimetry (TG/DTA) and Fourier transform infrared spectroscopy (FTIR) The protective properties associated with microcapsule-containing sol-gel coatings were assessed at lab scale by electrochemical impedance spectroscopy (EIS) and the scanning vibrating electrode technique (SVET), as well as by industrial standard testing (ASTM B 117-11, NP EN ISO 2409:2012 and ISO 16276-2:2007).

2. Experimental Section

2.1. Materials

Cyclohexane and *n*-butanol were acquired to Alfa Aesar and to VWR Chemicals, respectively. Span 85, diethylenetriamine (DETA) (99%), 2,4-toluene diisocyanate (TDI) (98%), 2-mercaptobenzothiazole (MBT) (97%), Poly(vinylpyrrolidone) (average mol wt 40,000) (PVP) and acetone were purchased from Sigma-Aldrich. Sodium chloride (NaCl) and buffer solutions were obtained from Riedel-de-Häen. Ethanol was supplied by Panreac. Titanium-isopropoxide (TPOT) (97%), 3-glycidoxypropyl trimethoxysilane (GPTMS) (97%) and acetylacetone were also purchased from Sigma-Aldrich. All chemicals were analytic grade and were used without further purification.

2.2. Synthesis of Polyurea microcapsules and encapsulation of 2-mercaptobenzothiazole

The synthesis of polyurea microcapsules (PU-MC) and the encapsulation of MBT in PU-MC were performed in a single step. Two different phases were prepared, a continuous phase where the non-ionic surfactant was dissolved in water and a dispersed phase where MBT (compound to be encapsulated) was dissolved. A similar process was previously reported for the encapsulation of phenolphthalein [23], but in this case TDI was used as

monomer and PVP as emulsion stabilizer. Briefly, a solution of 1 g Span 85 in 100 mL of water was prepared (continuous phase). A solution containing 0.25 g of PVP in 25 mL of water was prepared and added to the continuous phase. Then, 3 g of TDI was diluted in 20 mL of cyclohexane and, in parallel 150 mg of MBT dissolved in 10 mL of acetone. Both organic solutions were mixed (dispersed phase) and added to the continuous phase, resulting in an oil-in-water microemulsion. *n*-Butanol (1 mL) was added to the o/w microemulsion. After 15 minutes, 2 g of DETA were diluted in 20 mL of water and added dropwise to the microemulsion. Then, the mixture was heated until 60 ºC and stirred during 3 h. The obtained precipitate was filtered, washed with pure water and dried at room temperature.

2.3. Characterization of polyurea microcapsules loaded with MBT

The morphology of polyurea microcapsules loaded with MBT (MBT@PU-MC) was characterized by SEM using a Hitachi S-4100 system with electron beam energy of 25 keV. Particle size distribution was determined using an image processing and analysis in Java, free software, named "ImageJ" [24]. In order to characterize the chemical and thermal properties of PU-MC, FTIR-ATR spectra were recorded with a Bruker IFS55 spectrometer equipped with a single horizontal Golden Gate ATR cell. TG/DTA was carried out in a TGA-50 Shimadzu system under air atmosphere, with a heating rate of 10 C.min^{-1} from room temperature up to 800 ºC.

2.4. Release studies of MBT from polyurea microcapsules

The release profiles of MBT were monitored using a UV-1600 PC Spectrophotometer from VWR. The correlation coefficient of the calibration curves obtained with 5 MBT standards was higher than 0.999.

Briefly, 100 mg of MBT@PU-MC was dispersed in 20 mL of an aqueous solution where pH was varied (4, 7 and 10) and the MBT release profiles were determined by UV-Vis spectrophotometry at specific times. 1 mL sample of the mixture was extracted with a syringe and filtered with a specific syringe filter (PTFE membrane with 0.20 μm pore size). To determine the total amount of MBT encapsulated, 100 mg of MBT@PU-MC were dispersed in 20 mL of ethanol during 24 hours to guarantee the maximum release of MBT. Ethanol was selected because MBT is very soluble in this solvent and facilitates

MBT diffusion through the polymeric shell. The encapsulation efficiency was determined by the expression:

$$\%E = \frac{n_{MBText}}{n_{MBTi}} \times 100 \text{ (Eq. 1),}$$

where n_{MBText} is the amount of MBT extracted from PU-MC and n_{MBTi} is the initial amount of MBT used in the encapsulation. TG was also used to assess the MBT loading in PU-MC.

2.5. Substrate preparation

Aluminum alloy 2024-T3 substrates were cleaned and etched according to a standard commercial procedure: alkaline cleaning in Metaclean T2001 at 68 ºC for 15 min, alkaline etching in Turco Liquid Aluminetch N2 at 60 ºC for 45 s, acid etching in Turco Liquid Smutgo NC at 30 ºC for 7 min, each step followed by washing in distilled water.

2.6. Sol-gel preparation, application and characterization

Epoxy-functionalized SiO_2/TiO_2 based hybrid sol-gel was prepared using a similar approach to the one previously reported, except for the use of titanium alkoxide instead of zirconium alkoxide [9]. Briefly, hybrid sols (metalorganic and organosiloxane) were prepared separately and then combined to form a hybrid solution. Titanium(IV)-isopropoxide (TPOT) was mixed with acetylacetone and stirred in a water bath at constant temperature of 22 ºC during 20 minutes to stabilize the metalorganic precursor by acetylacetone complexant, followed by addition of 0.316 M HNO_3 solution (pH~0.5) drop wise to start the hydrolysis process of the metalorganic compound. The solution was stirred for 60 minutes. In parallel, 3-glycidoxypropyltrimethoxysilane (GPTMS) was dissolved in 2-propanol in 1:1 volume proportion, followed by addition of the acidic solution with pH~0.5 to promote the hydrolysis of silane and the final solution was stirred at room temperature during 60 minutes. After this time, both solutions were mixed and the resulting hybrid solution was stirred for 1h at room temperature. After sol-gel synthesis, MBT (or MBT@PU-MC) were dispersed in sol-gel and stirred until obtaining a uniform dispersion.

The resulting hybrid sol-gel was applied by dip-coating onto the alloy plates for electrochemical (EIS, SVET) measurements while samples for industrial tests were applied by spray coating. The coated plates were held in open air during 1 h to let sol–gel

hydrolyze and then cured at 120 ºC during 80 min in the oven. The dried thickness was measured using an "Elcometer" 456 Series Digital Coating Thickness Gauge.

Nanoindentation tests on the sol-gel coatings were performed using a CSM Micro-Hardness Tester facility and a Berkovich diamond tip was used as indenter. Hardness (*H*) and Young`s modulus (*E*) were determined from the unloading part of the force–depth curves. Hardness was calculated as the maximum applied load over the area of contact. The hardness measurements on the sol-gel coatings were performed with a load of 1 mN corresponding to a contact depth around 300 nm.

2.7. Assessment of corrosion protection performance of coated AA2024-T3

EIS measurements were carried out on coated aluminum alloy 2024-T3 at room temperature in a three-electrode cell consisting of a saturated calomel reference electrode (SCE), a platinum foil counter electrode and coated AA2024-T3 plate as the working electrode in the horizontal position (an exposed area of ca. 3.3 cm^2). The cell was placed in a Faraday cage to avoid the interference of external electromagnetic fields. The electrolyte was 0.5 M NaCl aqueous solution for coated plates (V = 10 mL), stagnant and in equilibrium with air. The measurements were performed using a Gamry FAS2 Femtostat with a PCI4 Controller. The selected frequency range was typically from 1×10^5 to 1×10^{-2} Hz, with a 10 mV RMS sinusoidal perturbation vs. open circuit potential. The impedance plots were fitted using different RC equivalent circuits, where pure capacitances were replaced by constant-phase elements (CPE). The software used for the fittings was Gamry Echem Analyst v5.61, and the χ^2 of the resulting spectra fittings varied between 10^{-2} and 10^{-4}.

For SVET measurements the Applicable Electronics Inc. (USA) measurement system was controlled by the ASET 2.0 software from ScienceWares Inc. (USA). The Pt-Ir vibrating microelectrode had a 10-20 µm spherical platinum black tip. The scanning distance from surface was 100 µm. SVET measures potential differences in solution caused by ionic fluxes arising from the sites of cathodic and anodic corrosion reactions at the surface [25]. Two artificial coating penetrating defects with diameter approximately 100 µm and depth around 50 µm were made by mechanical application of a stainless steel needle to all samples before immersion in 0.05 M NaCl.

Neutral salt spray (NSS) tests were performed according to Standard ASTM B 117-11 [26], where coated samples were assessed in terms of corrosion resistance in the presence of a strong electrolyte (NaCl). Adhesion corrosion tests were performed according to NP EN ISO 2409:2012 [27], where adhesion is tested in specific lattice pattern cuts made in the coatings followed by application of a pressure-sensitive tape over the lattice then removed, and according to ISO 16276-2:2007 [28], where an x-cut is made through the film to the substrate and immersed in deionized water for a defined time. All tests were performed in triplicate.

Samples used in NSS and adhesion tests were coated with a full coating system composed by the prepared sol-gel (modified with MBT@PU-MC or unmodified), followed by a waterborne primer and an epoxy based top-coat. All layers were applied by spray and the final thickness of those samples was 50 ± 1.5 μm.

3. Results and discussion

3.1. MBT encapsulation and characterization of polyurea microcapsules loaded with MBT

Polyurea microcapsules were synthesized by interfacial polycondensation through an oil-in-water microemulsion, where the dispersed phase containing MBT was encapsulated. The polymeric shell results from the reaction of isocyanate group from TDI with amine group from DETA in the interface between the continuous phase (hydrophilic) and the dispersed phase (hydrophobic), forming a urea linkage, as represented in Scheme 1.

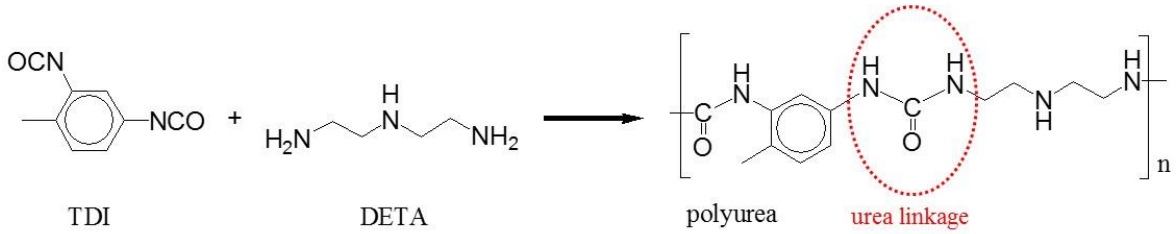

Scheme 1: Reaction of the amine groups of DETA with isocyanate group of TDI forming the urea linkage.

PU-MC prepared using this procedure have spherical and uniform morphology with a broad distribution of sizes. The encapsulation of MBT does not promote any significant modification on the microcapsules morphology when compared to empty ones, as observed in Figure 29. The largest microcapsules show some signs of shrinkage, probably due to the

high vacuum used during the SEM analysis. Both samples present signs of agglomeration. This is attributed to the drying process during sample preparation which precedes SEM analysis. To minimize this, only a small fraction of capsules was dried for characterization. The remaining material was kept in slurry form to avoid agglomeration. The mean size of obtained capsules is 277 and 219 nm for PU-MC and MBT@PU-MC, respectively. However, the standard deviation was large due to the broad size distribution and presence of microcapsules in the range of 1 - 2 μm.

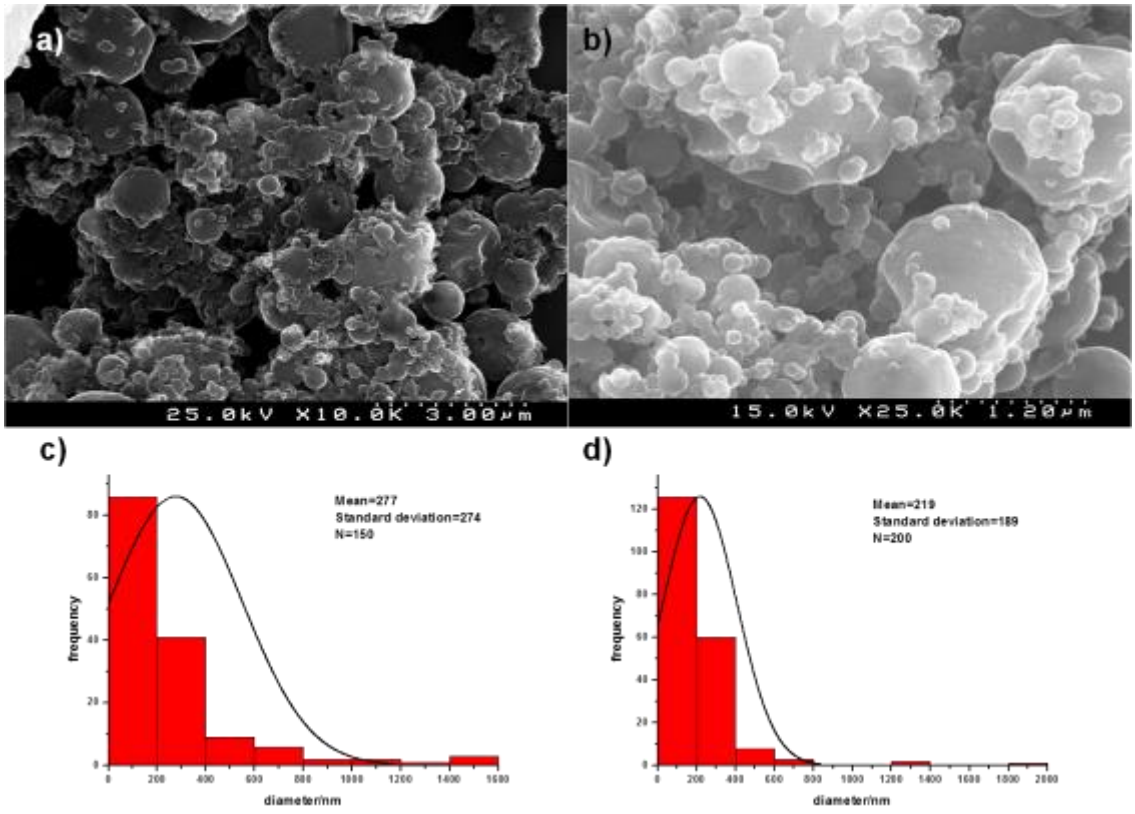

Figure 29: SEM images of (a) empty PU-MC, (b) MBT@PU-MC; Size distribution histograms of (c) empty PU-MC and (d) MBT@PU-MC.

The obtained MBT@PU-MC present a yellow pale coloration as result of MBT encapsulation, confirming its successful immobilization. FTIR measurements allow the identification of characteristic bands associated to the urea linkage at 1641 cm^{-1} and 1745 cm^{-1}, corresponding to the stretching of carbonyl group and at 1551 and 3314 cm^{-1} related to the stretching of N-H vibration from the urea linkage, directly connected to the carbonyl group [29], confirming the successful reaction represented in Scheme 1. Bands

associated with MBT cannot be detected. This may be due to overlapping with intense bands corresponding to urea linkage.

In order to verify the thermal stability of MBT@PU-MC and to quantify the amount of MBT encapsulated in PU-MC, thermogravimetric assays were performed and the obtained data are represented in Figure 30. Considering that both MBT and the polymeric shell (PU) are composed of organic material, they are affected by temperature in a similar way, as verified in Figure 30. However, for MBT@PU-MC profile there is a smaller weight loss when temperature reaches 400 ºC, showing a smaller weight loss rate due to the presence of MBT. MBT is a well-known organic vulcanization accelerator [30] and increases the thermal resistance of rubber. In this case, this feature can be used to estimate the loading content of MBT in MBT@PU-MC. According to the difference in TG profiles between 500 and 600 ºC, the value roughly estimated for MBT loading content is ~5 wt%. At temperatures higher than 600 ºC all the remaining organic material is completely decomposed.

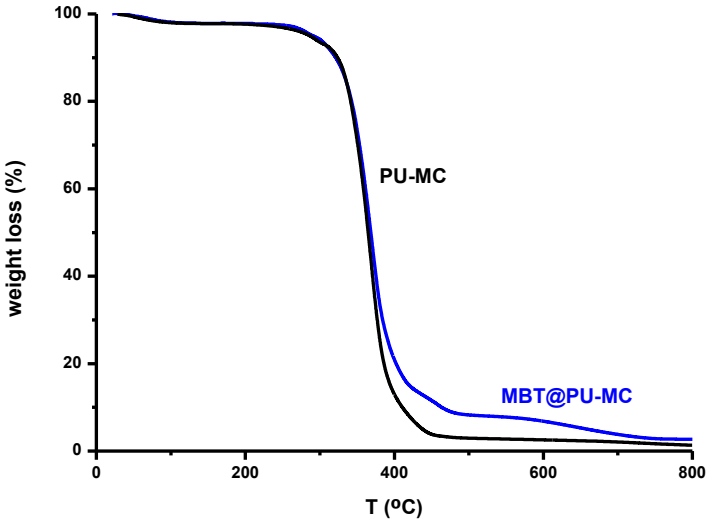

Figure 30: TG profiles of empty PU-MC and MBT@PU-MC.

3.2. Release studies of MBT from polyurea microcapsules

The methodology used for MBT encapsulation results in an encapsulation efficiency of 32 %, determined by extraction of MBT in ethanol (Equation 1). Ethanol was selected due to the high solubility of MBT in this solvent, and the loading content of MBT obtained in this way corresponds to 1 wt%, five times lower than the estimate from TG measurements

(~5 wt%). Although there may be some level of uncertainty associated with the estimate of loading content by TG, one can expect that the extraction of MBT with ethanol is limited and not all MBT inside the microcapsules is quantified in this manner.

MBT@PU-MC were dispersed in aqueous solutions with different pH conditions (3, 7 and 10). These conditions were selected because pH is a corrosion relevant trigger for AA2024 since localized corrosion is accompanied with pH changes in cathodic and anodic areas. Locally, pH can reach values around 3 at anodic zones and go up to 10 in cathodic areas [31].

The release profiles of MBT are depicted in Figure 31. The low solubility of MBT in aqueous solutions plays an important role in the extent of MBT released. Under neutral conditions the release of MBT is low, reaching only 3% of total loading content (determined by extraction with ethanol) after 48h of immersion, while for acidic conditions this value rises up to 5% and for alkaline conditions reaches 14%. The largest release of MBT under alkaline conditions is consistent with its solubility dependence upon pH and is in agreement with release studies of MBT reported in the literature [32]. A similar pH dependence was observed for the release of phenolphthalein from PU-MC, due to the barrier effect of the capsule and the low permeability of the organic compound in the polymeric shell under these conditions [23]. More importantly, this trend (higher release in acidic and alkaline conditions) matches well the localized nature of corrosion processes in AA2024, allowing for a more effective release of inhibitor when either anodic or cathodic processes occur. On the other hand, the relative low values of MBT released can be advantageous for long-term applications.

Experimental data from MBT release profiles were fitted using established kinetic-mechanistic models. The kinetic models selected were Higuchi's square root of time (diffusion) [33] and Power Law [34] equations, presented in Table 7. W represents the percentage of MBT released at time t and k_1 is the release rate constant of diffusion model. In the Power law equation, M_t/M_∞ represents the fractional drug (MBT) released into the dissolution medium and k_2 is a constant incorporating structural and geometric characteristic of the material. The parameter n is a diffusion exponent that characterizes the release transport mechanism of the active. When n=0.5, the drug diffuses through and is released from the polymeric matrix with a quasi-Fickian diffusion mechanism. For $n > 0.5$,

anomalous, non-Fickian drug diffusion occurs, and when n = 1, a non- Fickian, Case II or zero-order release kinetics occurs [34].

The parameter which significantly affects the release of MBT from PU-MC seems to be diffusion through the polymeric walls of the microcapsules. This influence is observed by the adjustment of experimental data to the Higuchi's model, as presented in Figure 3C and Table 7. On the other hand, Power Law model, a simple model which is typically used to characterize more complex systems also fits the experimental data with reasonable R2 values. The diffusional exponent n obtained is smaller than the theoretical value for spherical particles (n=0.43), probably associated with the broad distribution size diameter of MBT@PU-MC [34].

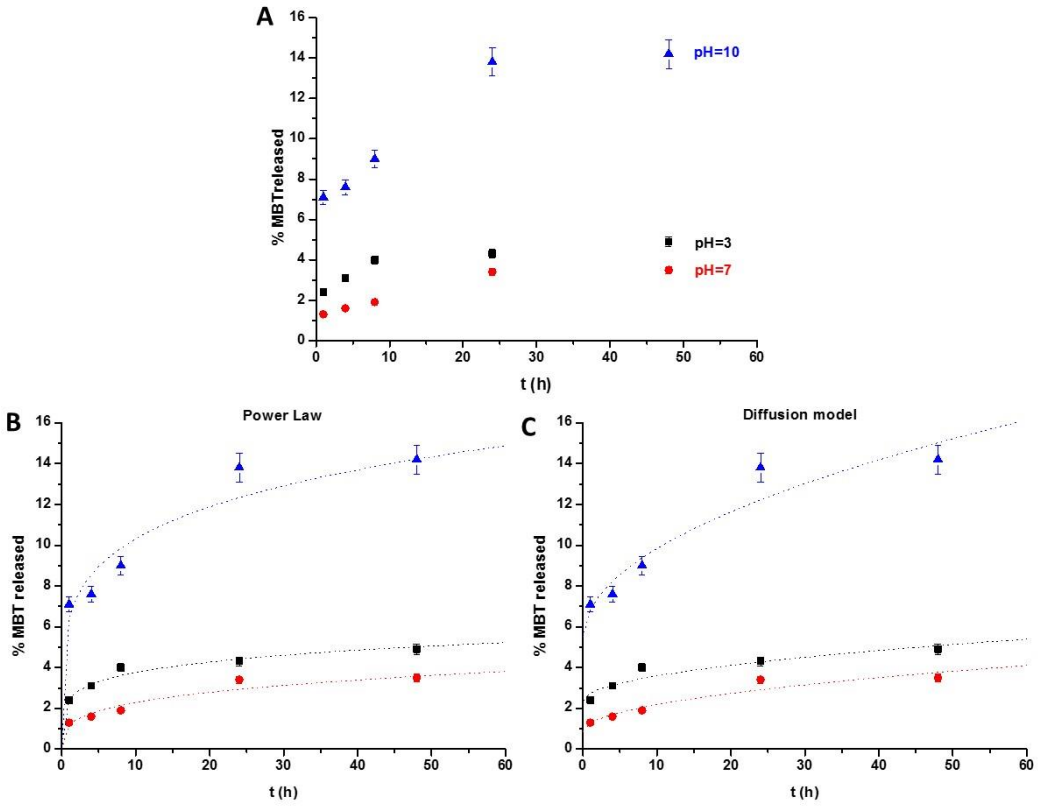

Figure 31: (A) Release profiles of MBT from MBT@PU-MC in different pH conditions. Fittings of experimental data using different kinetic models: (B) Power Law and (C) Higuchi's square root of time (diffusion model).

Table 7: Fitting kinetic models to MBT release experimental data at different pH's.

Kinetic models	Equation	Kinetic constants	Experimental conditions (pH): 3	7	10
Higuchi's square root of time	$W = k_1 t^{1/2}$	k	0.3926	0.4178	1.3764
		R^2	0.8883	0.9213	0.9196
Power law	$\frac{M_t}{M_\infty} = k_2 t^n$	k	0.0246	0.0119	0.0644
		R^2	0.9595	0.9321	0.8972
		n	0.1837	0.2850	0.2045

3.3. Coating properties and corrosion protection performance of coated AA2024-T3

MBT@PU-MC were dispersed in the prepared sol-gel and applied on etched AA2024 plates using dip-coating and spray methods, followed by thermal curing at 120 ºC. As observed before, in TG analysis (Figure 30), MBT@PU-MC shows good thermal stability and can be used at this temperature without significant changes.

The resulting coatings show good uniformity and thickness around 2-2.5 μm for coatings applied by dip-coating, while the ones applied by spray for industrial testing had thickness around 5 μm.

Mechanical properties of sol-gel coating were determined by nanoindentation tests. The average values obtained for sol-gel coating was 1.2±0.2 GPa and 6.4±0.7 GPa for hardness (*H*) and Young`s modulus (*E*), respectively. The values were calculated on the basis of five measurements. The obtained hardness value was found to be higher than the values reported in the literature, which was 0.15 GPa for GPTMS sol-gel coating [35]. The higher hardness obtained in this work is associated with the presence of titania nanoparticles (formed during the sol-gel synthesis procedure) and better reticulation of GPTMS matrix leading to more rigid matrix. Indeed, as the inorganic content in sol-gel matrix grows both hardness and Young`s modulus increase [36]. The latter was reported to be around 3-8 GPa for 25-50 % of organic content in a sol-gel coating, which is consistent with our measurements.

The corrosion protection of thinner samples was assessed by EIS and SVET, while thicker samples were tested industrially under standard conditions (ASTM D1654, ISO 2409:2007 (cross-cut test) and ISO 16276-2:2007 (x-cut test)).

Figure 32 shows Bode plots of coated AA2024 samples immersed in a 0.5M NaCl solution after 5 days (A) and after 14 days (B). The impedance data in the high frequency range, associated with the coating response, demonstrates that when MBT is directly added to sol-

gel, a significant decrease in impedance modulus (|Z|) occurs for both times of immersion, highlighting the negative effects of the MBT directly added to sol-gel. Contrastingly, when MBT is introduced in encapsulated form that negative effect on the sol-gel coating is negligible, resulting in a similar performance as the control (undoped sol-gel) system. Therefore, encapsulation limits the negative interaction of MBT with sol-gel matrix, maintaining the barrier properties of sol-gel layer. The same behavior related to sol-gel barrier is observed even after 14 days of immersion in NaCl solution (Figure 32 B). Additionally, the coating with MBT@PU-MC exhibits the highest |Z| in the low frequency region, ascribed to a lower rate of the corrosion-related electrochemical processes on the alloy surface, thereby demonstrating the active effect of MBT in the system.

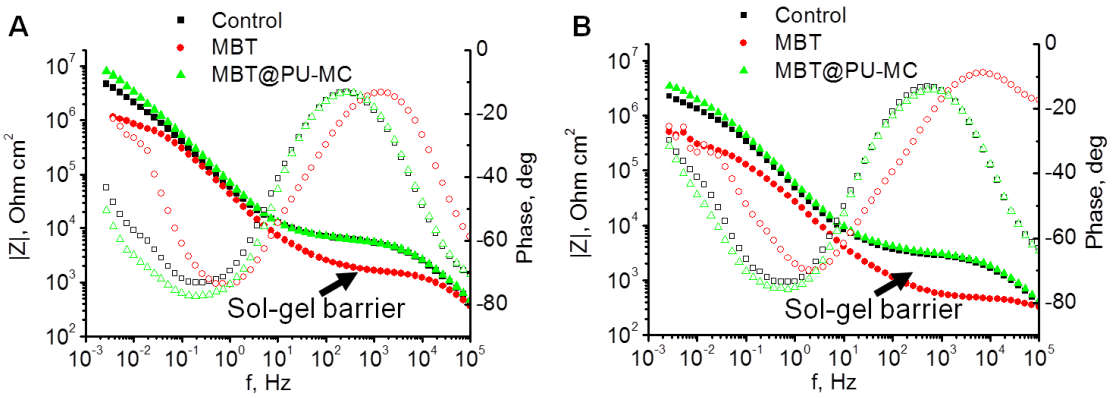

Figure 32: Bode plots of coated AA2024 immersed in 0.5M NaCl solution after (A) 5 days and (B) 14 days.

The typical Bode plot of a failed coating shows 3 time constant elements, attributed to sol-gel coating, intermediate oxide layer and corrosion activity [9].Values of resistances and capacitances associated with those elements can be determined using equivalent circuits to fit experimental data, as represented in the scheme of Figure 33.

The resistance associated with sol-gel coating provides valuable data on the stability of the coating upon addition of inhibiting compounds as well as on the evolution of coating barrier properties during immersion in corrosive electrolyte. On the other hand, the intermediate oxide layer is often seen on chemically cleaned alloy surface [38] and constitutes the last barrier against corrosive species. Thus, when damages occur in oxide, corrosion processes can easily initiate on the unprotected metal surface. In this context, monitoring the properties of intermediate oxide layer can unveil the improvement of corrosion protection of metal by coating with inhibitors. The evolution of sol-gel film and

intermediate oxide layer resistances (R_{coat}, R_{ox}) during immersion in 0.5M NaCl is depicted in Figure 34.

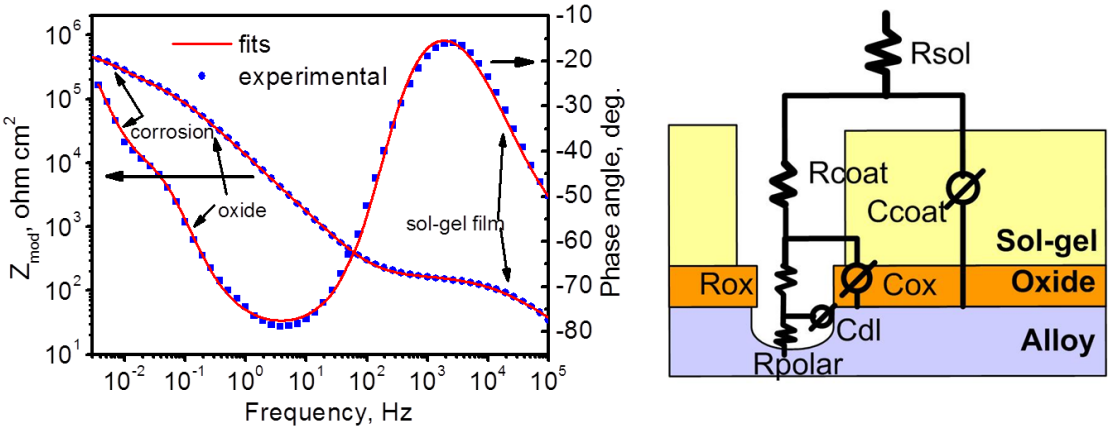

Figure 33: Schematic representation of EIS fitted data (left) using equivalent circuits model (right). Adapted from [37].

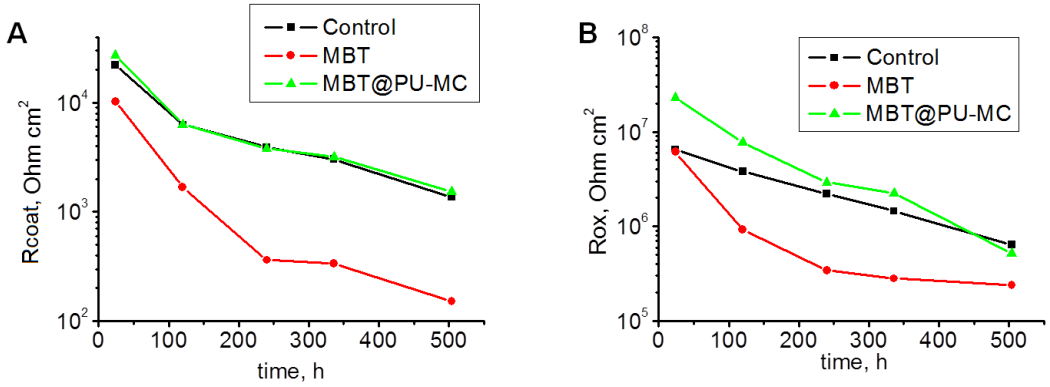

Figure 34: Evolution of sol-gel film resistance (A) and intermediate oxide layer resistance (B) for samples with unmodified sol-gel, sol-gel with MBT and MBT@PU-MC during immersion in 0.5 M NaCl.

The direct addition of MBT decreases the coating resistance with respect to the control system during the immersion time monitored, being more evident after 100 h of immersion until the end of the assay (Figure 34a). On the other hand, when MBT is added in its encapsulated form (MBT@PU-MC) there is no decrease in the film resistance when compared to the control (undoped sol-gel) system (Figure 34a). The same trend is observed for the intermediate oxide layer resistance. When MBT is directly added to the sol-gel, R_{ox} is similar to the control in the first measurement, but as time progress a significant decrease of approximately one order of magnitude is observed (Figure 34b), probably due to the fast

coating degradation promoted by MBT as a result of the chemical interaction between MBT and the sol-gel matrix. For MBT@PU-MC, R_{ox} values are significantly higher than control during most of the immersion time, except for the last measurement when that value is slightly lower than control (Figure 34b). Thus, three significant conclusions can be made from EIS data analysis: the first one is the degradation of barrier properties when MBT is added directly to sol-gel, being not favorable from the point of corrosion protection; the second one is related to the preservation of sol-gel matrix properties when MBT@PU-MC are added; and the third one is based on the improvement of corrosion protection of sol-gel modified with MBT@PU-MC observed and highlighted by higher oxide layer resistance values determined, showing signs of active corrosion protection.

The corrosion protection properties at localized defect sites were examined by SVET. All the sample coupons, with two artificially-inflicted defects made using a needle, were immersed in 0.05M NaCl solution. Usually, the cathodic and anodic corrosion processes occur at different defects [39]. The ionic fluxes caused by these activities can be detected by SVET. In Figure 35a the SVET maps taken after 2 hours of exposure in corrosive media are presented. The reference sample shows already high current densities, while the characteristic anodic peak reaches up to 12.1 µA cm^{-2}. The coating impregnated directly with MBT inhibitor shows only slightly lower activity (9.3 µA cm^{-2}) and the sample with MBT@PU-MC stays at 6.5 µA cm^{-2}. The visual degradation of coatings, especially at defect areas, can be seen in the optical micrographs (Figure 35b), where the ‘active spots’ in the reference sample have grown more than others after 72 hours of exposure in solution. The selected ionic current profiles in Figure 35c and SVET maps at Figure 35b demonstrate the level of corrosion activity on all samples after 72 hours of immersion. The sample with MBT@PU-MC performs clearly better than the others, as the maximum anodic current density slightly decreases down to 3.4 µA cm^{-2}, while for the reference sol-gel and coating with MBT the current densities raised up to 27.4 and 19.2 µA cm^{-2}, respectively. These results demonstrate that the impregnation of sol-gel matrix with MBT@PU-MC gives functional self-healing properties to the coating, while the direct addition of MBT corrosion inhibitor does not improve but degrades the sol-gel matrix.

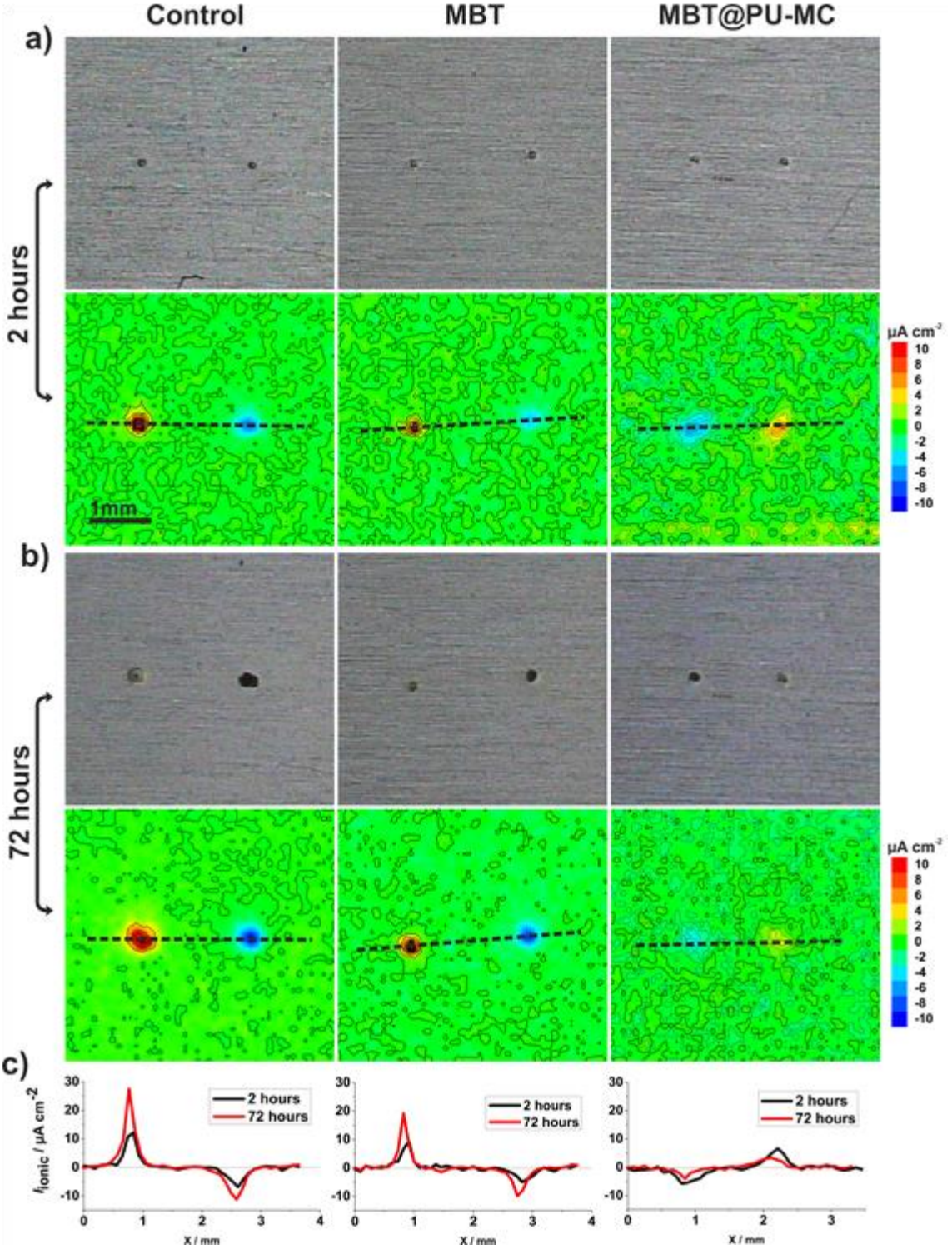

Figure 35: Optical micrographs and SVET maps after 2 hours of immersion (a) and after 72 hours of immersion in 0.05M NaCl (b) and selected ionic current profiles (c) for all samples.

Multilayer coatings (50 ± 1.5 μm), where sol-gel was applied by spray coating as pre-treatment, followed by primer and top layers, were subjected to standard tests. Coated

AA2024 were placed in neutral salt spray (NSS) chamber to assess the corrosion protection in corrosive environments according to ASTM B 117-11 standard. After one week in the NSS chamber coated AA2024 samples were removed and significant differences between samples with and without MBT@PU-MC were observed, as depicted in Figure 36. The sample coated with unmodified sol-gel presents numerous spots of corrosion (pitting), particularly in the vicinity of the hole and on the left side of the image. Oppositely, the sample coated with sol-gel mixed with MBT@PU-MC shows several pits on the left side and no signs of pitting near the hole. This evidence suggests that MBT@PU-MC not only limits the interaction between MBT and sol-gel matrix, keeping its barrier properties, but also improves the corrosion protection of modified sol-gel on the AA2024 surface.

In addition to corrosive testing, adhesion corrosion tests were performed according to NP EN ISO 2409:2012 (cross-cut test) and ISO 16276-2:2007 (wet x-cut test), being the results shown in Figure 37 and Figure 38, respectively.

Figure 36: Coated AA2024 with (A) unmodified sol-gel and (B) with sol-gel containing MBT@PU-MC, after 168 hours in NSS.

Cross-cut tests show signs of separation between the coating and surface of aluminum alloy on the right angle and some delamination in a few squares for sample pre-treated with unmodified sol-gel (samples A from Figure 37), being more evident for samples A2 and A3. According to the NP EN ISO 2409:2012 scale, sample A is classified with **3-4** ("Coating has flaked along the edges of the cuts partly or wholly in large ribbons, and/or it has flaked partly or wholly on different parts of the squares. A cross-cut area significantly greater than 15 %, but not significantly greater than 65 %, is affected"). On the opposite way, samples pre-treated with sol-gel containing MBT@PU-MC (samples B from Figure 9) show no significant signs of detachment and delamination, resulting in an improved ISO classification when MBT@PU-MC is added to the sol-gel. In this case, samples are classified with **1** ("Detachment of small flakes of the coating at the intersections of the cuts. A cross-cut area not significantly greater than 5 % is affected").

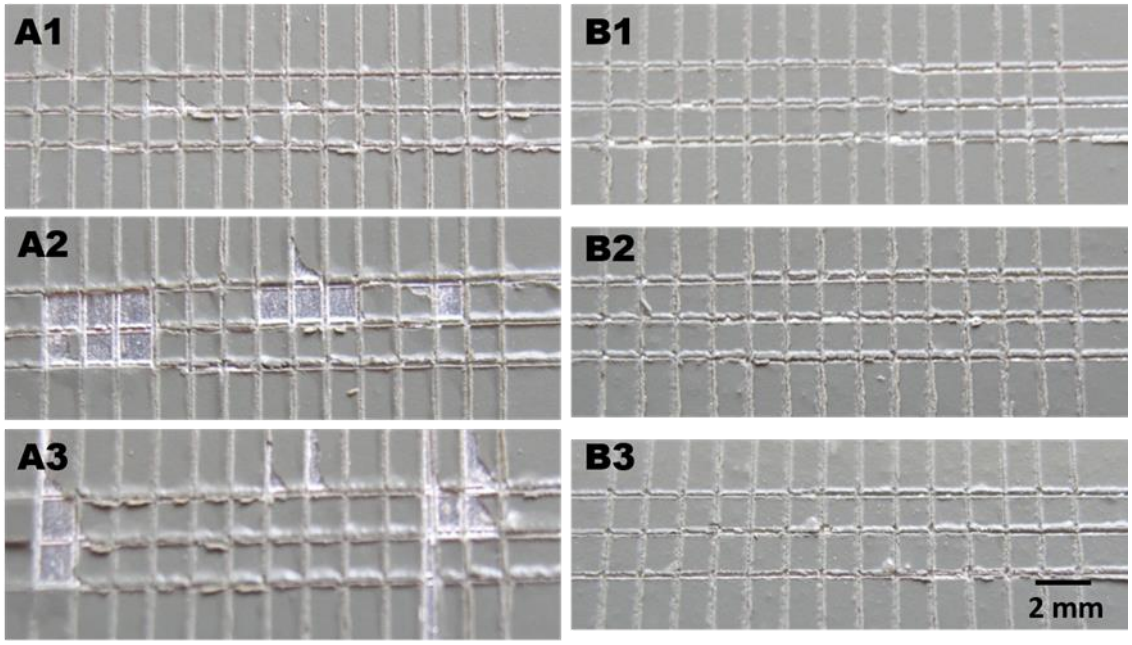

Figure 37: Coated AA2024 with (A) unmodified sol-gel + primer/top and (B) modified sol-gel with MBT@PU-MC + primer/top, after cross-cut test.

The same trend was observed in adhesion of x-cut tests performed after immersion in deionized water and depicted in Figure 38. The evaluation of samples was performed according to the scale used in ASTM D3359 – 09 [40]. Sample A (without sol-gel) shows trace peeling along incisions and was classified with **4A**. Sample B (unmodified sol-gel + primer/top) shows trace peeling along the incision and removal at the intersection, as

observed in Figure 38 B, being also classified with **4A**. Sample C containing MBT@PU-MC in the sol-gel matrix + primer/top presents a rough surface due to the presence of some capsules aggregates, nevertheless shows no peeling or coating removal (Figure 38 C), being classified with **5A**.

According to the scale used in ASTM D3359 – 09, the adhesion of samples containing MBT@PU-MC in the sol-gel matrix shows better performance when compared with samples coated with unmodified sol-gel (sample B) and without sol-gel (sample A).

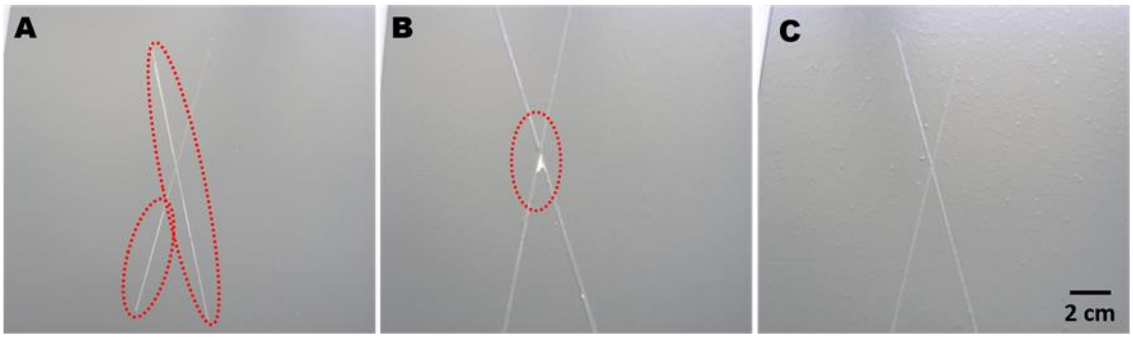

Figure 38: Coated AA2024 with (A) primer/top, (B) unmodified sol-gel + primer/top and (C) sol-gel with MBT@PU-MC + primer/top, after wet x-cut test.

In a general way, the addition of inhibitor in encapsulated form preserves barrier properties, avoiding the negative interaction between MBT and the sol-gel matrix, observed by EIS measurements, and improves the corrosion protection as also verified by EIS and when coated samples were submitted to corrosive atmospheres in the salt spray chamber. In terms of adhesion, samples containing MBT@PU-MC also demonstrate better performance than unmodified sol-gel, for both tests realized showing less signs of detachment or delamination.

The good performance of MBT@PU-MC when incorporated in sol-gel can be attributed to the presence of two "unreacted groups" (isocyanates and amines) from the polyurea polymer used in the encapsulation of MBT and the consequent formation of microcapsules. These two groups can react with sol-gel matrix, acting not only as filler but also as crosslinking agent, improving their protective properties.

Due to the performance of MBT@PU-MC in laboratory tests and in semi-industrial scale tests, they show a high potential to be incorporated in pre-treatment or in primer corrosion protective coatings for aeronautical applications.

4. Conclusions

In this work the successful synthesis and encapsulation of MBT in polyurea microcapsules is reported. As-prepared microcapsules show uniform and spherical morphology with a broad size distribution, from 100 nm up to 2 μm. The developed microcapsules have good thermal stability up to 300 ºC and have a MBT loading content around 5 wt%.

When incorporated into sol-gel matrix and applied in AA2024 pre-treatments, MBT@PU-MC corrosion protection was assessed by EIS, SVET, NSS and adhesion tests. The data obtained from different tests show the improvement of pre-treatment performance in the presence of MBT@PU-MC.

Therefore, the use of PU-MC seems an effective way of incorporating corrosion inhibitors within coating formulations, overcoming negative effects related to direct addition of inhibitors and resulting in an increase of the corrosion protective performance of the modified coating system.

Acknowledgements

This work was developed in the scope of the project CICECO - Aveiro Institute of Materials (Ref. FCT UID /CTM /50011/2013), financed by national funds through the FCT/MEC and when applicable co-financed by FEDER under the PT2020 Partnership Agreement and under the frame of NATAL Project Ref: 11474 Adi/QREN/FEDER. Dr. Igor Bdikin is greatly acknowledged for the provided help with mechanical properties measurements. FM, KY, SK and JT thank FCT for PhD SFRH/BD/72663/2010, Post-Doctoral SFRH/BPD/80754/2011, and Researcher IF/00856/2013 and IF/00347/2013 grants, respectively.

References

1. R.L. Twite, G.P. Bierwagen, Review of alternatives to chromate for corrosion protection of aluminum aerospace alloys, *Prog. Org. Coat.* **33**, 1998, 91–100.

2. J.A. DeRose, “Aluminum Alloy Corrosion of Aircraft Structures: Modelling and Simulation”, 2013, WIT Press.

3. Tammy L. Metroke, Robert L. Parkhill, Edward T. Knobbe, Passivation of metal alloys using sol–gel-derived materials - a review, *Prog. Org. Coat.* **41**, 2001 233–238.

4. Clément Sanchez, Beatriz Julián, Philippe Belleville and Michael Popall, Applications of hybrid organic–inorganic nanocomposites, *J. Mater. Chem*. **15**, 2005, 3559-3592.

5. N.N. Voevodin, N.T. Grebasch, W.S. Soto, F.E. Arnold, M.S. Donley, Potentiodynamic evaluation of sol-gel coatings with inorganic inhibitors, *Surf. Coat. Technol.* **140**, 2001, 24-28.

6. M.L. Zheludkevich, R. Serra, M.F. Montemor, K.A. Yasakau, I.M. Miranda Salvado, M.G.S. Ferreira, Nanostructured sol–gel coatings doped with cerium nitrate as pre-treatments for AA2024-T3: Corrosion protection performance, *Electrochim. Acta* **51**, 2005, 208–217.

7. A.M. Cabral, W. Trabelsi, R. Serra, M.F. Montemor, M.L. Zheludkevich, M.G.S. Ferreira, The corrosion resistance of hot dip galvanized steel and AA2024-T3 pre-treated with bis-[triethoxysilylpropyl] tetrasulfide solutions doped with $Ce(NO_3)_3$, *Corr. Sci.* **48**, 2006, 3740–3758.

8. D.G. Shchukin, Mikhail Zheludkevich, Kiryl Yasakau, Sviatlana Lamaka, Mario G. S. Ferreira, and Helmuth Möhwald, Layer-by-Layer Assembled Nanocontainers for Self-Healing Corrosion Protection, *Adv. Mater.***18**, 2006, 1672–1678.

9. K.A. Yasakau, M.L. Zheludkevich, O.V. Karavai, M.G.S. Ferreira, Influence of inhibitor addition on the corrosion protection performance of sol–gel coatings on AA2024, *Prog. Org. Coat.* **63**, 2008, 352–361.

10. Rudolph G. Buchheit, Hong Guan, Suhakar Mahajanam, Fariaty Wong, Active corrosion protection and corrosion sensing in chromate-free organic coatings, *Prog. Org. Coat.* **47**, 2003, 174–182.

11. A.N. Khramov, N.N. Voevodin, V.N. Balbyshev, M.S. Donley, Hybrid organo-ceramic corrosion protection coatings with encapsulated organic corrosion inhibitors, *Thin Solid Films* **447–448**, 2004, 549–557.

12. D.G. Shchukin, S.V. Lamaka, K.A. Yasakau, M.L. Zheludkevich, M.G.S. Ferreira and H. Möhwald, Active Anticorrosion Coatings with Halloysite Nanocontainers, *J. Phys. Chem. C* **112**, 2008, 958–964.

13. E.D. Mekeridis, I.A. Kartsonakis, G.C. Kordas, Multilayer organic–inorganic coating incorporating TiO2 nanocontainers loaded with inhibitors for corrosion protection of AA2024-T3, *Prog. Org. Coat.* **73**, 2012, 142–148.

14. V. Dalmoro, J.H.Z. dos Santos, E. Armelin, C. Alemán, D.S. Azambuja, Sol–gel hybrid films based on organosilane and montmorillonite for corrosion inhibition of AA2024, *J. Colloid Interface Sci.* **426**, 2014, 308–313.

15. E.L. Ferrer, A.P. Rollon, H.D. Mendoza, U. Lafont, S.J. Garcia, Double-doped zeolites for corrosion protection of aluminum alloys, *Micropor. Mesopor. Mater.* **188**, 2014, 8-15.

16. D. Snihirova, S.V. Lamaka, M.M. Cardoso, J.A.D. Condeço, H.E.C.S. Ferreira, M.F. Montemor, pH-sensitive polymeric particles with increased inhibitor-loading capacity as smart additives for corrosion protective coatings for AA2024, *Electrochim. Acta* **145**, 2014, 123–131.

17. H. Wei, Y. Wang, J. Guo, N.Z. Shen, D. Jiang, X. Zhang, X. Yan, J. Zhu, Q. Wang, L. Shao, H. Lin, S. Wei and Z. Guo, Advanced micro/nanocapsules for self-healing smart anticorrosion coatings, *J. Mater. Chem. A* **3**, 2015, 469–480.

18. M.L. Zheludkevich, J. Tedim and M.G.S. Ferreira, "Smart" coatings for active corrosion protection based on multi-functional micro and nanocontainers, *Electrochim. Acta*, **82**, 2012, 314–323.

19. M.L. Zheludkevich, K.A. Yasakau, S.K. Poznyak and M.G.S. Ferreira, Triazole and thiazole derivatives as corrosion inhibitors for AA2024 aluminum alloy, *Corr. Sci.* **47**, 2005, 3368-3383.

20. J. Tedim, S.K. Poznyak, A. Kuznetsova, D. Raps, T. Hack, M. L. Zheludkevich and M. G. S. Ferreira, Enhancement of Active Corrosion Protection via Combination of Inhibitor-Loaded Nanocontainers, *ACS Appl. Mater. Interfaces* **2**, 2010, 1528-1535.

21. F. Maia, J. Tedim, A.D. Lisenkov, A.N. Salak, M.L. Zheludkevich and M.G.S. Ferreira, Silica nanocontainers for active corrosion protection, *Nanoscale* **4**, 2012, 1287–1298.

22. E. Koh, S.-Y. Baek, N.-K. Kim, S. Lee, J. Shin and Y.-W. Kim, Microencapsulation of the triazole derivative for self-healing anticorrosion coatings, *New J.Chem.* **38**, 2014, 4409-4419.

23. F. Maia, J. Tedim, A.C. Bastos, M.G.S. Ferreira and M.L. Zheludkevich, Active sensing coating for early detection of corrosion processes, *RSC Adv.* **4**, 2014, 17780-17786.

24. W. Burger and M.J. Burge, "Digital Image Processing: an Algorithmic Introduction Using Java", 2008, Springer London.

25. C. Scheffey, Two approaches to construction of vibrating probes for electrical current measurement in solution, *Rev. Sci. Instrum*. **59**, 1988, 787-792.

26. Standard ASTM B 117-11 – "Standard Practice for Operating Salt Spray (Fog) Apparatus".

27. NP EN ISO 2409:2012 – "Paints and varnishes - Cross-cut test".

28. ISO 16276-2:2007 – "Corrosion protection of steel structures by protective paint systems - Assessment of, and acceptance criteria for, the adhesion/cohesion (fracture strength) of a coating - Part 2: Cross-cut testing and X-cut testing".

29. M. M. Coleman, M. Sobkowiak, G. J. Pehlert and P. C. Painter, Infrared temperature studies of a simple polyurea, *Macromol. Chem. Phys*. **198**, 1997, 117-136.

30. H.-W. Engels, H.-J. Weidenhaupt, M. Pieroth, W. Hofmann, K.-H. Menting, T. Mergenhagen, R. Schmoll, and S. Uhrlandt, **2004**. Rubber, 4. Chemicals and Additives. Ullmann's Encyclopedia of Industrial Chemistry.

31. K.A. Yasakau, M.L. Zheludkevich, S.V. Lamaka and M.G.S. Ferreira, Mechanism of Corrosion Inhibition of AA2024 by Rare-Earth Compounds, *J. Phys. Chem. B* **110**, 2006, 5515–5528.

32. J. Carneiro, J. Tedim, S.C.M. Fernandes, C.S.R. Freire, A. Gandini, M.G. S. Ferreira and M.L. Zheludkevich, Chitosan as a Smart Coating for Controlled Release of Corrosion Inhibitor 2-Mercaptobenzothiazole, *ECS Electrochem. Lett.* **2**, 2013, C19-C22.

33. T. Higuchi, Mechanism of sustained-action medication. Theoretical analysis of rate of release of solid drugs dispersed in solid matrices, *J. Pharm. Sci.*, **52**, 1963, 1145–1149.

34. P.L. Ritger and N.A. Peppas, A simple equation for description of solute release I. Fickian and non-Fickian release from non-swellable devices in the form of slabs, spheres, cylinders or discs, *J. Control. Release*, **5**, 1987, 23-36.

35. B.A. Latella, M. Ignat, C.J. Barbé, D.J. Cassidy and J.R. Bartlett, Adhesion behavior of organically-modified silicate coatings on stainless steel. *J. Sol-Gel Sci. Technol.*, **26**, 2003, 765-770.

36. B.A. Latella, Indentation Creep and Adhesion of Hybrid Sol-Gel Coatings, *Adv. Mat. Res.*, **41-42**, 2008, 305-311.

37. M.L. Zheludkevich, D.G. Shchukin, K.A. Yasakau, H. Mohwald, and M.G.S. Ferreira, Anticorrosion Coatings with Self-Healing Effect Based on Nanocontainers Impregnated with Corrosion Inhibitor, *Chem. Mater.* **19**, 2007, 402-411.

38. M.L. Zheludkevich, I.M.M. Salvado and M.G.S. Ferreira, Sol-Gel Coatings for Corrosion Protection of Metals, *J. Mater. Chem.* **15**, 2005, 5099-5111.

39. K.A. Yasakau, S. Kallip, M.L. Zheludkevich and M.G.S. Ferreira, Active corrosion protection of AA2024 by sol–gel coatings with cerium molybdate nanowires, *Electrochim. Acta* **112**, 2013, 236-246.

40. ASTM D3359 – 09: Standard Test Methods for Measuring Adhesion by Tape Test.

CHAPTER 5

"Nanocontainer-based corrosion sensing coating"

IOP PUBLISHING NANOTECHNOLOGY
Nanotechnology **24** (2013) 415502 (9pp) doi:10.1088/0957-4484/24/41/415502

Nanocontainer-based corrosion sensing coating

F Maia, J Tedim, A C Bastos, M G S Ferreira and M L Zheludkevich

Department of Materials and Ceramic Engineering, CICECO, University of Aveiro, 3810-193 Aveiro, Portugal

E-mail: mzheludkevich@ua.pt

Received 27 June 2013, in final form 13 August 2013
Published 17 September 2013
Online at stacks.iop.org/Nano/24/415502

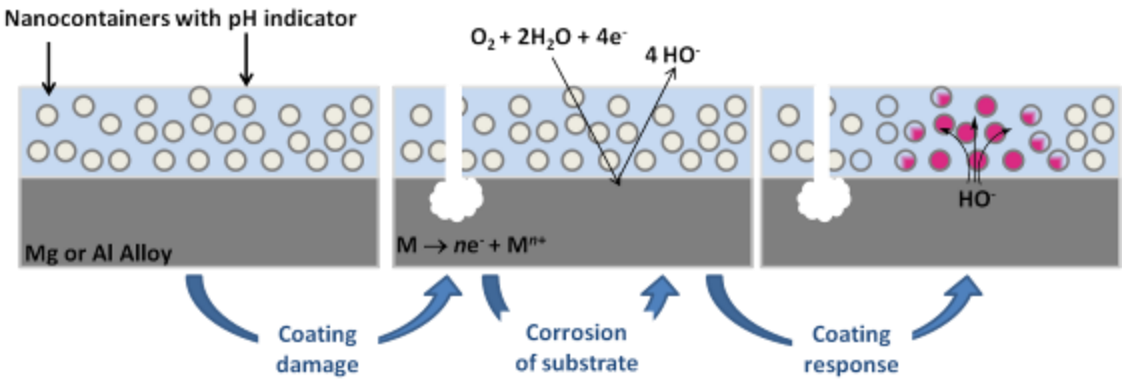

Abstract

The present paper reports on the development of new sensing active coating on the basis of nanocontainers containing pH-indicating agent. The coating is able to detect active corrosion processes on different metallic substrates. The corrosion detection functionality based on the local colour change in active cathodic zones results from the interaction of hydroxide ions with phenolphthalein encapsulated in mesoporous nanocontainers which function as sensing nanoreactors. The mesoporous silica nanocontainers are synthesized and loaded with pH indicator phenolphthalein in a one-stage process. The resulting system is mesoporous, which together with bulkiness of the indicator molecules limits their leaching. At the same time, penetration of water molecules and ions inside the container is still possible, allowing encapsulated phenolphthalein to be sensitive to the pH in the surrounding environment and outperforming systems when an indicator is directly dispersed in the coating layer.

The performed tests demonstrate the pH sensitivity of the developed nanocontainers being dispersed in aqueous solutions. The corrosion sensing functionality of the protective coatings with nanocontainers are proven for aluminium- and magnesium-based metallic substrates. As a result, the developed nanocontainers show high potential to be used in a new generation of active protective coatings with corrosion-sensing coatings.

Introduction

Corrosion prevention remains an important challenge of the technological world, affecting everyone's lives, with great economic impact, often associated with safety and environmental hazards [1]. The most widespread method for preventing corrosion is the use of protective coatings which create a barrier between the metal and the corrosive environment and optionally contain active elements in their composition to actively suppress the corrosion (e.g. inhibitors) [1]. However, the barrier layers also hide the corrosion processes from human eyes and complicate the detection of an initiated degradation processes in the substrate. The early detection of corrosion and coating damage can avoid catastrophic accidents and trigger simpler and less onerous maintenance actions.

Corrosion is typically characterized by a reaction of two part, one anodic (oxidation of the metal) and another cathodic (reduction of oxygen or water molecules from the environment),

Anodic reaction: $M \rightarrow ne^- + M^{n+}$ (1)

Cathodic reaction: $O_2 + 2H_2O + 4e^- \rightarrow 4HO^-$ (2) [1].

With the onset of corrosion, pH increases in the local cathodic areas due to the formation of hydroxide ions whilst acidification often occurs at anodic sites as a result of hydrolysis reactions. The cathodic and anodic sites are often separated in space especially in the case of coated metallic substrates. Thus, the respective pH variations can be used to detect and locate the active corrosion spots in confined defects of the coatings or under the coatings if pH indicators are incorporated in a polymer protective layer.

In recent years there have been several reports published on the development of high-performance coatings with functionalities capable of 'sensing' and 'responding' to external stimuli that may cause coating degradation and, as a result, undermine the integrity of metallic structures [2–9].

Zhang and Frankel showed that the addition of phenolphthalein to an acrylic-based coating confers sensing functionality [2]. The sensitivity of the sensing coatings was determined by passing a cathodic current and determining the charge at which a colour change occurs. A similar approach was employed by El-Nahhal *et al* for monitoring acid–base reactions using a silica-based sol–gel matrix doped with phenolphthalein as pH sensing agent [3]. In both cases phenolphthalein was the selected pH indicator because of its good colour intensity at high pH and high contrast between the low-pH (colourless) and high-pH (pink) states. Another important aspect of this indicator is the colour transition occurring at alkaline but close to neutral pH (pH > 8.2), being very useful for the indication of corrosion onset, avoiding false-positive corrosion indication.

The active compounds can be sometimes added directly to the coating formulations without compromising their intrinsic properties [2]. However, in many cases the interaction of active functional compounds with components of the coating formulation leads to undesirable effects such as loss of functionality, decrease of barrier properties and compromised adhesion [4]. One way to overcome this negative effect is by the

encapsulation of the active compounds before their introduction to the coating formulation, which can be considered as a promising alternative in such situations [5]. The immobilization of active molecules in different nanocontainers confers control over the release and prevents undesirable interactions.

In the specific example of phenolphthalein, Engelmann *et al* have suggested dextran carbamate derivatives for encapsulation of this indicator [6]. The encapsulation of phenolphthalein in pH-sensitive microcapsules based on film-forming monomers and pre-polymers including urea-formaldehyde and melamine-formaldehyde, combined with a cross-linking agent that has one or more ester and mercapto groups such as pentaerythritol tetrakis (3-mercaptopropionate), was also reported [7–9]. According to these works, the shell of microcapsules breaks down under alkaline conditions, releasing the pH indicator as a result of corrosion activity. Nevertheless, the important questions of the capsule mechanical stability and the container size constraints are not resolved in such systems.

In the present work we suggest the encapsulation of phenolphthalein in a new nanocontainer system based on mesoporous silica nanocapsules. A new mechanism for detection of corrosion-induced pH changes is suggested. The main idea is to provide a colour change signal as a result of pH change in the vicinity of a nanocontainer with consecutive diffusion of hydroxide ions into the mesopores reacting with pH indicator within the container. The suggested approach is significantly different from the situations reported in the literature in which the indicator is released from the nanocontainer and reacts in the surrounding solution. To the best of our knowledge it is the first time that nanocontainers have been used as nanoreactors in the active sensing coatings.

Experimental section

Materials

Phenolphthalein (PhPh), cetyltrimethylammonium bromide (CTAB) (99%), tetraethoxysilane (TEOS) (99.9%) and acetone were purchased from Sigma-Aldrich. Ammonia solution (NH4OH) (25–28%), sodium hydroxide (NaOH), sodium chloride (NaCl), ethyl ether (99.5%) and buffer solutions were obtained from Riedel-de-Häen. Ethanol was supplied by Panreac (Spain) and acetonitrile (HPLC grade) from ROMIL. All chemicals were analytic grade and were used without further purification.

Phenolphthalein encapsulation

The silica-based nanocontainers (Si_NC) were prepared via an oil-in-water microemulsion approach as shown in scheme 1.

The nanocontainers were prepared using CTAB as cationic surfactant, ethyl ether as co-solvent and ammonia solution as catalyst. First, a CTAB solution was prepared (0.25 g in 35 ml of water) and 0.25 ml of ammonia solution (25–28%) was subsequently added (aqueous phase). Afterwards, 0.1 g of PhPh dissolved in 25 ml of ethyl ether was added to the aqueous phase, and an oil-in-water microemulsion was obtained (scheme 1). Then, 2.0 ml of TEOS was added drop wise to the microemulsion under vigorous stirring and kept in a closed vessel for 24 h at room temperature. The obtained precipitate was filtered, washed with pure water and dried at room temperature. A small portion of these nanocontainers was calcined at 550 ºC during 5 h, with a heating rate of 10 ºC.min^{-1}, in order to determine PhPh loading content.

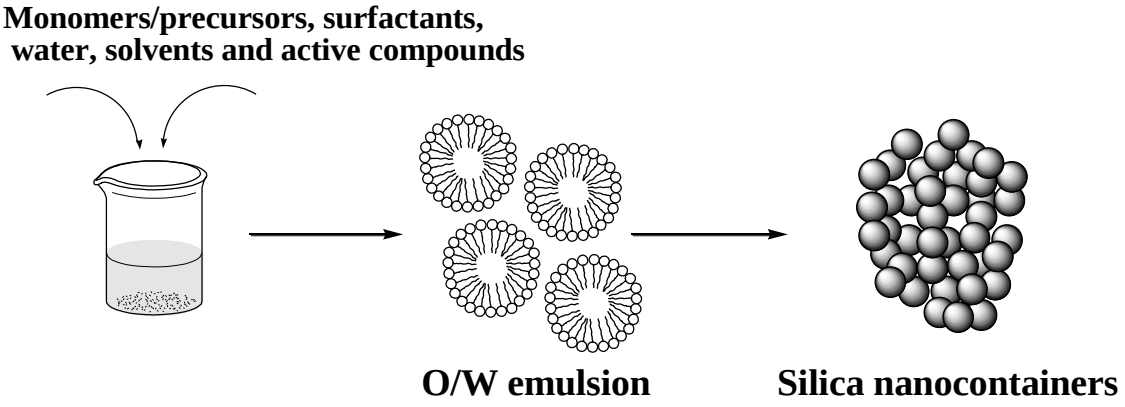

Scheme 1: Encapsulation of PhPh in mesoporous Si_NC.

Characterization of silica nanocontainers

The morphology of obtained nanocontainers was characterized by scanning electron microscopy (SEM) coupled with energy dispersive spectroscopy (EDS), (Hitachi S-4100 system with electron beam energy of 25 keV), and by transmission electron microscopy (TEM) (Hitachi H9000 TEM system with electron beam energy of 300 keV).

Thermogravimetric analysis (TG/DTA) was carried out in a Sataram–Labsys system under air atmosphere, with a heating rate of 10 ºC.min^{-1} from room temperature up to 800 ºC.

The textural properties of samples were evaluated based on the adsorption–desorption isotherms of N_2 at -196 ºC, performed on the equipment Quantachrome NOVA 4200e.

Samples were previously degassed at 180 ºC for 6 h. The specific area (S_{BET}) was calculated by the BET method (Brunauer, Emmett and Teller), the volume of micropores (V_{micro}) was determined from the method-*t*, and the total pore volume ($V_{P/p^o=0.98}$) was obtained from the total volume of N_2 adsorbed to p/p^o=0.98 [10]. The most frequent diameter of pores (mode of pore diameter distribution) was calculated by two different methods: the BJH method (Barrett–Joyner–Halenda) [10, 11], applied to the desorption branch of isotherm, and the DFT method (density functional theory) using a routine available in the Quantachrome equipment software that was developed for the adsorption of N_2 on porous materials based on silicon, assuming a cylindrical pore model.

Release studies of PhPh

The release profiles were monitored by high-performance liquid chromatography (HPLC) using a Shimadzu chromatograph equipped with a SPP-M20A diode array detector, using a C18 column as stationary phase and acetonitrile/pure water (90:10, v/v) as the mobile phase with a flow of 1 mL.min^{-1}. The correlation coefficient of the calibration curves obtained with 5 PhPh standards was higher than 0.999, using the wavelength 275 nm as maximum.

100 mg of Si_NC with PhPh were dispersed in 20 mL of aqueous solutions where NaCl concentration and buffered pH were systematically varied: NaCl concentrations of 0.005 M, 0.05 M and 0.5 M; pH = 4, 7 and 9. These conditions were selected as relevant parameters found in corrosive environments. 1 mL sample of each mixture was extracted with a syringe, and filtered with a specific syringe filter (PTFE membrane with 0.20 μm pore size). In order to determine the total amount of PhPh encapsulated, 100 mg of Si_NC–PhPh was dispersed in 20 mL of ethanol during 24 h to guarantee the maximum release of PhPh. 1 mL of the resulting solution was extracted with a syringe, filtered, and then analysed by HPLC as well. The encapsulation efficiency was determined by the expression $\%E = n_{PhPhext} / n_{PhPhi} \times 100\%$, where $n_{PhPhext}$ is the amount of PhPh extracted from silica nanocontainers and n_{PhPhi} is the initial amount of PhPh used in the encapsulation.

Preparation of substrates and coating

Two different substrates were selected as representatives of light alloys widely used in different industrial applications, such as aeronautics, where detection of early corrosion is

essential considering the high reliability requirements and elevated maintenance costs. Substrates of aluminium alloy 2024 were cleaned and etched according to a standard commercial procedure (alkaline cleaning in Metaclean T2001 - Chemie Vertrieb Hannover GmbH and Co KG - at 68 ºC for 25 min, alkaline etching in Turco Liquid Aluminetch N2 - Turco Chemie GmbH - at 60 ºC for 45 s, acid etching in Turco Liquid Smutgo NC - Turco Chemie GmbH - at 30 ºC for 7 min, each step followed by washing in distilled water). Magnesium alloy AZ31 coupons were abraded with sandpaper of different grain sizes to remove all oxides and impurities followed by cleaning with ethanol.

Dried and cleaned substrates (Mg and Al alloys) were coated with an aqueous-based two-component room temperature cured epoxy non pigmented paint provided by Mankiewicz GmbH (Germany). The nanocontainers with PhPh were incorporated into the resin (5 wt% with respect to the resin) and stirred until uniform dispersion (~30 min) was obtained. Subsequently, the hardener was added to the dispersion and the coating was applied on metal plates using a bar coater (30 μm thickness). Samples were left to cure at room temperature (~25 ºC) for 12 h.

Sensing activity in solution and in coated substrates

The sensitivity of the developed nanocontainers to pH changes was verified using different approaches, including dispersion of the encapsulated indicator in the corrosive electrolytes and corrosion tests on the alloy coupons coated with polymer layers containing PhPh-loaded nanocontainers. The first and simplest test consisted of suspending PhPh nanocontainers in distilled water and then changing the pH of the suspension by the addition of one drop of sodium hydroxide solution (5% (m/m)). A second test consisted of deposition of PhPh nanocontainer slurry on top of a glass plate by casting, followed by drying at room temperature, creating a layer of PhPh-loaded nanocontainers. Then, one drop of sodium hydroxide solution (5% (m/m)) was placed on the formed layer and the evolution of the drop spreading was monitored by the change of colour in the affected zone. In a third test the PhPh-containing nanocontainers were dispersed in a 0.5 M NaCl electrolyte used for corrosion testing of zinc–iron galvanic couple embedded in an epoxy resin. The colour change in the vicinity of the cathodic site was then observed. Finally, to evaluate the sensing activity of indicator-containing nanocontainers incorporated in coatings, the painted metal substrates were immersed in a corrosive electrolyte (0.5 M

NaCl) and monitored over time to detect the colour changes. The evolution of the colour was followed by visual inspection and recorded with a digital camera.

Results and discussion

Encapsulation of phenolphthalein in Si_NC

Silica nanocontainers were prepared by oil-in-water microemulsion polymerization, using CTAB as emulsion stabilizer and template surfactant, ethyl ether as co-solvent and ammonia as catalyst, in a single-step process. After the formation of a stable microemulsion, TEOS was added to the reaction medium and was hydrolyzed in the interface of both phases, followed by alkaline condensation, forming a porous wall around the organic phase promoting the encapsulation of PhPh. The resulted porosity in the nanocontainer shell is a consequence of the gasification of co-solvent, ethyl ether, due to in situ temperature increase as a result of exothermic condensation of TEOS.

The formation of Si_NC is the result of a dynamic cross-coupling of two processes, namely, the dynamic gasification of the template and the stabilization process of condensation together with self-assembly controlled by the presence of CTAB, as explained in our previous publication [12].

The prepared empty mesoporous silica nanocapsules display a regular, spherical shape with size diameter between 100 and 150 nm as shown in Figure 39. Gradual porosity of the Si_NC shell and narrow particle size distribution can be confirmed by TEM (image inset in Figure 39 (left)). Nonetheless, the encapsulation of PhPh promotes a few modifications on the final structure of silica nanocontainers. As can be observed in Figure 39 (right side), the silica nanocontainers have a consistent size distribution but irregular shape. In the inset of the same figure, TEM highlights the irregularity of the Si_NC–PhPh, with part of the capsule shell not completely formed resulting in higher porosity probably due to the bulkiness of PhPh molecules.

This irregular shape found in Si_NC–PhPh seems to be also related to the increase of pore diameter promoted by the encapsulation of PhPh. To verify this hypothesis, textural properties of silica nanocontainers (Si_NC and Si_NC–PhPh) were evaluated based on adsorption–desorption isotherms of N_2 at -196 ºC. Figure 40(a) shows the isotherms for both samples. The observed results are typical for the case of multilayer adsorption in mesoporous materials with a wide pore size distribution [10, 11]. Table 8 presents the main

textural parameters of the silica nanocontainers: specific surface area (S_{BET}), the volume of micropores (V_{micro}), the total pore volume ($V_{P p/p^o=0.98}$) and the most frequent diameter of pores (mode of distribution of pore diameter). The pore size distribution in the silica nanocontainers increases with the PhPh encapsulation as can be observed in Figure 40(b), (c) and in Table 8. The pore diameter also grows by more than three times, from 3.7 to 13.1 nm, according to the BJH method, and 5.5 to 17.3 nm, according to the DFT method. As a result of the pore size increase, the surface area (S_{BET}) decreases from 151 to 144 $m^2.g^{-1}$.

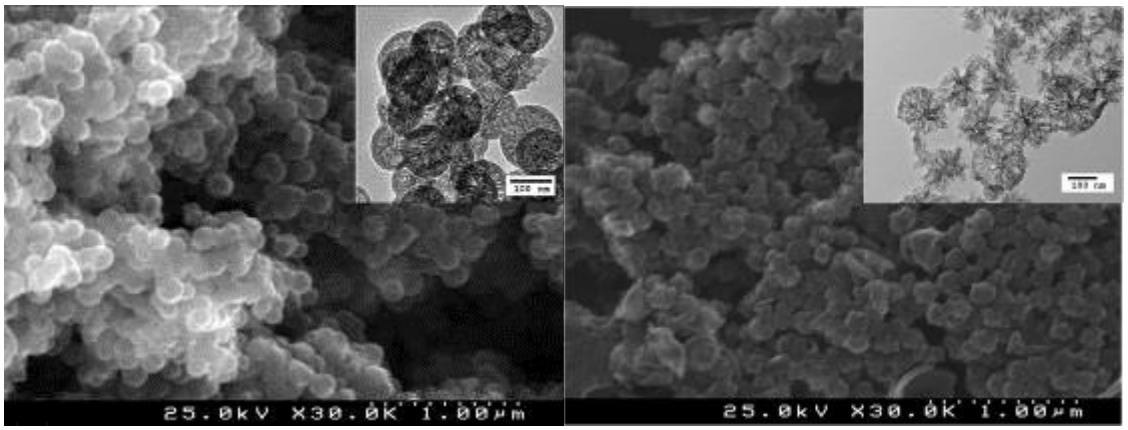

Figure 39: SEM picture of Si_NC: (left) empty (inset: TEM picture of Si_NC with scale bar of 100 nm) and (right) with PhPh (inset: TEM picture of Si_NC–PhPh with scale bar of 100 nm).

The porosity analysis has demonstrated that the obtained nanocontainers have mesoporosity and high specific surface area available for the absorption of the active species. The achieved loading of the developed nanomaterials was tested using thermal analysis. The thermogravimetry experiments in air were performed to verify the thermal stability of Si_NC and to determine the amount of PhPh encapsulated (Figure 41). The curve of calcined Si_NC (used as reference) shows no significant weight loss with temperature. The difference between the weight reduction of the as-synthesized Si_NC and the calcined nanocontainers is approximately 27% and mostly originates from thermal degradation of residual TEOS and traces of surfactant. The plot corresponding to Si_NC–PhPh shows a similar profile from room temperature until 300 ºC, but then an additional mass reduction can be observed in the temperature range from 350 to 500 ºC. Around 10% of the observed weight loss can be attributed to the selective degradation that occurs preferentially from relatively weak bonds (C–N and C–O) to form free radicals, which

undergo a variety of reactions, such as recombination, rearrangement, degradation, etc, and further degradation at elevated temperatures is attributed to PhPh [13] and to part of TEOS degradation. The following step from 530 ºC until 800 ºC is completely attributed to PhPh degradation. The resulting mass loss is significantly higher in this case ant 36%. Therefore, the difference of mass loss for loaded and unloaded nanocontainers can be used to estimate the PhPh loading in Si_NC, which in this situation is at least 9 wt%.

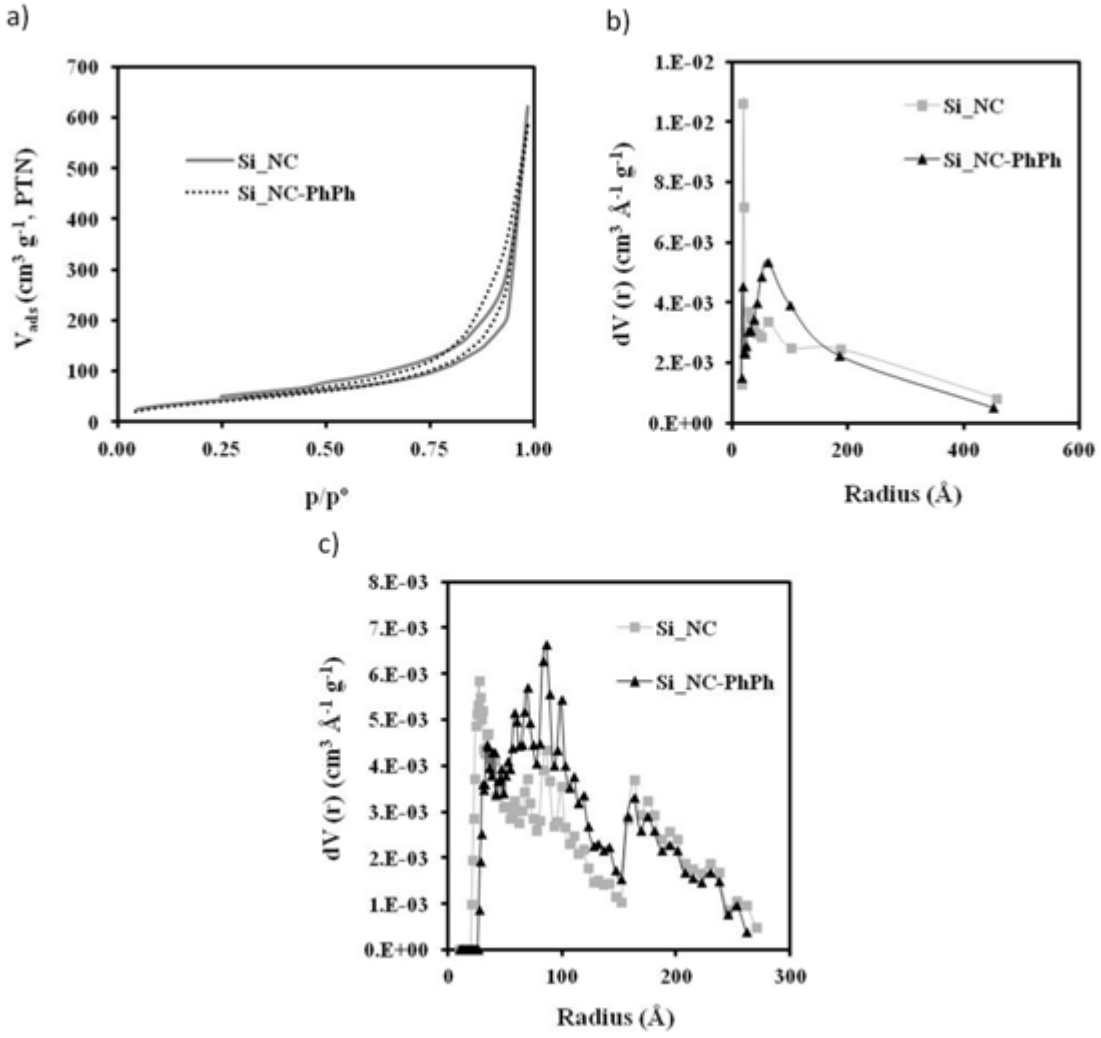

Figure 40: (a) Nitrogen adsorption–desorption isotherms of Si NC; and pore size distribution by two methods: (b) BJH and (c) DFT.

Table 8: **Textural properties of the samples determined from the adsorption-desorption isotherms of N_2.**

Sample	S_{BET} ($m^2\ g^{-1}$)	V_{micro} (*t*-method) ($cm^3\ g^{-1}$)	$V_{P\ p/p^o=0.98}$ ($cm^3\ g^{-1}$)	ϕ_{pores} BJH [(a)] (nm)	ϕ_{pores} DFT [(a) (b)] (nm)
Si_NC [12]	151	0	0.96	3.7	5.5
Si_NC-PhPh	144	0	0.91	13.1	17.3

(a) The values shown represent the most frequent (mode) value of the distribution of pore diameter. (b) Applying a routine that assumes porous silicon-based cylindrical geometry.

The loading of the indicator was additionally verified by extraction experiments. The extraction of PhPh from Si-NC was performed using ethanol and the obtained result was about 6 wt% which is lower than the value obtained by the thermogravimetry. This difference can arise from possible chemisorption of PhPh or a kind of grafting to Si-NC preventing the leaching during the extraction. It can also be related to the retention of PhPh in small pores. As pores are closed, PhPh is not accessible to solvent and it can be removed only with temperature.

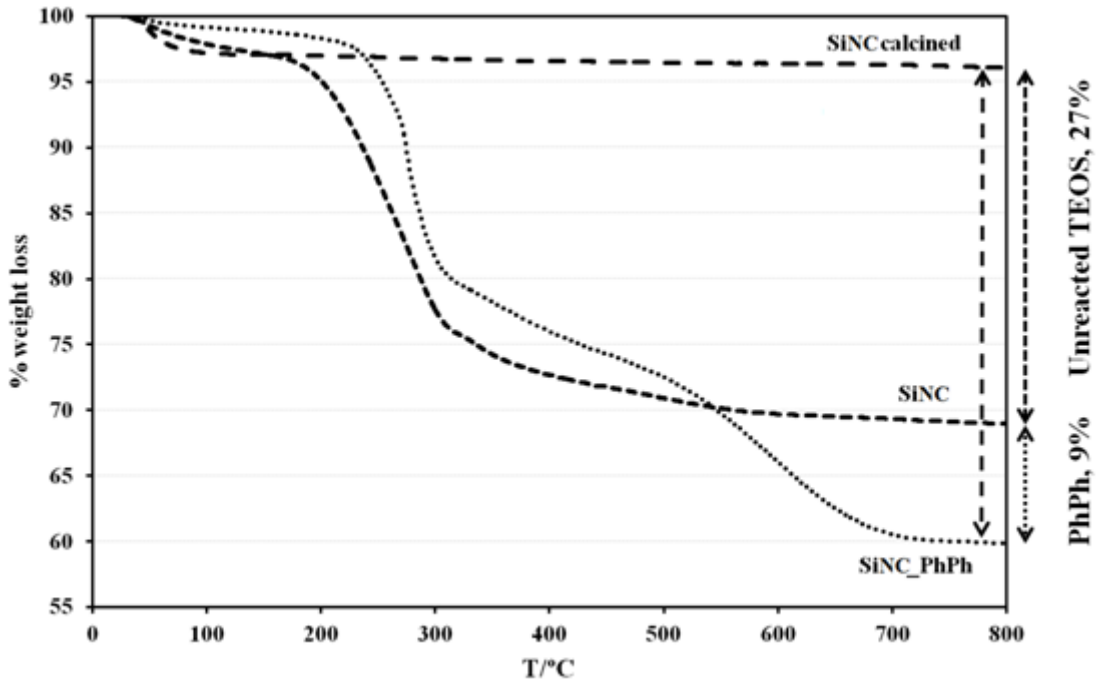

Figure 41: TG profile of Si NC calcined, non-calcined and with PhPh encapsulated.

According to the above-described numbers for loading content, an encapsulation efficiency of 57% was achieved, which corresponds to ~284 ppm of PhPh of loading content. The release of PhPh from mesoporous silica nanocontainers in aqueous electrolytes at different pH conditions and NaCl concentration was studied in order to understand the behaviour of the system in corrosive conditions (Figure 42). The acidity and chloride concentration were varied since they are the most relevant parameters in corrosive environments. The ionic strength and pH also have an important influence on the diffusion of species absorbed in mesoporous nanocontainers [12]. The release studies were carried out at pH equal to 4, 7 and 9; and the NaCl concentrations used were 0.005, 0.05 and 0.5 M. All the experiments were performed four times for each condition in order to guarantee reproducibility.

The release of PhPh from Si NC significantly depends on pH value of the electrolyte. The amount released is very low (1.6 ppm) at neutral pH while at pH = 9 the value is slightly higher (2.7 ppm) and under acidic conditions the released amount reaches 12.1 ppm. The higher value in acidic conditions can be associated with additional hydrolysis of non-hydrolyzed TEOS precursors unblocking the pores [12]. However, after the first hours of immersion this value drops because of possible precipitation of PhPh-containing products, as visually observed. Before injection to HPLC the solution is filtered and precipitates are trapped by the filter leading to a decrease in the level of PhPh detected. Overall, the amount of released indicator is relatively small even in acidic conditions. Also, the level of chlorides in the electrolyte has a certain effect on the release of (Figure 42 (b)). The higher the NaCl concentration, the more PhPh is released. However, this correlation is not very significant because all the values are very low (less than 2 ppm), near the detection limit of the technique, and consequently the errors associated with them are very high, as can be observed in the error bars in Figure 42 (b).

The highest observed value was 12 ppm of PhPh at pH = 4, corresponding to 4% of the full amount of indicator encapsulated. This value is significantly lower than in the case of similar but even denser nanocontainers with 2-mercaptobenzothiazole where 28% of the total loaded inhibitor was released [12]. This significant difference can be attributed to the differences in structural size and stereochemistry (in other words bulkiness) of PhPh [14, 15] with respect to MBT and also due to the possible interactions of PhPh with silica surface.

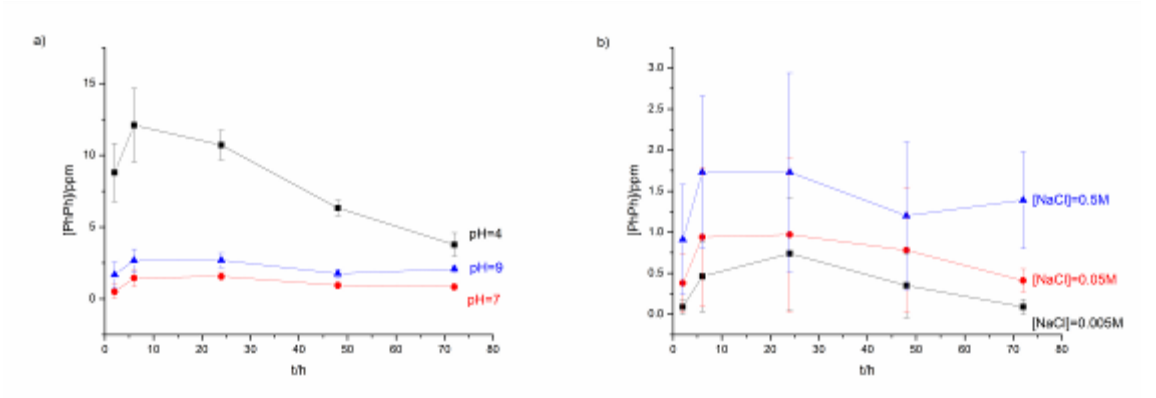

Figure 42: Release studies of PhPh from Si NC at different: (a) pH and (b) sodium chloride concentration.

Sensing ability of nanocontainers in solution

The pH sensing ability of the developed nanocontainers was tested before their incorporation in the polymer protective coating. First, a glass slide was covered with silica nanocontainers. The slurry of nanocontainers was applied by casting on glass substrate forming a uniform layer of Si_NC after drying at room temperature. A small drop of NaOH solution (5% (m/m)) was spread through this dried layer. The colour has locally changed from colourless to pink as a result of pH increase, as observed in Figure 43 (top). A similar test was performed using PhPh-loaded nanocontainers suspended in an aqueous solution (figure 5.5, bottom). When one drop of 0.5 M NaOH was added to the suspension, the colour immediately changed to pink. After a few minutes, due to poor stability of the suspension, the silica nanocontainers deposited at the bottom of the beaker and a clear separation appeared between the colourless solution and the pink bottom. This fact suggests that change in colour occurs by diffusion of hydroxide anions into the nanocontainers and not by release of PhPh from the mesoporous silica nanoparticles. This is consistent with the release studies presented before, where the amount of PhPh released at different conditions of pH is very low (less than 5 ppm). The relative sizes of PhPh and hydroxide anions play an important role, the ingress of hydroxide anions into the nanocontainers being easier than the release of PhPh molecules, causing the colouration of loaded nanoparticles instead of the solution. In this situation the developed nanocontainers with PhPh molecules can be considered as a kind of ‘sensing nanoreactor’.

Approaching real conditions, another pH sensing test was performed using a Zn–Fe galvanic couple on Si-NC–PhPh containing corrosive electrolyte as shown in Figure 44(a).

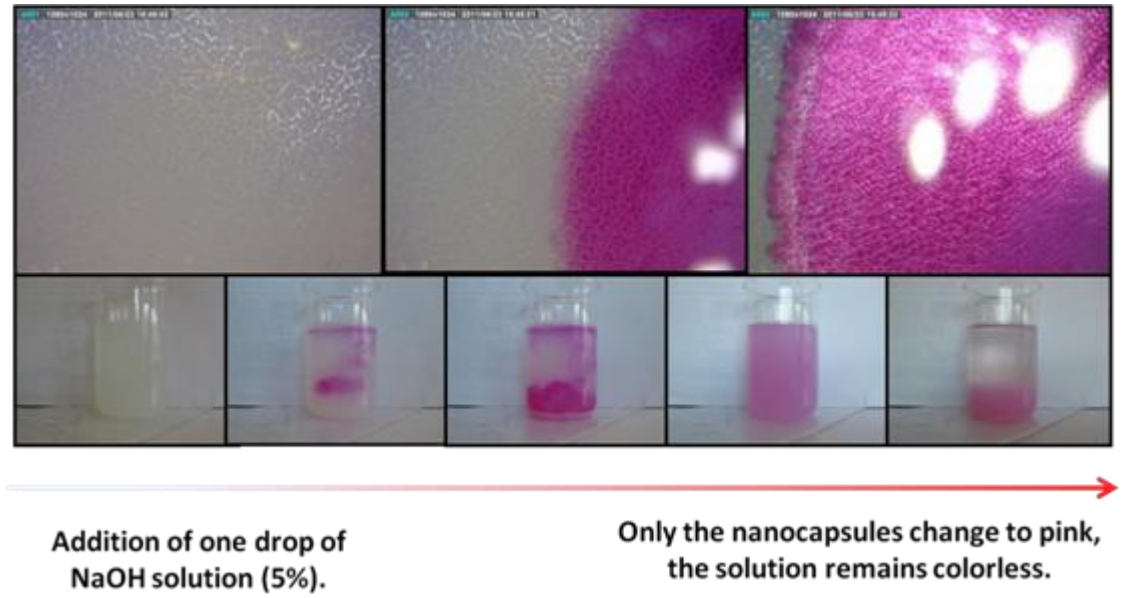

Figure 43: Colour development of PhPh-containing nanocontainers in solution.

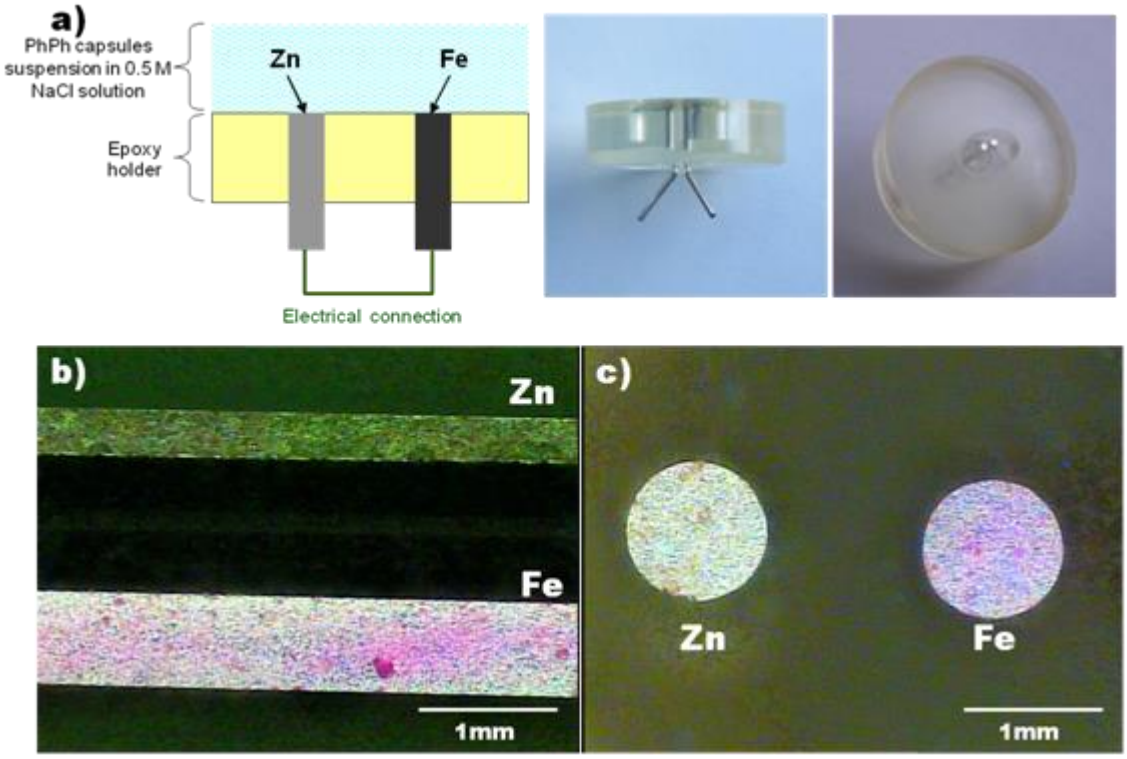

Figure 44: (a) Scheme of Zn–Fe galvanic couple embedded in an epoxy holder; colouration of PhPh nanocontainers in the cathodic area of Zn–Fe couple, using different forms of metallic substrates: (b) plates and (c) rods.

The idea of this experiment was to prove that the nanocontainers are able to detect cathodic activities on the Fe electrode. When the electrical connection between both metals is

established, two electrochemical parallel reactions occur: zinc starts to oxidize (being the anode) and the cathodic reduction of dissolved oxygen begins on the iron/solution interface. The cathodic process results in the formation of hydroxide anions on Fe surface according to reaction 2. The observed colour change (Figure 44(b) and (c)) proves that the addition of the sensing nanocontainers permits detection of local alkalinization resulted from the cathodic processes on iron. The colouration of loaded PhPh nanoreactors occurred only above Fe (the cathode), due to the ingress of hydroxide to the core of mesoporous silica nanoparticles in that location. No colour change was visible in other zones not associated with the cathodic electrochemical activities. The performed model experiments clearly demonstrate that the cathodic processes can be visualized when PhPh-containing nanocontainers are added to the corrosive medium. An additional advantage of this method is the possibility to reuse the PhPh nanocontainers, because they can be recovered by filtration and washed with water until they turn colourless again.

Active corrosion sensing coatings with nanocontainers of pH indicator

The main aim of the present work was to achieve sensing of the corrosion activity on the coated substrates in the confined defects or under paint without compromising the coating intrinsic properties, such as barrier and adhesion. Aluminium and magnesium alloy substrates were coated with a transparent water-based epoxy paint loaded with Si_NC–PhPh. The resulting coating had 20 μm dry thickness and the incorporated nanocontainers were very well dispersed without signs of aggregation. Even with some clusters, their medium size was very small compared to the coating thickness. The coated substrates were tested in a 0.5 M NaCl solution to promote corrosion and monitored by visual inspection.

After several days of immersion a few pink spots appeared showing local pH changes under the paint or in local defects. The colour change can be associated with the local alkalinization at the cathodic corrosion sites. The increase of pH led to a colouration of pH sensing nanocontainers incorporated in the coating as schematically shown in Figure 45.

In the case of coated aluminium alloy an artificial scratch was created on the coated surface in order to accelerate the corrosion processes. The defected zone normally becomes preferentially anodic while the cathodic activity is distributed along the surface and especially concentrated in places where oxygen is most accessible. The coloured spots can be seen in Figure 46(b) in more detail, as a result of the magnification of the Figure 46(a).

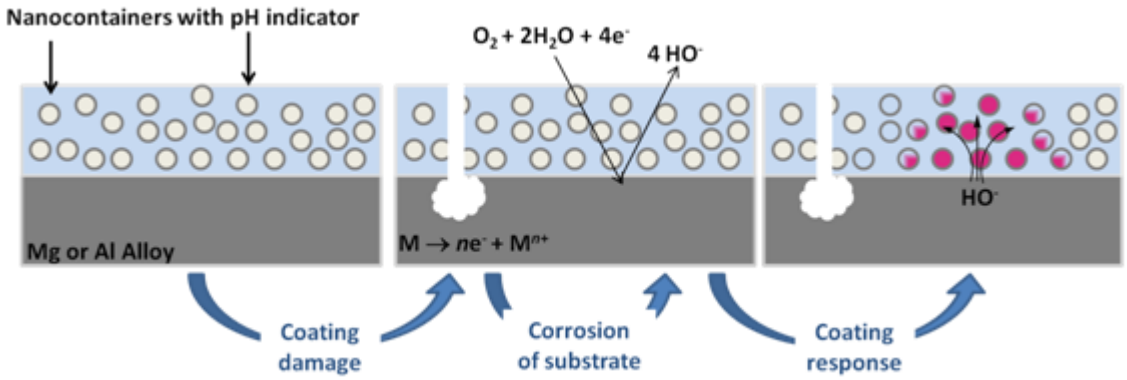

Figure 45: Scheme of pH sensing response from coating.

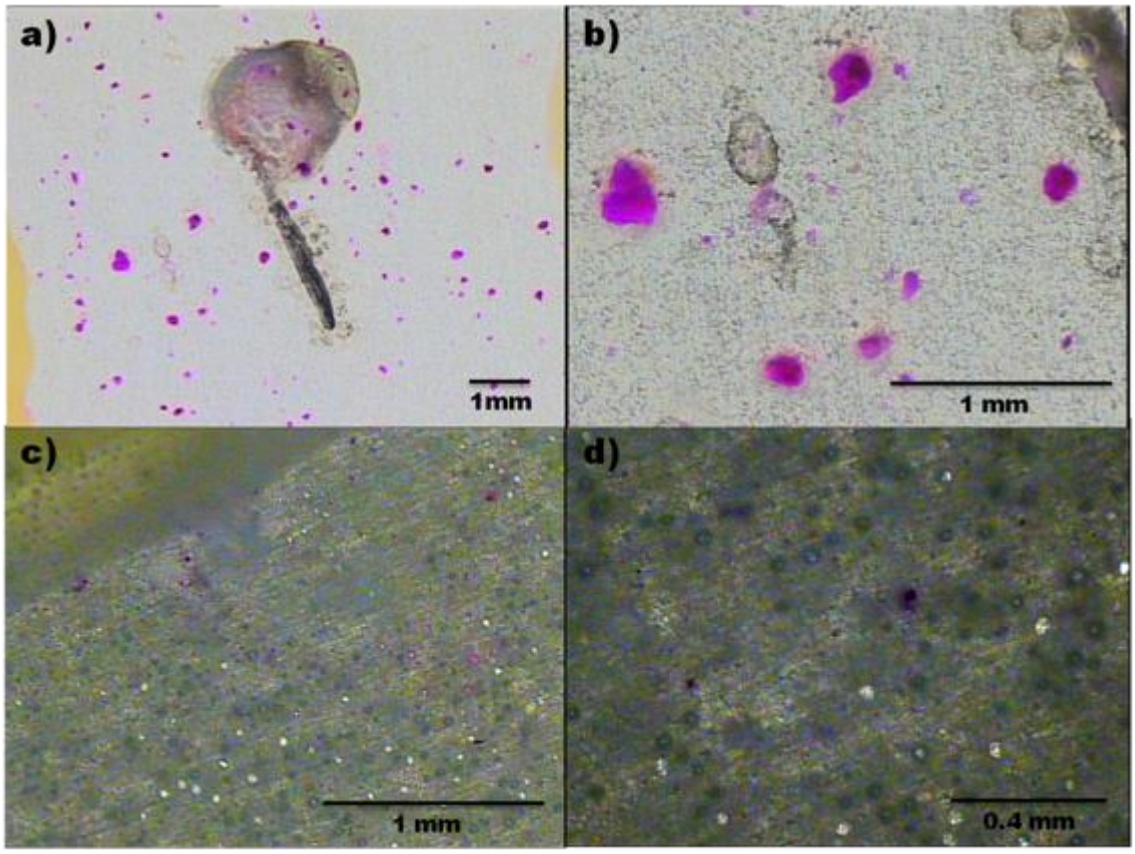

Figure 46: Pictures of coated substrates doped with Si NC–PhPh and tested during 3 days in 0.5 M NaCl: (a) and (b) coated aluminium alloy with artificial scribe, (c) and (d) coated magnesium alloy without scribe.

In the case of magnesium alloy the corrosion was indicated even without any defect or artificial scribe as shown in figures Figure 46(c) and (d). The change in colour was faster in magnesium than aluminium alloys because of the higher corrosion rate of the former

[16] and also because magnesium hydroxide precipitates only at pH higher than 11 [17], i.e. the initial OH^- formed were free to penetrate to the mesoporous nanoreactors and react with PhPh, changing the colouration of coating.

As one can clearly see, the developed nanoreactor sensing system based on nanocontainers with pH indicator can be used for conferring a corrosion sensing functionality to the protective coatings on different metallic substrates.

Conclusions

Active corrosion-sensing coatings based on nanocontainers with pH-indicating agent introduced in the polymer matrix are reported in the present work.

The synthesis of the mesoporous silica nanocontainers is performed in a one-stage process allowing high encapsulation degree and reasonable loading of phenolphthalein. The loaded pH indicator is efficiently stored in the nanocontainers without significant uncontrollable leaching in the aqueous environments.

The nanocontainers act as pH sensing nanoreactors in solution, detecting the onset of an alkaline environment since hydroxide anions can react with PhPh immobilized into the container, turning them from colourless to pink. The pH sensing ability was retained when the silica nanocontainers were incorporated in a water-based organic coating applied to aluminium and magnesium alloys.

The developed approach seems to be a simple and promising solution to be used in general structures for warning of their degradation at an early stage. Other corrosion detection coatings can be created on a similar basis using various sensing agents for specific metallic cations as well as for tuned pH ranges. The inclusion of sensing mechanism in self-healing protective coatings can be also a way to monitor their service life.

Acknowledgments

FM and JT thank FCT for PhD grant SFRH/BD/72663/2010 and post-doc grant SFRH/BPD/64335/2009, respectively.

References

[1] Ghali E, Sastri V S and Elboujdaini M 2007 Corrosion Prevention and Protection: Practical Solutions (Chichester: Wiley).

[2] Zhang J and Frankel G S 1999 Corrosion 55 957–67.

[3] El-Nahhal I M, Zourab S M and El-Ashgar N M 2001 J. Dispersion Sci. Technol. 22 583–90.

[4] Raps D, Hack T, Wehr J, Zheludkevich M L, Bastos A C, Ferreira M G S and Nuyken O 2009 Corros. Sci. 51 1012–21.

[5] Ferreira M G S, Zheludkevich M L and Tedim J 2011 Nanocoatings and Ultra-Thin Films: Technologies and Applications ed A S H Makhlouf and I Tiginyanu (Cambridge: Woodhead Publishing).

[6] Engelmann G, Jobmann M and Rafler G 2004 Indust. Crops Prod. 20 37–48.

[7] Li W and Calle L M 2007 NACE Corrosion 2007 (Nashville).

[8] Li W and Calle L M 2007 Proc. Smart Coatings 2007 (Orlando).

[9] 2010 US Patent Specification 7790225.

[10] Sing K S W, Everett D H, Haul R A W, Moscou L, Piertti R A, Rouquerol J and Siemieniewska T 1985 Pure Appl. Chem. 57 603–19.

[11] Gregg S J and Sing K S W 1982 Adsorption, Surface Area and Porosity (London: Academic).

[12] Maia F, Tedim J, Lisenkov A D, Salak A N, Zheludkevich M L and Ferreira M G S 2012 Nanoscale 4 1287–98.

[13] Ghetiya R M, Kundariya D S, Parsania P H and Patel V A 2008 Polym. Plast. Technol. Eng. 47 836–41.

[14] Tamuras Z, Abe S, Ito K and Maeda M 1996 Anal. Sci. 12 927–30.

[15] Sugiura H, Kato T, Senda H, Kunimoto K K, Kuwae A and Hanai K 1999 Anal. Sci. 15 611–2.

[16] Song G and Atrens A 2003 Adv. Eng. Mater. 5 837–58.

[17] Pourbaix M 1974 Atlas of Electrochemical Equilibria in Aqueous Solutions (Houston: NACE).

CHAPTER 6

"Active sensing coating for early detection of corrosion processes"

RSC Advances

PAPER

Active sensing coating for early detection of corrosion processes

Cite this: *RSC Adv.*, 2014, 4, 17780

Frederico Maia,[a] João Tedim,[a] Alexandre C. Bastos,[a] Mário G. S. Ferreira[a] and Mikhail L. Zheludkevich*[ab]

Received 28th January 2014
Accepted 2nd April 2014

DOI: 10.1039/c4ra00826j

www.rsc.org/advances

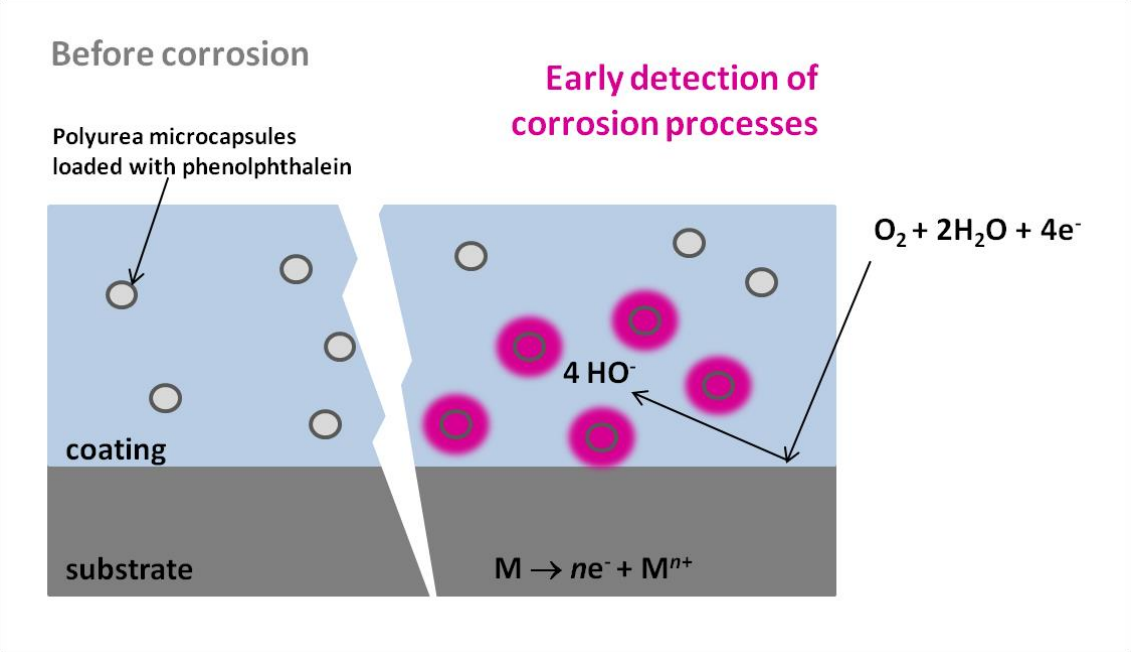

Abstract

A corrosion sensing coating based on specially developed polymeric microcapsules with a pH-indicator is reported. The synthesis of the microcapsules is designed in a way to ensure their optimal compatibility with the polyurethane protective coatings and to allow release of the indicator at higher pH values. The obtained polyurea microcapsules have a regular and microsized morphology and a loading content of 12 wt%. The developed sensing coating applied on aluminium and magnesium alloys is able to indicate initiation of corrosion processes through a pink coating coloration, as a result of local pH increase in the cathodic areas.

Introduction

Corrosion processes lead to degradation of metal and corresponding alloys, which ultimately can cause structural failures if no action is promptly taken to tackle this issue at the initial stages. Early detection of corrosion can be a way to trigger necessary maintenance actions reducing the probability of potential structural failures and high costs associated with repair.

Very often the metallic structures are protected by coating systems to increase the service life. One of the most used types of coatings is based on polyurethane/polyurea due to its high performance, easy functionalization and ability to form different nanocomposites by incorporation and interaction with nano-pigments [1]. The range of PU coating applications is so wide due to versatility in selection of monomeric materials from a vast list of macrodiols, diisocyanates and chain extender [1]. According to the type of reaction promoted with diisocyanate compounds is possible to obtain different characteristic groups. The reaction of diisocyanate with a diol or with an amine, results in urethanes and ureas (Scheme 1), respectively.

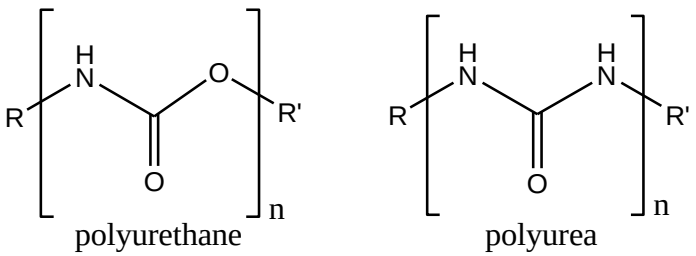

Scheme 1: Generic chemistry of polyurethane and polyurea.

The incorporation of corrosion sensors in a protective coating, simple and accessible to non-specialized personnel, is an important improvement with respect to traditional coatings and potentially complement some of the existing technologies for corrosion assessment of structures (electrochemical methods such as polarization resistance) and visual inspection of corrosion products.

Commonly, corrosion occurs according to two parallel processes: (i) metal oxidation in the anodic zone with possible hydrolytic acidification, and (ii) reduction of oxygen and/or water in the cathodic areas, leading to the formation of hydroxide anions [2]. The corrosion induced change of pH in the local defects of coatings or in confined areas can be used to detect the corrosion onset and locate the cathodic or anodic spots.

Different pH indicators can be employed for visualization of pH changes. For example phenolphthalein seems to be one of the best options because it is colourless at pH below 8.2 and turns pink at pH higher than 8.2. Therefore, it can be used to monitor the raise in pH associated with the cathodic reaction and overall with ongoing corrosion activity.

Since the pioneering work of Zhang and Frankel [3], where a paint system containing phenolphthalein and sensitive to corrosion processes was presented, several other researchers followed the idea. El-Nahhal and co-workers reported the immobilization of phenolphthalein in a sol–gel matrix for monitoring acid–base reactions.4 Showing the industrial relevance of this approach, Frankel and co-workers published a patent based on the introduction of a pH indicator in a gel based corrosion sensing coating able to modify its colour as a response to a change in hydrogen ions concentration near the surface of the material [5].

Although the direct incorporation of active compounds to some coating formulations can be simple but effective, normally it encloses some drawbacks such as deactivation or degradation of the active compound, and a decrease in adhesion and barrier properties provided by the coating itself [6]. One of the best ways to overcome these problems can be the encapsulation or immobilization of active compounds in capsules that protect the compound from deactivation or interaction with the coating matrix and can additionally provide a triggered and localized response.

Some examples available in literature show the application of nanostructured materials for phenolphthalein encapsulation. Engelmann and co-workers proposed dextran carbamates with hydrophobic properties as wall material for microparticles with core/shell structure

for phenolphthalein encapsulation [7]. In another work, Li and Calle described a new type of pH-sensitive microcapsules, based on film-forming monomers and pre-polymers including urea–formaldehyde and melamine–formaldehyde. The shell of those microcapsules is sensitive to alkaline pH, breaking down and releasing the pH indicator as a result of corrosion activity [8–10]. A different approach for the application of encapsulated phenolphthalein was presented recently by Maia and coworkers, where silica nanocontainers filled with phenolphthalein were used as nanoreactors, with the colour change taking place inside the nanocontainers. Accordingly, no release of phenolphthalein was detected, only diffusion of hydroxide anions into the porous silica shell reacting with phenolphthalein inside the nanocontainer, and acting as a corrosion sensor when tested in solution or incorporated in coatings applied different metal substrates [11].

In this paper we report the encapsulation of phenolphthalein in polyurea microcapsules for the first time. The aim of this work is the incorporation of polyurea microcapsules containing phenolphthalein in a coating formulation based on polyurethane, resulted from the polymerization of hydroxyfunctional polyacrylic with aliphatic polyisocyanates. The polymeric system for the microcapsule walls (polyurea) is suggested in order to improve the compatibility between the microcapsules and the coating matrix, due to their similar (polyurethane/polyurea) chemistry. This way is possible to obtain corrosion sensing feature in a uniform, homogeneous and compatible coating without compromising the barrier properties.

Experimental section

Materials

Phenolphthalein (PhPh), Span 85, diethylenetriamine (DETA) (99%), isophorone diisocyanate (IPDI) (98%) and acetone were purchased from Sigma-Aldrich. Sodium hydroxide (NaOH), sodium chloride (NaCl) and buffer solutions were obtained from Riedel-de-Häen. Ethanol was supplied by Panreac. All chemicals were analytic grade and were used without further purification.

Phenolphthalein encapsulation

The synthesis of polyurea microcapsules (PU_MC) and the encapsulation of PhPh in PU_MC were performed for the first time in a single step, as described in Scheme 2.

PU_MC were prepared using Span 85 as non-ionic surfactant and PhPh as encapsulated product. Firstly, a solution of 1 g Span 85 in 100 mL of water was prepared. Then, 3 g of IPDI and 150 mg of PhPh were dissolved in 20 mL of acetone and added to the aqueous solution, leading to an oil-in-water microemulsion (Scheme 2). With a vigorous agitation, 2 g of DETA were diluted in 20 mL of water and added drop-by-drop to microemulsion. Then the mixture was heated at 60 ºC and stirred for 3 h. The obtained precipitate was filtered, washed with pure water and dried at room temperature.

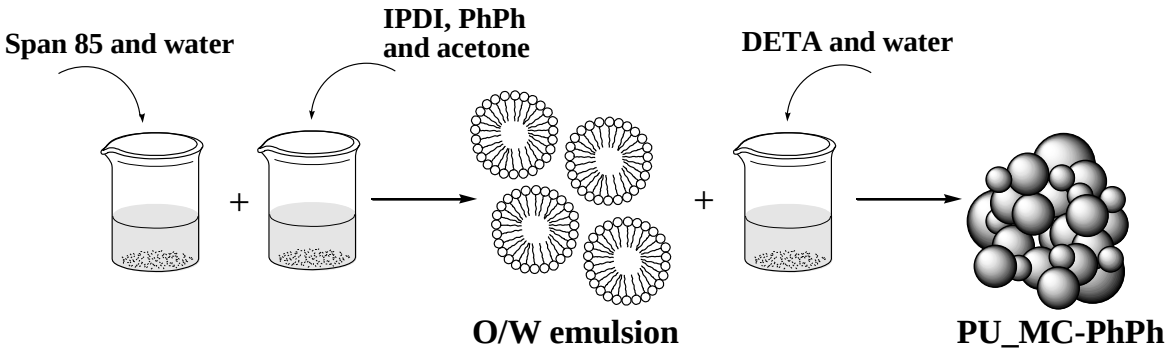

Scheme 2: Preparation of PU_MC and encapsulation of PhPh.

PU_MC–PhPh morphology characterization

PU_MC–PhPh morphology was characterized by scanning electron microscopy (SEM) coupled with energy dispersive spectroscopy (EDS), using an Hitachi S-4100 system with electron beam energy of 25 keV, and by transmission electron microscopy (TEM) using an Hitachi H9000 system with electron beam energy of 300 keV.

In order to characterize the chemical and thermal properties of PU_MC, ATR-FTIR spectra were recorded with a Bruker IFS55 spectrometer equipped with a single horizontal Golden Gate ATR cell. Thermogravimetric analysis (TG/DTA) was carried out in a TGA-50 Shimadzu system under nitrogen atmosphere, with a heating rate of 10 ºC.min^{-1} from room temperature up to 800 ºC.

Release studies of PhPh

The release profiles of PhPh were monitored by ScanSpec miniature UV-Vis spectrophotometer (ScanSci) at wavelength ≈ 280 nm. The correlation coefficient of the calibration curves obtained with 5 PhPh standard solutions was higher than 0.999.

For that purpose 100 mg of PU_MC–PhPh were dispersed in 20 mL of aqueous solutions where temperature and pH were systematically varied: T = 40, 60 and 80 ºC; pH = 4, 7 and 9 (pH buffer solutions were used to maintain the pH constant during the release studies). Then 1 mL sample of each mixture was extracted with a syringe, and filtered with a specific syringe filter (PTFE membrane with 0.20 μm pore size). In order to determine the total amount of PhPh encapsulated, 100 mg of PU_MC–PhPh were dispersed in 20 mL of ethanol during 24 hours to guarantee the maximum release of PhPh. Ethanol was the solvent selected because it is one of the solvents where phenolphthalein dissolves better [12]. 1 mL of the resulting solution was extracted with a syringe, filtered, and then analyzed. The encapsulation efficiency was determined by the expression:

$$\%E = n_{PhPhext}/n_{PhPhi} \times 100,$$

where $n_{PhPhext}$ is the amount of PhPh extracted from capsules and n_{PhPhi} is the initial amount of PhPh used in the encapsulation.

Preparation of substrates and coating

Magnesium alloy AZ31 specimens were abraded with sandpaper of different grain sizes finishing with 600/1200 grades to remove all oxides and impurities followed by cleaning with ethanol and immediately dried.

Aluminium alloy 2024 substrates were cleaned and etched according to a standard commercial procedure: alkaline cleaning in Metaclean T2001 (Chemie Vertrieb Hannover GmbH & Co KG) at 68 ºC for 25 min, alkaline etching in Turco Liquid Aluminetch N2 (Turco Chemie GmbH) at 60 ºC for 45 s and acid etching in Turco Liquid Smutgo NC (Turco Chemie GmbH) at 30 ºC for 7 min, each step followed by washing in distilled water.

Dried and cleaned substrates (Mg and Al alloys) were coated with Bayhydrol® A 145, a water-reducible, hydroxyfunctional polyacrylic dispersion, used in combination with aliphatic polyisocyanates (Bayhydur® 304) with fast drying at room temperature, from Bayer. PU_MC–PhPh were incorporated into the formulation (5 wt% with respect to the total wet formulation) and stirred during 30 minutes until obtaining uniform dispersion. Subsequently, the coating formulation was applied on metal plates (AA2024 and

Mg AZ31) using a bar coater with a wet thickness of 30 μm. Samples were left to dry at room temperature (~25 ºC) for 48 h. Finally, the edges and the backside of the metal plates were covered by a protective varnish (Lacomit® from Agar Scientific).

The remnants of the formulation were applied in a Teflon mould, dried and detached, in order to obtain a free standing coating composed by the PU matrix with the developed microcapsules (Film 1 and Film 2).

Sensing activity in solution, inside the coating matrix and on coated substrates

A suspension of PU_MC–PhPh in water was prepared and one drop of 0.5 M sodium hydroxide solution was added to assess the ability of the prepared capsules in sensing pH changes in solution. The colour evolution was recorded with a digital camera during one week. A similar test was carried out with coatings modified with PU_MC–PhPh. Film 1 was immersed in distilled water and one drop of 0.5 M sodium hydroxide solution was added. Film 2 was immersed for 48 hours and then removed before the addition of hydroxide solution to verify whether PhPh was released under neutral conditions. For evaluation of the corrosion sensing activity, aluminium and magnesium alloy specimens coated with coatings modified with PU_MC–PhPh were immersed in a corrosive electrolyte (0.5 M NaCl) and monitored over time to follow any colour development. The colour evolution was followed by visual inspection and recorded with a digital camera.

Results and discussion

Encapsulation of phenolphthalein and characterization of PU_MC

Polyurea microcapsules of PhPh were synthesized by interfacial polymerization in an oil-in-water microemulsion. The suggested methodology allows the microcapsule synthesis and the encapsulation of hydrophobic compounds in a single step. The polymerization occurs at the interface between phases, where the surfactant plays an important role in the stabilization of the emulsion droplets. Initially, the hydrophobic phase containing PhPh and IPDI – a hydrophobic monomer – was dispersed in water, forming the emulsion. Then DETA, hydrophilic monomer, was added to the emulsion drop-by-drop to react with IPDI at the interface between phases (Scheme 3). This reaction, which consists of polymerization between IPDI and DETA, results in the formation of a shell and consequently encapsulation of PhPh within the hydrophobic core. For the best of our

knowledge this is the first time that PhPh is encapsulated in polyurea capsules and also the combination of IPDI and DETA as monomers for the shell formation.

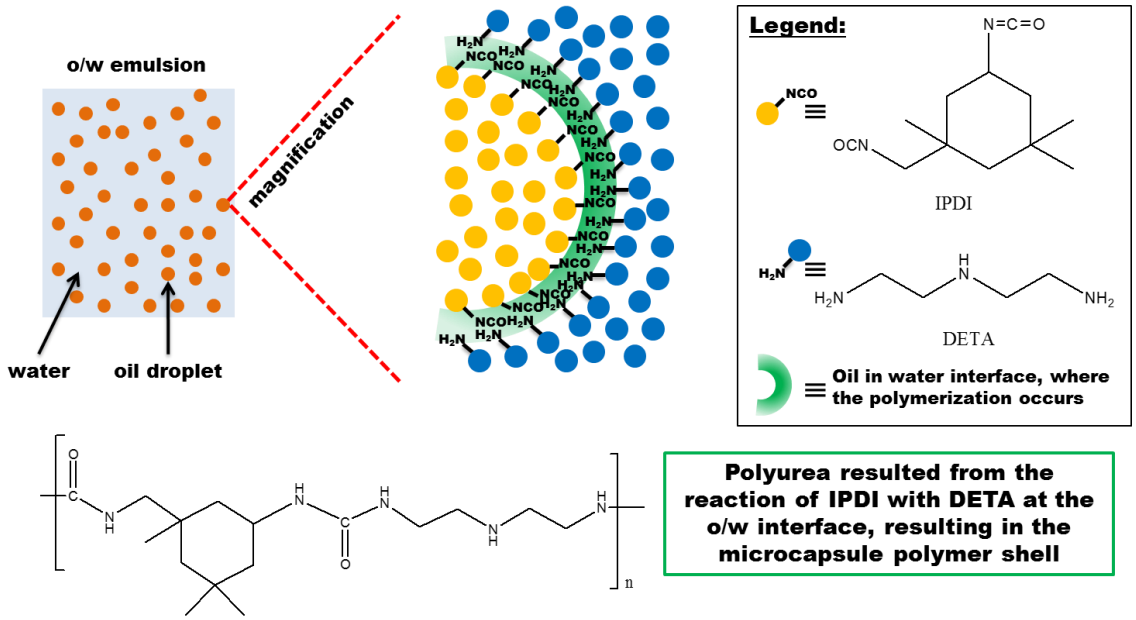

Scheme 3: Representation of the polyurea microcapsule shell formation at the oil in water interface.

The obtained PU_MC have spherical morphology and broad size distribution between 100 nm and 1 mm as shown in Figure 47. The encapsulation of PhPh, when compared to empty capsules did not promote any significant morphological modification on PU_MC and the obtained capsules do not appear to be porous. The TEM image of PU_MC–PhPh (Figure 48) shows that the wall thickness is approximately ~8 nm.

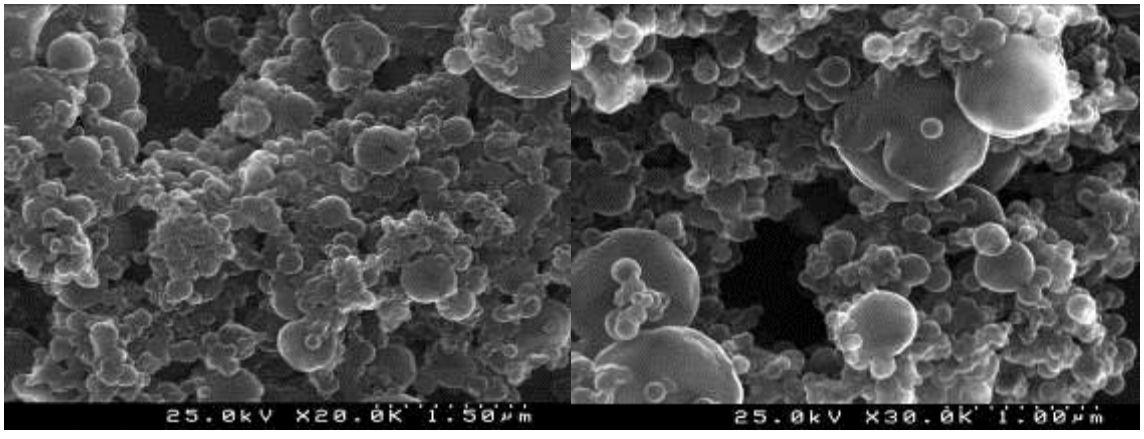

Figure 47: SEM micrographs of: (left) empty PU_MC and (right) PU_MC–PhPh.

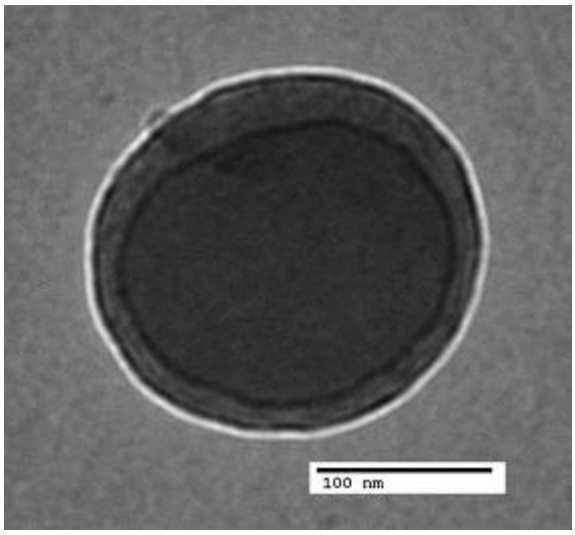

Figure 48: TEM micrograph of a typical single PU_MC–PhPh microcapsule.

The resulting polyurea polymer used as a microcapsule shell presents the typical vibration bands of polyurea as depicted in Figure 49. The most important bands for this specific polymer are the ones resulted from the vibration of N–H and C=O bonds, representing the urea linkage. In the spectra of Figure 49 two bands are observed at 1738 cm^{-1} and 1633 cm^{-1} related to stretching of carbonyl group, corresponding to the hydrogen bonded to the carbonyl group [13]. The broad band at 3334 cm^{-1} is related to stretching of NH [13] in particular to the secondary amines from DETA and the strong band at 1552 cm^{-1} is related to the vibration of the stretching bond N–H from the urea linkage, directly connected to the carbonyl group. The band presented at 2257 cm^{-1} corresponds to the stretching vibration of NCO bond, probably due to unpolymerized residues from the diisocyanate (IPDI) that was not fully consumed.

Thermogravimetry was used to investigate the thermal behaviour of polyurea as can be observed in Figure 50. The resulted thermogravimetric profile shows that PU microcapsules are thermally stable until 300 ºC and after this temperature the degradation of soft and hard segments of the urea linkage [14] is observed.

Using FTIR and TG techniques to characterize the prepared PU_MC was possible to demonstrate the typical chemical and thermal properties of the polyurea polymer.

The encapsulation of PhPh in PU_MC was successful and the loading content of PhPh, determined by extraction with ethanol (see Experimental section), was 611.5 ppm (loading content of 12.2 wt% in the capsules), corresponding to an encapsulation efficiency of 82%.

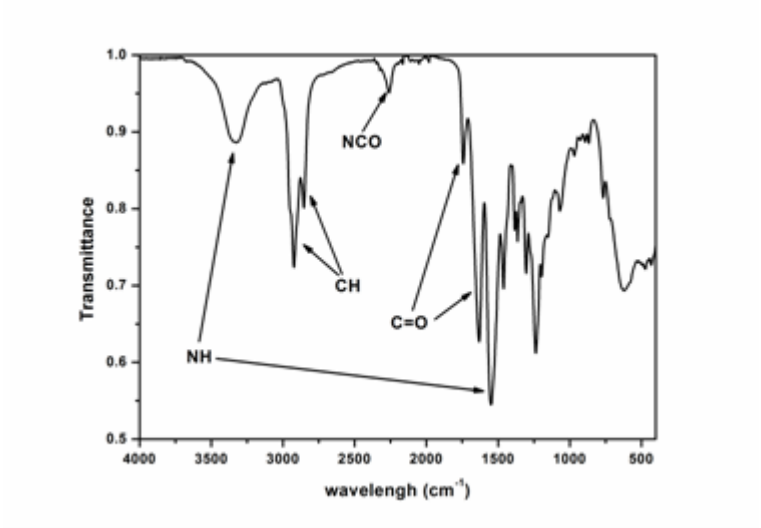

Figure 49: FTIR spectra of polyurea microcapsules.

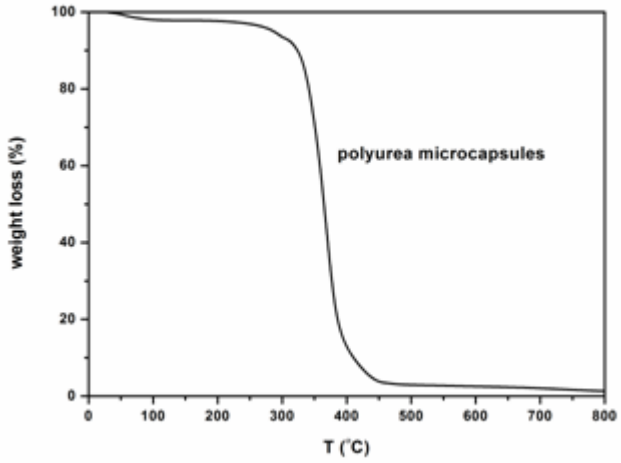

Figure 50: TG profile of polyurea microcapsules.

Release studies were performed under different pH and temperature conditions. Since PU_MC has a polymeric structure, temperature should play an important role on the viscoelastic behaviour and consequently on the release of PhPh. At the same time, sensing of corrosion via pH is a very important factor for assessing the application of PU_MC–PhPh in protective coatings for corrosion, so pH was the second parameter under survey.

The release of PhPh under different conditions of pH (4, 7 and 9) and temperature (40, 60 and 80 ºC) was performed four times for each condition and the mean is depicted in Figure 51.

The concentration of PhPh released at different pH is less than 1% of the total loading content, due to the very low solubility of phenolphthalein in water, only with the increase of pH their solubility slightly increases [12], and also due to the barrier effect of the microcapsule, limiting the PhPh release. More specifically, the concentration of PhPh released in neutral conditions (3.6 ppm) is lower than in alkaline (5.9 ppm) and acid conditions (4.4 ppm), as observed in Figure 51a. The values have a high uncertainty associated because of very low concentrations near the detection limit of the analytical method.

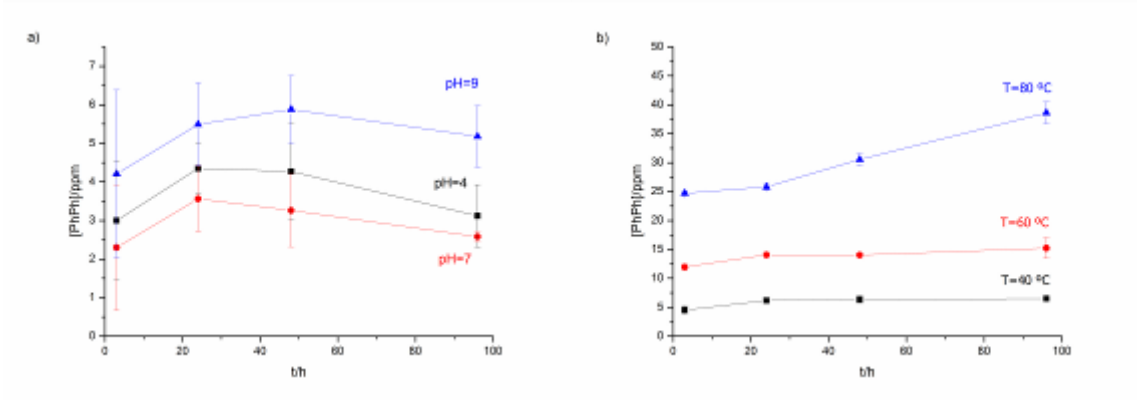

Figure 51: Release of PhPh from PU_MC at different: (a) pH and (b) temperature.

PhPh release profiles at different temperatures are shown in Figure 51b. The amount of released PhPh increases with temperature but is still lower than 10% of the total loading content: at 40 ºC the concentration released is 6.5 ppm, at 60 ºC is 15.2 ppm and at 80 ºC the value reaches 42.4 ppm. The results obtained suggest that the increase of temperature promotes a higher mobility of the polymeric chains and consequently the PhPh permeation across the capsule wall to solution increases.

Sensing activity of PU_MC–PhPh in suspension and incorporated into the coating matrix

In order to verify the pH sensitivity of PU_MC–PhPh, one drop of 0.5 M sodium hydroxide solution was added to an aqueous suspension of PU_MC–PhPh, and the results are depicted in Figure 52. Immediately after the addition of sodium hydroxide the colour of solution turned pink, as a result of pH increase. After homogenization of the pink suspension, by manual stirring, part of the microcapsules begins to deposit in the bottom of

the beaker and after 30 minutes the solution was found to remain pink while the microcapsules presented a very pale coloration. These findings imply that even the small amount of PhPh released under alkaline condition is sufficient to promote a visible coloration of the suspension.

Some materials lose their functionality when incorporated into a coating matrix, and before the characterization of the coated metallic alloys, the sensitivity of the free standing films composed by the coating matrix with PU_MC–PhPh to pH changes was tested in contact with water.

Figure 52: Colour evolution of a PU_MC–PhPh suspension: (a) PU_MC–PhPh aqueous suspension, (b) after addition of one drop of sodium hydroxide solution (0.5 M), (c) after colour homogenization, (d) after 30 minutes (microcapsules deposition and solution with pink coloration) and (e) magnification of previous picture (microcapsules in the bottom with a very pale coloration).

Detached films (Film 1 and Film 2), with white coloration, were immersed in distilled water and one drop of 0.5 M sodium hydroxide solution was added. The pH of the solution increased up to ≈10 and the detached film started to be coloured, with a pink coloration, as can be observed in Figure 53.

The coloration of Film 1 in the solution becomes more intense with time, due to the release of PhPh from PU_MC. It seems that polyurea polymeric matrix allows the diffusion of hydroxide ions and phenolphthalein molecules, resulting into a pink coloration of the solution present in the Petri dish. One similar test was done with Film 2 to verify the influence of pH in the PhPh release form the coating matrix. Film 2 was immersed for 48 hours in the same conditions as Film 1, without the addition of sodium hydroxide solution. After that time, Film 2 was removed from the aqueous solution and one drop of 0.5 M sodium hydroxide solution was added and the coloration of the solution was not observed. It means that under neutral conditions the release of PhPh from the coating with capsules is very low being not sufficient to promote the colour change of the solution, which is in agreement with release studies performed before. To confirm that Film 2 was in good

conditions, it was immersed again in the same solution, now with alkaline pH (due to the addition of sodium hydroxide) and the pink coloration was observed in a similar way like with Film 1. This experiment shows that PhPh is only released from polyurea microcapsules and from the coating matrix with alkaline pH, not only because of the higher solubility of PhPh at this pH, and probably, due to the higher mobility of the polymeric network, allowing the diffusion of the PhPh through the PU shell and the coating matrix. This is exactly the trigger that is intended to be used for self-sensing of corrosion protection.

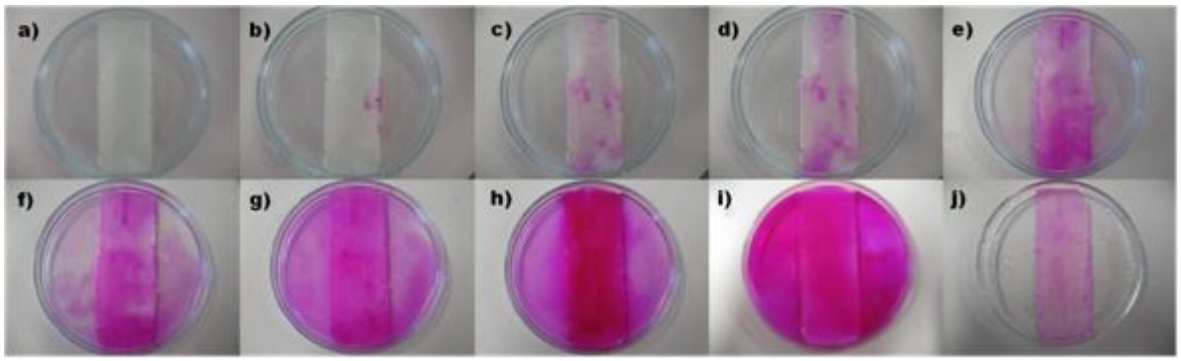

Figure 53: Scheme of pH sensing response detached Film 1, after addition of one drop of sodium hydroxide solution (0.5 M). (a–i) Colour evolution with time; (j) after removing the solution from *Petri dish*.

Sensing activity of PU_MC–PhPh in coated metallic substrates

In order to verify the ability of PU_MC–PhPh to sense the corrosion onset, these microcapsules were incorporated into the coating formulation and applied on two metallic alloys (2024 Al alloy and AZ31 Mg alloy).

Since the polymeric shell of these microcapsules and the coating formulation have the same chemistry (based on polyurethane), the compatibility was visually good, leading to uniform and homogeneous coatings with no signs of aggregates or defects. The coated substrates were immersed in a 0.5 M sodium chloride solution to promote the corrosion activity and to verify the sensing ability of PU_MC–PhPh.

After 24 h of immersion coatings applied on AA2024 substrates showed small pink spots, as a result of the corrosion activity (Figure 54). However, these spots fade away rapidly due to the diffusion of hydroxide ions into the bulk solution.

Using a similar strategy, coated AZ31 magnesium alloy was immersed in a 0.5 M NaCl solution. After 20 hours of immersion the effects of the cathodic reaction are remarkably different compared to AA2024 (Figure 55). There is formation of bubbles as a result of hydrogen evolution and the pink coloration comes from the formation of hydroxide ions.

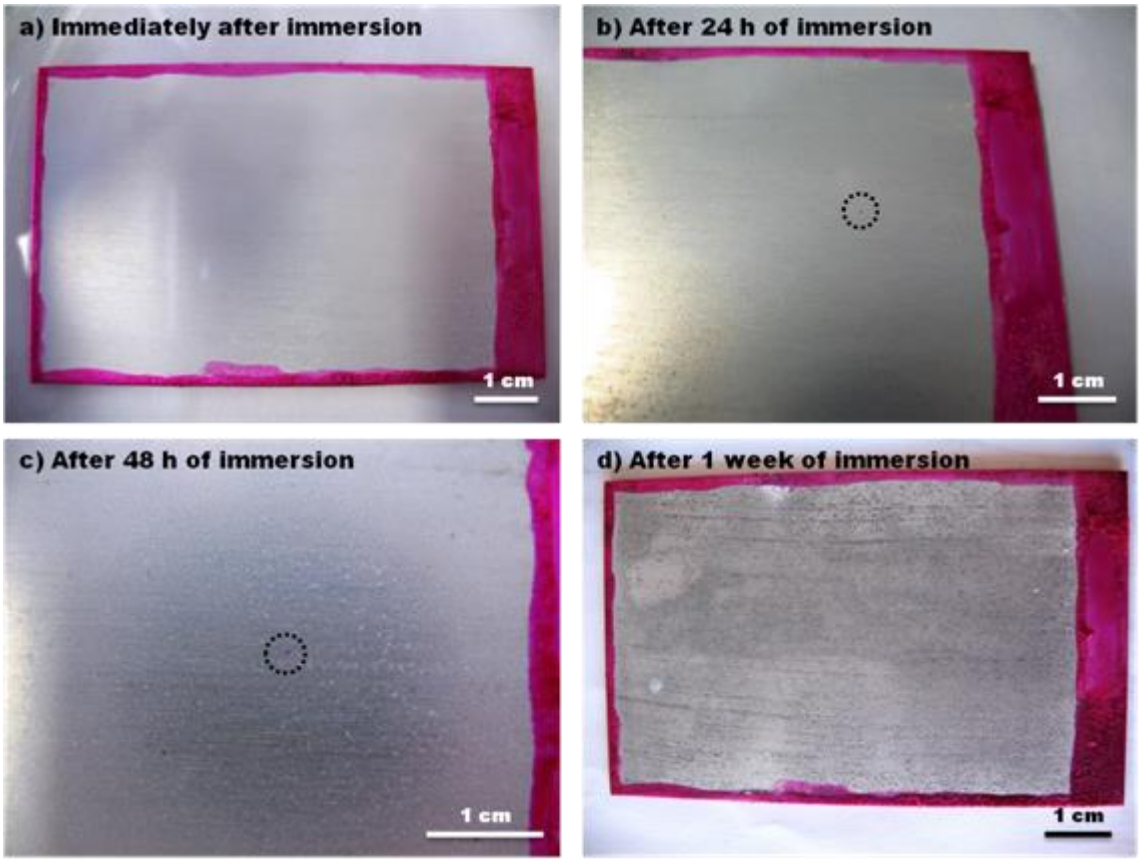

Figure 54: Evolution of coated AA2024 immersed in a 0.5M NaCl solution.

For this coated substrate the sensing ability of the modified coating (with PU_MC–PhPh) is more evident due to the higher reactivity of magnesium and consequently to the higher amount of hydroxide ions formed. Additionally, Mg^{2+} is stable in solution up to pH 10–11 [15, 16], thus allowing for the accumulation of OH^- and its detection by PhPh. As observed before, the coating matrix allows the diffusion of ions and molecules, particularly under these alkaline conditions and the reaction between phenolphthalein and hydroxide ions is clearly observed by the coloration of the coating.

The importance of this type of functional coatings is recognized, but for very reactive substrates, such as magnesium, it is even more important because their degradation rate is

very high [17]. Thus, it is very important to detect the degradation in early stages and act in a preventive way in order to guarantee the structural safety of the materials.

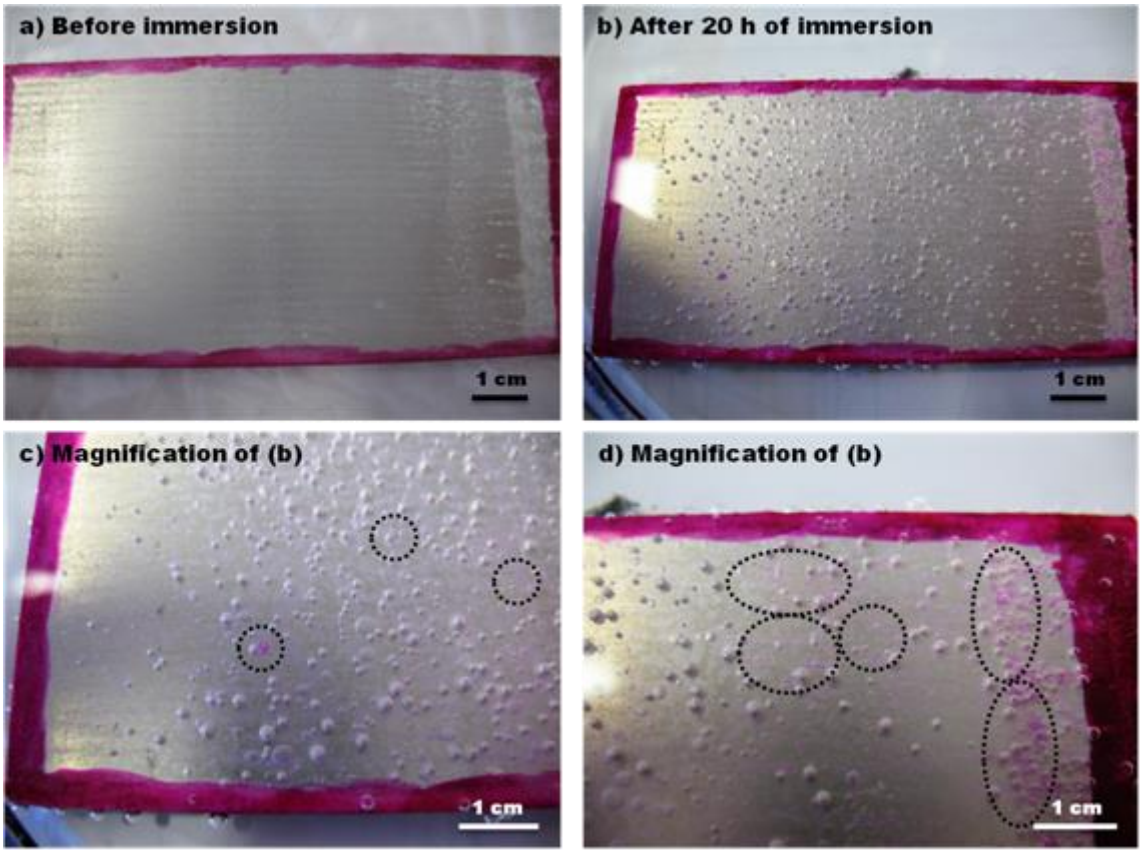

Figure 55: Evolution of coated AZ31 Mg alloy immersed in a 0.5 M NaCl solution.

Figure 56 depicts the specimen of Figure 55 after 72 hours of immersion. The Mg alloy is damaged and the coating is heavily delaminated, as a result of the corrosion processes and associated coating degradation. An intense pink coloration is also observed, underlining the ability and usefulness of this system (PU_MC–PhPh). After one week of immersion, coated samples were removed from NaCl solution and dried at room temperature. In Figure 57, is possible to observe the corroded surfaces of both alloys. Those surfaces present signs of corrosion activity, namely pitting and delamination. This observation confirms that the coloration observed in the coating is due to the beginning of corrosion activity and not only due to the release of PhPh. And also because PhPh needs the hydroxide ions (to increase pH) resulted from the cathodic process to turn pink, otherwise it continues colourless.

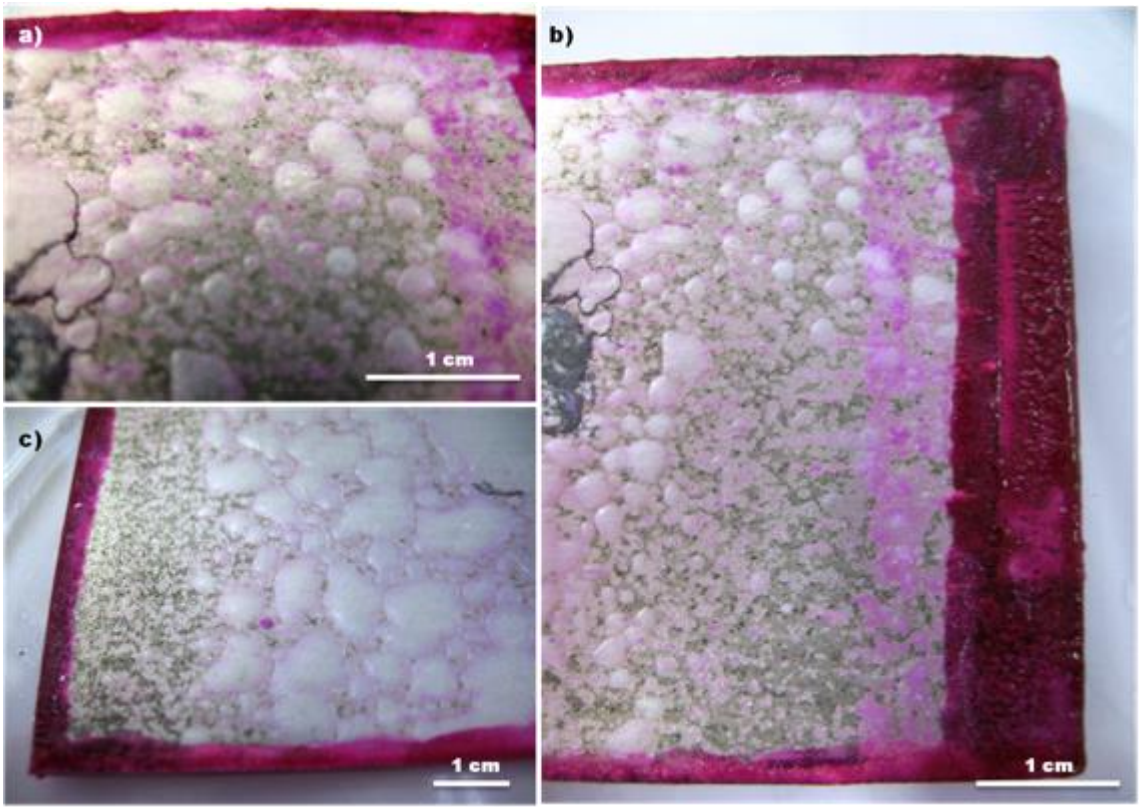

Figure 56: Coated AZ31 Mg alloy after 72 h of immersion in 0.5 M NaCl.

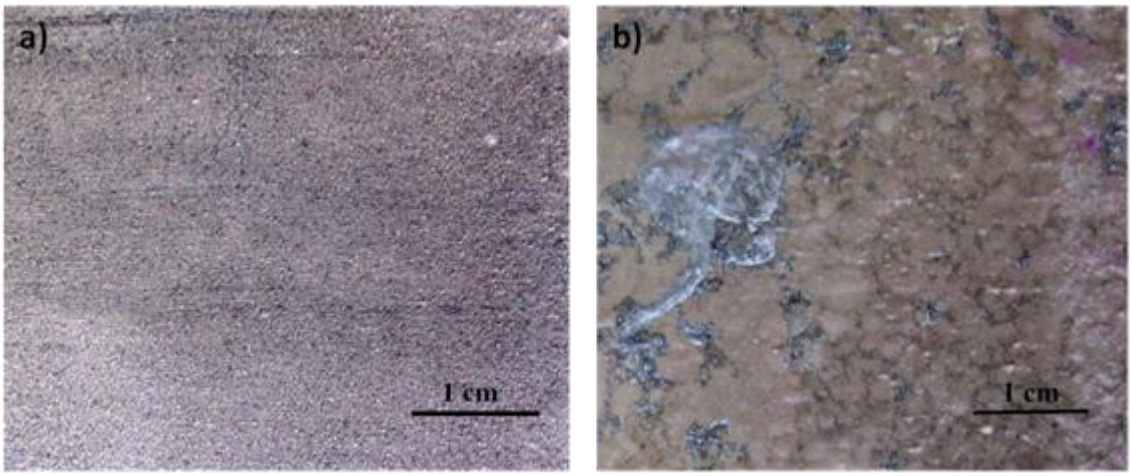

Figure 57: Surface of coated (a) AA2024 and (b) AZ31 Mg alloy after immersion tests.

Conclusions

This paper reports the new synthesis for encapsulation of phenolphthalein to be used as corrosion sensor in multifunctional protective coatings.

This system is based on polyurea microcapsules with a regular and microsized morphology and with a loading content of 12 wt%. The same chemical nature of coating and capsules

improves their compatibility resulting in very uniform and homogeneous coatings. Alkaline pH induces the release of phenolphthalein which ensures sensing the localised corrosion onset.

Aluminium and magnesium alloys coated with a formulation, containing polyurea microcapsules with encapsulated phenolphthalein, acted as a corrosion sensor, displaying the corrosion processes, through a pink coating coloration, as a result of local pH increase in the cathodic areas. The sensing performance expectedly works better for magnesium alloy than for aluminium alloy. This seems to be a simple, compatible and promising solution to be used in general coating technologies for metallic structures, being useful to identify the corrosion degradation in early stages. These PU microcapsules confer a way to immobilize/encapsulate different functional compounds to attribute different functionalities to protective coatings, i.e. anticorrosive and antifouling properties.

Acknowledgements

The authors thank CICECO (ref. PEst-C/CTM/LA0011/2013) and FM thanks FCT for PhD grant SFRH/BD/72663/2010.

Notes and references

1 D. K. Chattopadhyay and K. V. S. N. Raju, Prog. Polym. Sci., 2007, 32, 352.

2 E. Ghali, V. S. Sastri and M. Elboujdaini, Corrosion Prevention and Protection: Practical Solutions, John Wiley & Sons Ltd, 2007.

3 J. Zhang and G. S. Frankel, Corrosion, 1999, 55, 957.

4 I. M. El-Nahhal, S. M. Zourab and N. M. El-Ashgar, J. Dispersion Sci. Technol., 2001, 22, 583.

5 US Pat., 20030068824A1, Corrosion-sensing composition and method of use, 2003.

6 D. Raps, T. Hack, J. Wehr, M. L. Zheludkevich, A. C. Bastos, M. G. S. Ferreira and O. Nuyken, Corros. Sci., 2009, 51, 1012.

7 G. Engelmann, M. Jobmann and G. Rafler, Ind. Crops Prod., 2004, 20, 37.

8 W. Li and L. M. Calle, NACE Corrosion 2007, Paper 07228, Nashville, TN, March 2007.

9 W. Li and L. M. Calle, Proceeding of the Smart Coatings, Orlando, Florida, 2007, p. 191.

10 US Pat., 7790225, Coatings and methods for corrosion detection and/or reduction, 2010.

11 F. Maia, J. Tedim, A. C. Bastos, M. G. S. Ferreira and M. L. Zheludkevich, Nanotechnology, 2013, 24, 415502.

12 B. Fantus and J. M. Dyniewicz, Am. J. Dig. Dis., 1936, 3, 573.

13 M. M. Coleman, M. Sobkowiak, G. J. Pehlert and P. C. Painter, Macromol. Chem. Phys., 1997, 198, 117.

14 W. H. Awad and C. A. Wilkie, Polymer, 2010, 51, 2277.

15 M. Pourbaix, Atlas of Electrochemical Equilibria in Aqueous Solutions, NACE, Houston, USA, 2nd edn, 1974, pp. 141 and 171.

16 W. Stumm and J. J. Morgan, Aquatic Chemistry – Chemical Equilibria and Rates in Natural Waters, Wiley Interscience, New York, USA, 3rd edn, 1996, pp. 273 and 396.

17 G. Song and A. Atrens, Adv. Eng. Mater., 2003, 5, 837.

CHAPTER 7

"Incorporation of biocides in nanocapsules for protective coatings used in maritime applications"

Chemical Engineering Journal 270 (2015) 150–157

Contents lists available at ScienceDirect

Chemical Engineering Journal

journal homepage: www.elsevier.com/locate/cej

Incorporation of biocides in nanocapsules for protective coatings used in maritime applications

F. Maia [a], A.P. Silva [b], S. Fernandes [b], A. Cunha [b], A. Almeida [b], J. Tedim [a,*], M.L. Zheludkevich [a,c], M.G.S. Ferreira [a]

[a] CICECO, Department of Materials and Ceramic Engineering, University of Aveiro, 3810-193 Aveiro, Portugal
[b] Biology Department and CESAM, University of Aveiro, 3810-193 Aveiro, Portugal
[c] Institute of Materials Research, Helmholtz-Zentrum Geesthacht, Max-Planck-Str. 1, 21502 Geesthacht, Germany

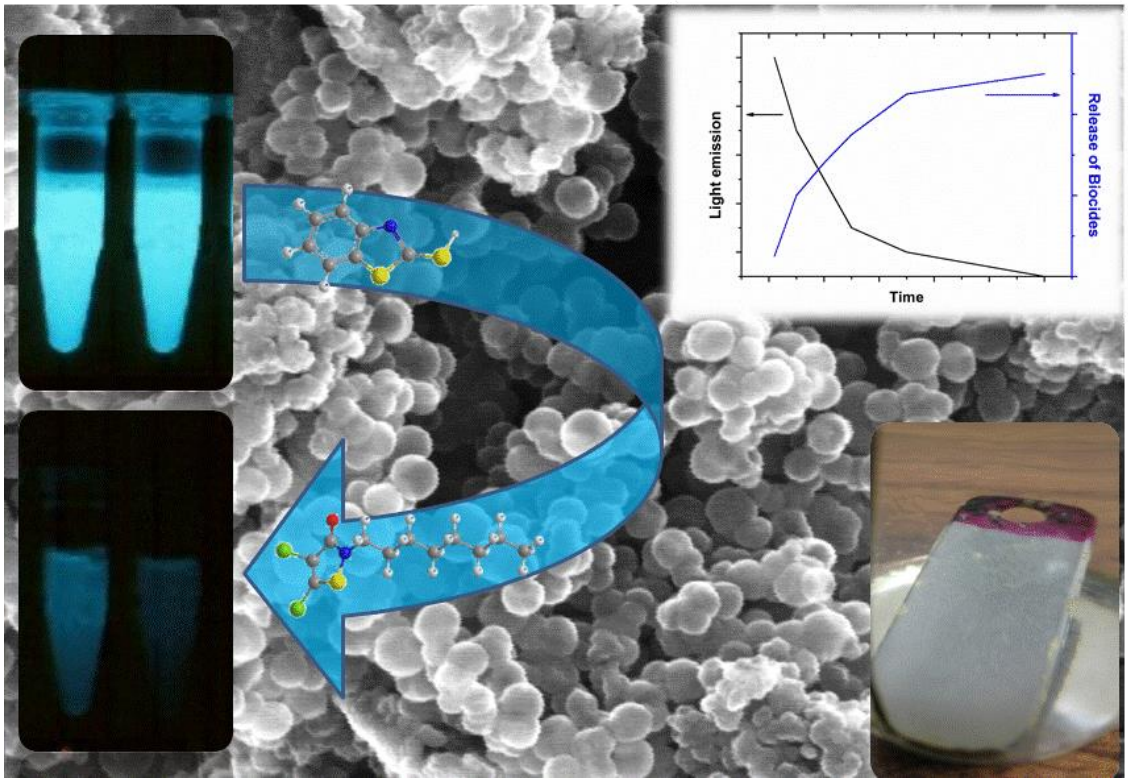

Highlights:

- Successful encapsulation of biocides in silica nanocapsules.
- Expedite and real-time screening method to assess the inactivation of bacteria.
- Antibacterial activity of silica nanocapsules loaded with biocides.
- The developed nanomaterials show high potential to be used in antifouling coatings.

Abstract

This work reports the synthesis and characterization of silica nanocapsules with biologically-active compounds 2-mercaptobenzothiazole and 4,5-dichloro-2-octyl-4-isothiazolin-3-one. The resulting particles were characterized by scanning electron microscopy, thermogravimetry and adsorption–desorption isotherms of N_2. The antibacterial activity was assessed for both nanocapsules dispersed in solution as well as incorporated in coating systems, using a recombinant bioluminescent Escherichia coli expressing the *luxCDABE* genes from the marine bioluminescent bacterium *Aliivibrio fischeri*. The decrease in light emission of the bacterial model, indicative as decrease of metabolic activity, was directly correlated with the level of biocide detected in solution by UV–Visible spectrophotometry. The results show that the developed nanomaterials show great potential for application in antifouling coatings.

Keywords: Antifouling coatings, encapsulation of biocides, silica nanocapsules, antibacterial activity.

1. Introduction

Marine environments are particularly aggressive for metals and corresponding alloys because of the high salinity, presence of microorganisms, algae, plants and nutrients which lead to the occurrence of biofouling and corrosion issues [1,2]. Despite the settlement of macro and microorganisms on the substrate occurring at the coating/aquatic environment interface, the presence of living organisms can generate a set of specific conditions that weakens the coating. The result is the occurrence and propagation of cracks and pores, thereby contributing to the initiation and progress of corrosion at the metal/coating interface. The economic impact of these processes is considerable and includes costs

associated with maintenance operations, replacement of offshore structures, expenditure of extra fuel in maritime transportation and consequent increase in greenhouse gas (GHG) emissions associated with the increase of drag forces [3].

To overcome biofouling, antifouling agents have traditionally been used and added to coating formulations, most notably tributyltin (TBT). However, since 2003, TBT was banned by the International Maritime Organization due to its high toxicity and bioaccumulation [1]. The rapid change enforced by the prohibition of organotin paints, combined with the current low carbon revolution, rising of fuel prices and heightened environmental awareness, have stimulated massive research efforts in the last decade or so in the area of antifouling technology.

In the last couple of years, several reviews reporting current antifouling technologies and highlighting strategies to achieve more environment friendly approaches were published [1,4–8]. Generally, the innovative approaches to prevent the settlement of microorganisms and the development of biofilms involve the modification of the physicochemical properties of surfaces or the embedding of antimicrobial compounds in coating materials [9]. Surface functionalization decreases surface energy and prevents adhesion of molecules and microorganisms. This has been achieved by modification of surface topography and biomimetic strategies using natural products, cells and enzymes [6,7], application of sol–gel systems [7,10], by the use of biodegradable polymers [11], self-assembly polymers and nanostructured polymer thin films [12]. On the other hand, the encapsulation of biocides to control the release of bioactive species has been attempted by the entrapment/encapsulation in latex nanocapsules [13] and chitosan/xanthan gum microcontainers with a core–shell structure [14]. An approach based on the combination of nanocontainers loaded with a formulation of corrosion inhibitors and biocides, combining anticorrosive and antifouling properties in the same coating, has been recently proposed [15].

Although the biocidal activity of encapsulated materials has been experimentally demonstrated, the potential toxic effects introduced by capsules and their performance in coatings with different properties in terms of propensity to biocide release have not been sufficiently addressed. In this work we investigated two compounds with known biocidal properties, in their free and encapsulated form: 2-mercaptobenzothiazole (MBT) which has a minimum inhibitory concentration (MIC) for *Escherichia coli* of 50 ppm [16] and the

antifouling agent, 4,5-dichloro-2-octyl-4-isothiazolin-3-one (DCOIT) with a MIC of 16 ppm for *E. coli* [17]. These compounds were encapsulated in silica nanocapsules [18] and the resulting materials were fully characterized by scanning electron microscopy (SEM), thermogravimetric analysis (TG/DTA) and adsorption/desorption isotherms. The antibacterial activity was assessed using a recombinant bioluminescent *E. coli* expressing the *luxCDABE* genes from the marine bioluminescent bacterium *Aliivibrio fischeri* [19]. This expedite method allow the real-time monitoring of the inactivation of the bacterium as result of the biocide release from silica nanocapsules. The activity observed for the encapsulated biocides, either in solution or incorporated into coatings applied on carbon steel substrates was correlated with the release profiles of biocides obtained by UV–Visible spectrophotometry as a function of time.

2. Experimental Section

2.1. Materials

The active compounds used for encapsulation were 2-mercaptobenzothiazole (MBT) from Sigma-Aldrich and the marine antifouling agent SEA-NINE™ 211N, which is 30% of 4,5-dichloro-2-octyl-4-isothiazolin-3-one (DCOIT) in xylene, obtained from Rohm and Haas Company. For the preparation of capsules, cetyltrimethylammonium bromide (CTAB) (99%) and tetraethoxysilane (TEOS) (99.9%) were purchased from Sigma-Aldrich. Ammonia solution (NH4OH) (25-28%), sodium hydroxide (NaOH), sodium chloride (NaCl), ethyl ether (99.5%) and buffer solutions were obtained from Riedel-de-Haën. Phosphate buffered saline (PBS) pH 7.4, containing 0.138 M NaCl; 0.0027 M KCl, was prepared with Sigma-Aldrich reagents. The recombinant bioluminescent strain of *E.coli* was provided by Alves et al [19]. All chemicals were analytic grade and were used without further purification.

2.2. Encapsulation of MBT and DCOIT in Silica Nanocapsules, SiNC

The encapsulation of MBT was performed as reported in our previous paper [18]. The encapsulation of DCOIT (SEA-NINE™ 211 N) was performed in a similar way. Briefly, an aqueous solution containing 0.1 g of CTAB dissolved in 35 mL of water was prepared and placed under stirring. Then, 0.25 mL of ammonia solution was added. In parallel, 5 mL of DCOIT solution (SEA-NINE™ 211 N) was diluted in 20 mL of ethyl ether, and added

to the aqueous solution under constant stirring, forming an oil-in-water emulsion. After 30 min of emulsion stabilization 2 mL of TEOS was added to the emulsion. The reaction was left during 24 h at room temperature and under constant stirring. The resulting nanocapsules were filtered under vacuum and washed several times with distilled water and dried at room temperature.

2.3. SiNC characterization

The morphology of obtained nanocapsules was characterized by scanning electron microscopy (SEM) coupled with energy dispersive spectroscopy (EDS), (Hitachi S-4100 system with electron beam energy of 25 keV). Particle size distribution was determined using a free software named "ImageJ" for image processing and analysis with Java [20]. Thermogravimetric analysis (TG/DTA) was carried out in a Sataram–Labsys system under air atmosphere, with a heating rate of 10 °C min^{-1} from room temperature up to 800 °C. The textural properties were evaluated based on the adsorption–desorption isotherms of N_2 at −196 °C, performed on Gemini V2.00 equipment (Micromeritics Instrument Corp.) - samples were previously degassed at 180 °C for 6 h.

The specific area (S_{BET}) was calculated by the BET method (Brunauer, Emmett and Teller) [21, 22].

2.4 Preparation of substrates and coating

Carbon steel AISI 1008 samples were blasted with glass microspheres until reaching a roughness of ≈30–40 μm, followed by degreasing with an alkaline solution (10% Extran (Merck)), rinsed with water and ethanol, and dried with hot air.

Two types of formulation were used to coat carbon steel substrates: (i) water-based and (ii) solvent-based. The first one was a water-reducible, hydroxyfunctional polyacrylic dispersion (Bayhydrol® A 145), used in combination with aliphatic polyisocyanates (Bayhydur® 304) with fast drying at room temperature, from Bayer (Germany).

The second one was a bi-component Sumadur120 without pigments composed by an epoxy based resin (component A) cured with a polyamide (component B) from Sherwin Williams Sumare (Brazil). In general, a specific amount of nanocontainers loaded with biocides was added to the component A, mixed, and followed by addition of component B, in a 1:1 proportion between both components. Carbon steel samples were coated with the prepared

formulations using a brush. In Table 9 the composition of all the coatings prepared is shown.

Table 9: Composition of prepared coatings.

Sample Name	Type of formulation	wt% of nanocontainers*	[biocide]/ppm*
Reference	-	-	-
AC Blank	PU (aqueous based coating)	-	-
AC MBT 0.5%		0.5-0.6	~20
AC MBT 5%		5-6	~200
AC DCOIT 0.5%		0.4-0.5	~8
AC DCOIT 5%		4-5	~80
OC Blank	Epoxy (organic based coating)	-	-
OC MBT 0.5%		0.5-0.6	~20
OC MBT 5%		5-6	~200
OC DCOIT 0.5%		0.4-0.5	~8
OC DCOIT 5%		4-5	~80

*For 10 g of coating formulation.

2.5. Microbiological studies of MBT@SiNC and DCOIT@SiNC in suspension and immobilized in coatings

The antimicrobial effect of biocides MBT and DCOIT encapsulated in silica nanocapsules was evaluated using a recombinant bioluminescent strain of *E. coli* [19], in liquid suspensions and immobilized in a paint for carbon steel. Bacterial cells suspensions (107 cell mL^{-1}) in PBS were exposed to the nanocontainers, during 6 h time course experiments. The concentration of nanocontainers was that corresponding to 20 and 200 mg L^{-1} MBT or 8 and 80 mg L^{-1} DCOIT. The inactivation was assessed, in real time, as the decrease in bacterial light emission, read in a luminometer (TD-20/20, Turner Designs). A negative control corresponding to cell suspensions in PBS without any amendment and controls corresponding to an equivalent concentration of SiNC without biocides, and to equivalent concentrations of the biocides delivered in the form of solution were also included.

For experiments with coated carbon steel, a similar methodological approach, based on bioluminescence detection, was used. Carbon steel panels (2 cm × 6 cm × 0.15 cm) were coated with two different formulations, one aqueous and other solvent based, containing MBT@SiNC and DCOIT@SiNC, as described earlier. The amount of nanomaterials added to the formulations was determined to achieve 20 and 200 ppm of MBT and 8 and 80 ppm for DCOIT, as shown in Table 9. The metal panels were immersed in sterile PBS solution for 8 days and incubated at room temperature, in the presence of ambient light. During the incubation, aliquots of the immersion liquid were collected and added to a fresh PBS suspension of bioluminescent *E. coli*. Light emission was determined as a measure of the biocidal effect of the immersion liquid. In order to evaluate the long-time effect of immersion on the coating stability, the metal panels were left in immersion after the initial 8-day experiment, for a total period of 4 months.

2.6. Release studies of MBT and DCOIT

The release profiles of MBT and DCOIT were monitored by ScanSpec miniature UV–Vis spectrophotometer (ScanSci) at wavelength ≈310 nm and ≈280 nm, respectively. The correlation coefficient of the calibration curves obtained with 6 standard solutions was higher than 0.999 for both compounds.

The aliquots collected to quantify light emission were also used to quantify the amount of biocide released in solution.

An extraction using ethanol was made, by dispersing 50 mg of DCOIT@SiNC in 10 mL of ethanol to determine total loading content. The suspension was stirred at room temperature during 24 h and the ethanolic solution was analyzed by UV–Visible spectrophotometry.

3. Results and Discussion

3.1. Encapsulation of MBT and DCOIT in SiNC and their characterization

The SiNC synthesis and encapsulation of biocide (MBT or DCOIT) in a single step is the result of the TEOS condensation at the interface of an oil-in-water miniemulsion, using CTAB as surfactant and template for silica shell formation. This encapsulation methodology was already reported for MBT encapsulation [18] and small adjustments were performed to promote the encapsulation of DCOIT, reported here for the first time (stabilization of the emulsion and in the selection of a compatible solvent with

SEANINE™ 211 N composition). Silica nanocapsules loaded with DCOIT show a yellowish coloration as result of the encapsulation of DCOIT and other components (organic solvents) of SEA-NINE™ 211 N. The synthesized capsules present a uniform spherical morphology. SiNC have a narrow size distribution centered at 126 nm with a standard deviation of 22 nm for 100 measurements, as observed in Figure 58. Capsules resulting from the encapsulation of DCOIT seem larger than empty ones, resulting in a broad distribution size centered at 300 nm, with a standard deviation of 126 nm, for 40 measurements. The broadening in the size distribution and the enlargement of the capsules, are probably related to the presence of xylene (less soluble in water) in the dispersed phase resulting in a small increase of the droplet size during the miniemulsion step, which leads to a small increase in the size of the filled nanocapsules when compared to empty ones, as depicted in Figure 58. Oppositely, when encapsulation of MBT was performed, no significant variation on the size of filled capsules was observed [18]. The differences in the effect of the encapsulation of DCOIT and MBT in SiNC may be explained by differences in size and arrangement of DCOIT and MBT molecules, as presented in Figure 59.

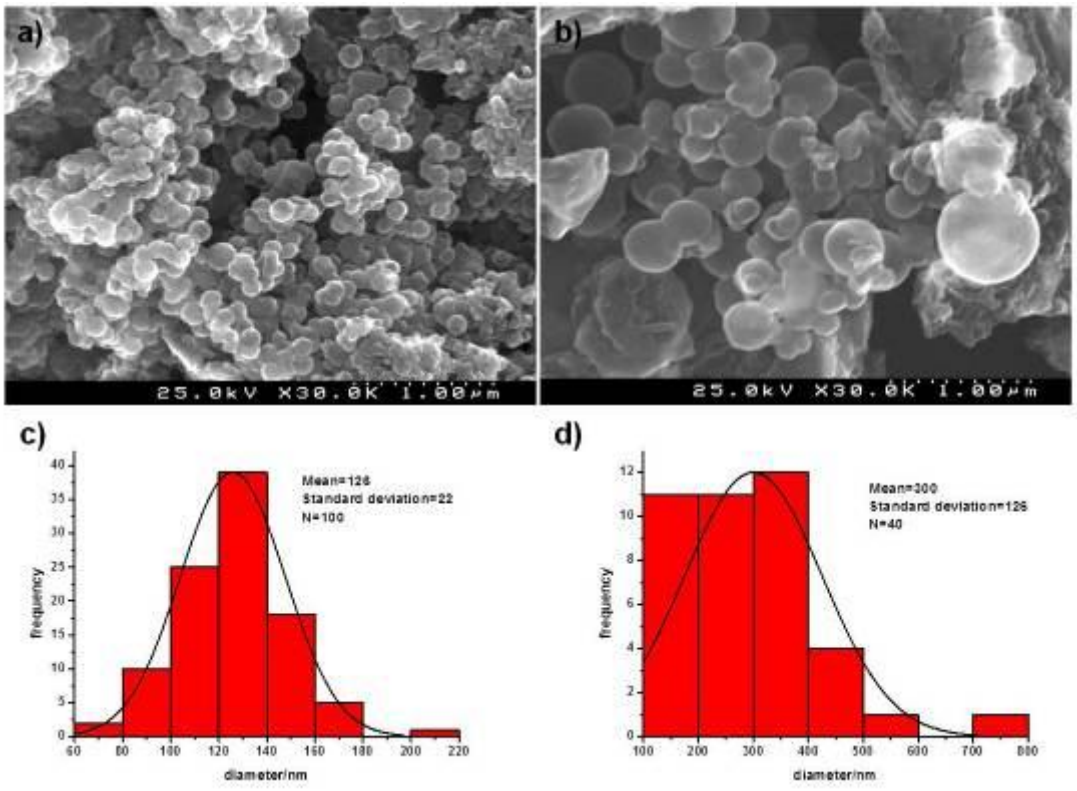

Figure 58: **SEM pictures of synthesized (a) SiNC and (b) DCOIT@SiNC. Histograms with size distribution of (c) SiNC and (d) DCOIT@SiNC, determined using *ImageJ*.**

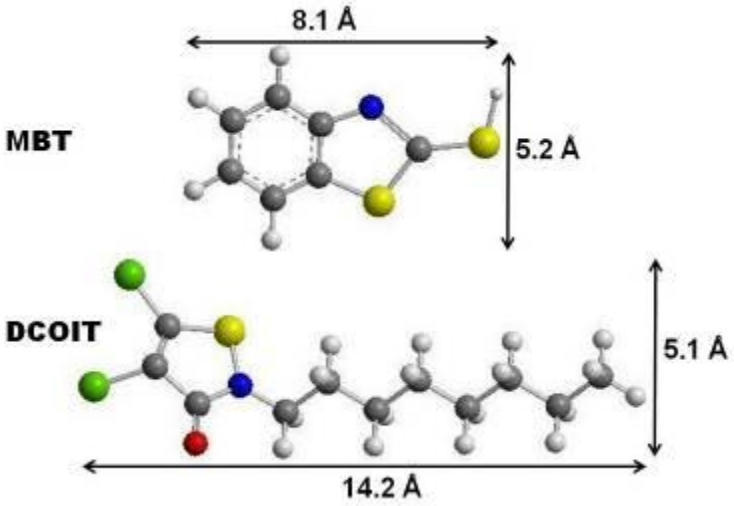

Figure 59: Molecular structure of MBT and DCOIT. Approximated length values were determined using *ImageJ* software, based on bond lengths of crystal structure of MBT [23].

Samples presented in Figure 58 show some degree of agglomeration because they were completely dried to be observed by SEM. However, silica nanocapsules were used in coating formulations in the form of slurry to facilitate the dispersion.

Another important property of this type of nanomaterials is porosity which can affect the release of encapsulated biocides. The nitrogen adsorption–desorption isotherms were recorded to assess the influence of DCOIT and MBT encapsulation on the textural properties of silica nanocapsules (Figure 60). Silica nanocapsules show a curve of isotherm type IV representing an adsorption of nitrogen in multiple overlapping layers with a hysteresis type H3 which indicates capillary condensation in meso and macropores, associated to soft aggregates of particles, resulting in large pores or voids with slit-shape [22]. Surface area and pore size distribution were determined according to BET theory [21] and BJH model [22], respectively, and are depicted in Table 10 and in Figure 61b. The analysis of nitrogen adsorption isotherms (Figure 61) and data presented in Table 10 demonstrates the increase in the surface area with the encapsulation of DCOIT. Values for SiNC and for MBT@SiNC are similar, 157 and 162 $m^2\ g^{-1}$, respectively, whereas for DCOIT@SiNC it reaches 214 $m^2\ g^{-1}$. This increase of surface area is due to the increase in the meso and macroporosity in the nanocapsule shell, as shown in Figure 61b. There is a shift in the pore size distribution to larger pores: SiNC < MBT@SiNC < DCOIT@SiNC. This increase in the pore size distribution is due to the increase of the size of the encapsulated molecules. DCOIT has an approximated length of 14.2 Å, while MBT is

smaller with 8.1 Å. This difference conjugated with solvation of these molecules can result in larger pores in the former case. The solvent used during the synthesis of silica nanocapsules and encapsulation of MBT and DCOIT also plays an important role in the formation of pores, acting as porogen (material used in the formation of pores) [24–27]. For MBT encapsulation only ethyl ether was used, and due to the low boiling point (~37 °C), channels and gradual porosity was formed during the vaporization of ethyl ether [18]. For DCOIT, xylene was mixed with ethyl ether, so the composition of the dispersed phase was a mixture of ethyl ether/xylene in a proportion of 4:1. The composition of this mixture has a direct influence in textural properties, mainly in the porosity of synthesized DCOIT@SiNC. In a first step ethyl ether is vaporized (acting as gaseous porogen) creating micro and small mesoporous, but xylene has higher boiling point (~140 °C) and stays entrapped in the initial structure formed during the condensation step, resulting in bigger mesopores when compared to empty capsules and the ones with MBT.

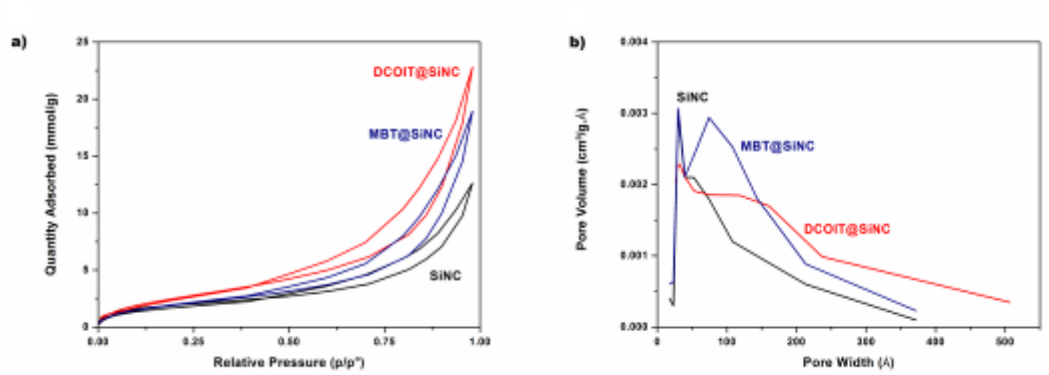

Figure 60: **Nitrogen adsorption–desorption isotherms and pore size distribution of SiNC, MBT@SiNC and DCOIT@SiNC.**

Table 10: **Surface area of the samples determined from the adsorption-desorption isotherms of N_2, according with BET theory.**

Sample	S_{BET} ($m^2.g^{-1}$)
SiNC	157
MBT@SiNC	162
DCOIT@SiNC	214

In order to assess the thermal properties of developed silica nanocapsules and to quantify the amount of MBT and DCOIT encapsulated, thermogravimetric experiments were performed (Figure 61). As previously reported, calcined silica is thermally stable, while SiNC (not calcined) and MBT@SiNC have a total weight loss of 27 % and 37 %, respectively, with the difference ascribed to MBT loading content (10 wt%) [18]. Concerning DCOIT encapsulation and corresponding TG profile (DCOIT@SiNC), the difference for SiNC is only 3 %, corresponding to 3 wt% of loading content. To confirm this value, the extraction of DCOIT from SiNC was performed and quantified by UV–Vis spectrophotometry. The amount of DCOIT extracted was ≈ 190 mg.L^{-1}, corresponding to 3.8 ± 0.2 wt%, close to the DCOIT loading content previously determined by TG.

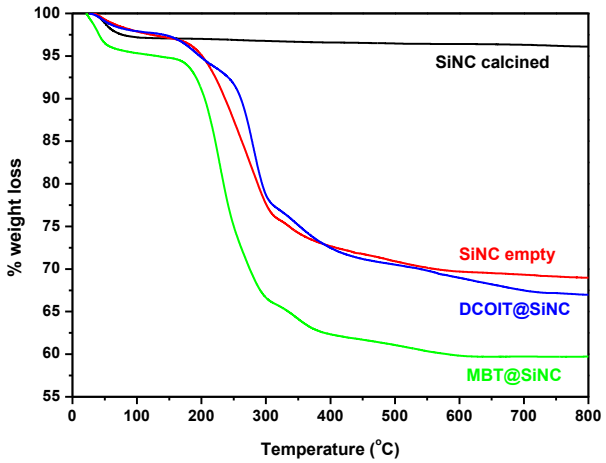

Figure 61: TG profile of calcined SiNC, SiNC, MBT@SiNC and DCOIT@SiNC.

3.2. Biological activity of developed silica nanocapsules in suspension

The antimicrobial activity of the developed silica nanocapsules containing MBT and DCOIT was assessed using a simple and fast method to monitor the photodeactivation process of *E. coli* involving the use of recombinant bioluminescent bacterial strain, previously reported [19]. In parallel with the light emission measurements, the amount of active species released from SiNC at those specific times was also monitored by UV–Vis spectrophotometry in cell-free extracts, as depicted in Figure 62. The amount of DCOIT released is almost four times higher than that of MBT, which can be explained by differences in the textural properties of SiNC@MBT and SiNC@DCOIT.

Under neutral conditions (pH 7.4) the release of MBT is very low (around 1 ppm), as previously reported [18], although MBT solubility (118 ppm) is significantly higher than that of DCOIT. The released MBT is ascribed to those molecules adsorbed in the outer, external surface of SiNC only. The release is much more limited by the shell constituted by micropores (<2 nm). When exposed to solutions with different pH values, these pores may open, namely by dissolution of non-hydrolyzed silica precursor [18]. Increasing the concentration of SiNC@MBT 10 times results in an increase of MBT released of around 5–10 times. Considering that the amount of MBT released is well below the solubility limit, the results indicate that the porosity is an important factor in the regulation of the release of MBT.

On the other hand, the amount of DCOIT released is higher than MBT, reaching 4 ppm, but there is no direct relation between the amount of DCOIT@SiNC added to the suspension and the amount of DCOIT released (Figure 62). In this case, the porosity of DCOIT@SiNC is the greatest among the studied systems and the shell has a larger number of big mesopores, which allows the release of DCOIT up to values near the solubility limit (4 ppm), regardless of the amount of SiNC@DCOIT added. In this case, the solubility of DCOIT is the parameter determining the release extent and not the textural properties of SiNC.

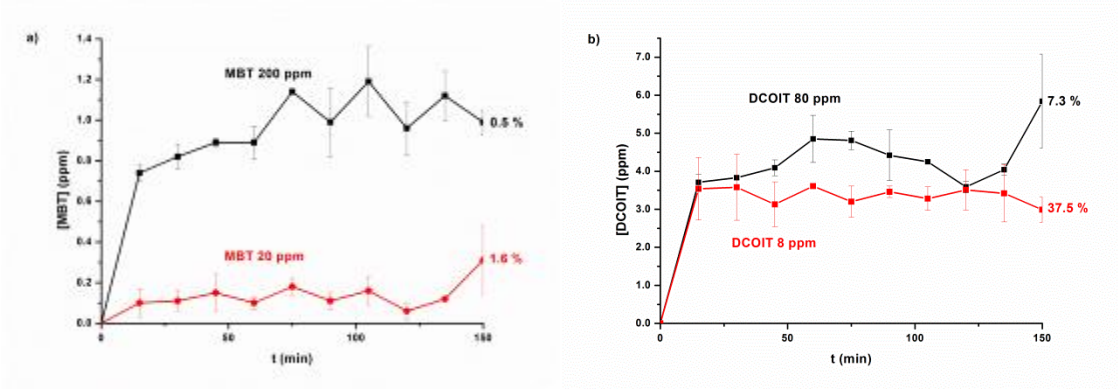

Figure 62: Release profiles of (a) MBT and (b) DCOIT, during the biological activity tests in solution. The percentage values correspond to the fraction of MBT/DCOIT released.

The release extent of MBT (or DCOIT) can be correlated with the corresponding biological activity, detected by the decrease in light emission of the suspension of the bioluminescent bacterial strain. The inactivation of the bioluminescent *E. coli* upon exposure to MBT, DCOIT, MBT@SiNC and DCOIT@SiNC, as a function of time, is

represented in Figure 63. The bioluminescence of the negative control (cell suspension in PBS) shows a decrease that is typical for this model microorganism [19], and represents the reference light emission of the strain for each experiment. SiNC did not significantly inhibit *E. coli* bioluminescence, indicating a negligible level of toxicity. For the lowest concentration of the biocide (Figure 63a), a significant decrease in the light emission of the luminescent bacteria was observed upon exposure to DCOIT. For free dissolved DCOIT, there was a significant and immediate decrease in light emission and the detection limit was reached within 45 min. A similar pattern was observed for DCOIT@SiNC, but the inactivation was delayed in relation to the condition in which the biocide was in the free-(non-encapsulated) form, due to the release of DCOIT from SiNC. Nevertheless, it seems that when encapsulated in a concentration that corresponds to half the MIC, DCOIT is more efficient in the inactivation of modified *E. coli* than MBT. At 20 ppm, MBT showed no significant inactivation, neither in the free state nor encapsulated, as expected from the MIC values. When the concentration of active species was increased ten-fold, the inactivation of E. coli was much faster (Figure 63b). Immediately after the exposure, the values of light emission dropped significantly for both free species (MBT and DCOIT) and after 15 min, bacteria are completely inactivated. The inactivation level achieved with the encapsulated biocides was similar to that of the dissolved biocides although delayed, such as observed in the experiments with the low concentrations, because of the time needed for the release of biocides from SiNC. After 45 min, complete inactivation occurred in the presence of the highest concentrations of MBT@SiNC (equivalent to 200 ppm of biocide) and DCOIT@SiNC (80 ppm of biocide). Despite the lower MIC of DCOIT, in experiments with the highest concentrations, MBT@SiNC promoted faster inactivation of *E. coli* than DCOIT@SiNC.

MBT antimicrobial action has been demonstrated against virus, bacteria and fungi and it is considered more of a microbialstatic type [28]. In bacteria, MBT affects outer cellular structures, namely membrane integrity, and the transference of electrons between donors and acceptors involved in the bacterial membrane respiratory chains, without the absolute requirement of entering the cell [29]. The biocidal activity of DCOIT is thought to involve translocation through the membrane to the intracellular compartment where it reacts with intracellular sulfur-containing proteins inhibiting vital cellular functions [30]. This difference between the initial mechanisms of action of the two tested biocides and the fact

that whereas the release of MBT is much higher at high biocide concentration, the release of DCOIT does not change significantly between the low and high concentrations, may contribute to the difference on the kinetics of bacterial inactivation of the two biocides in experiments conducted with concentrations below or above the MIC.

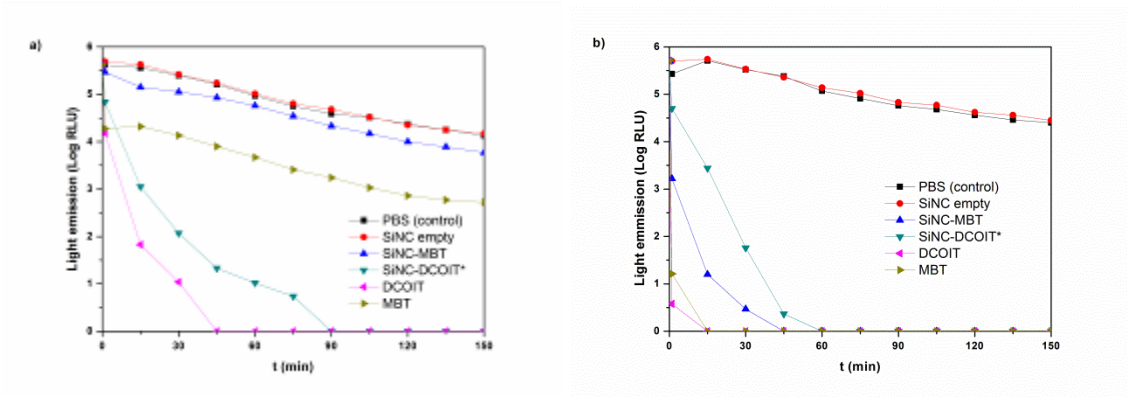

Figure 63: Biological activity of developed silica nanocapsules in solution containing: (a) 20 ppm and (b) 200 ppm of active species. (*In the case of DCOIT@SiNC the concentration is lower than initially expected, being 8 and 80 ppm, respectively.)

3.3. Biological activity of developed silica nanocapsules in coatings

Using the same methodology to assess the biological activity (by measuring the inactivation of a recombinant bioluminescent strain of *E. coli*) of SiNC loaded with MBT and DCOIT, carbon steel panels were coated with two different formulations (one aqueous and other solvent-based) containing MBT@SiNC and DCOIT@SiNC.

The amount of nanomaterials added to the formulations was determined to achieve 20 and 200 ppm of MBT and 8 and 80 ppm for DCOIT, as shown in Table 9 (Section 2), while the obtained data from release studies and biological activity for both aqueous- and organic-based formulations are depicted in Figure 64 and Figure 65, respectively.

Comparisons between the amount of MBT and DCOIT released from the AC systems (Figure 64a) and biological activity (Figure 64b) show a direct correlation between amount of biocide and biological activity. The highest level of inactivation was observed for coatings with the highest concentration of biocide (MBT 5% and DCOIT 5%), after 8 days of immersion, which is consistent with the amount of MBT and DCOIT detected in solution. In these cases, the bioluminescence signal decreased 45% and 90% (normalized units), respectively.

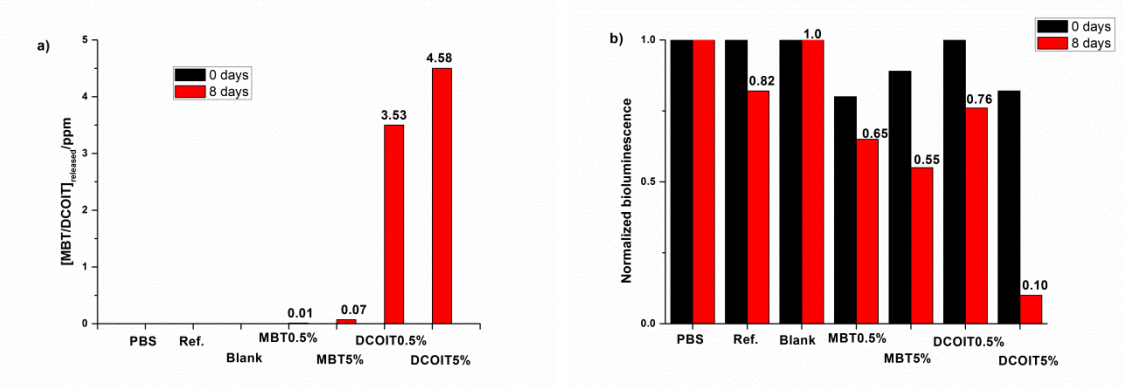

Figure 64: (a) release studies and (b) biological activity of MBT@SiNC and DCOIT@SiNC when incorporated in carbon steel aqueous based coating.

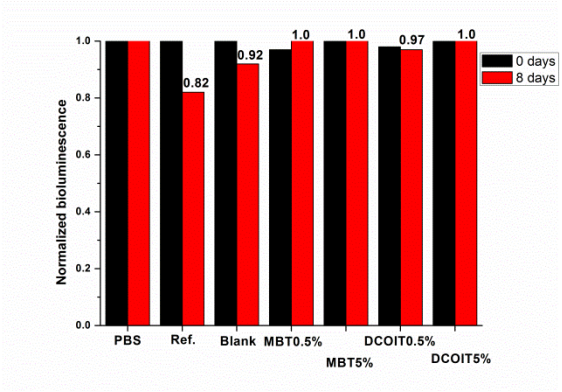

Figure 65: Biological activity of MBT@SiNC and DCOIT@SiNC when incorporated in carbon steel organic based coating.

The application of developed nanomaterials in organic-based coating formulations failed to cause significant biological effects for this period of time, as observed in Figure 65. This is in full agreement with absence of spectroscopic signal ascribed to MBT or DCOIT in solution (not shown) which indicates that biocide was not released from the coating during the experiment.

Additionally, the decrease in bioluminescence in the negative control [31] may be due to the corrosion of uncoated carbon steel which may have led to a considerable release of iron-derived species, with inhibitory effect on the bioluminescent bacteria.

The results depicted in Figure 64 and Figure 65 show clear differences in terms of coating degradation as visually inferred from the photographs presented in Figure 66. After 8 days of immersion, signs of blistering were already visible in the aqueous coating sample without SiNC (blank). Moreover, after 4 months of exposure, corrosion products, blisters

and “wires” of iron oxide are clearly visible. Contrastingly, the solvent-based coating appeared intact even after 4 months of immersion, with the exception of the uncoated area (coated with pink varnish) which led to the formation of the “iron oxide wire-like products” in the edge of the beaker.

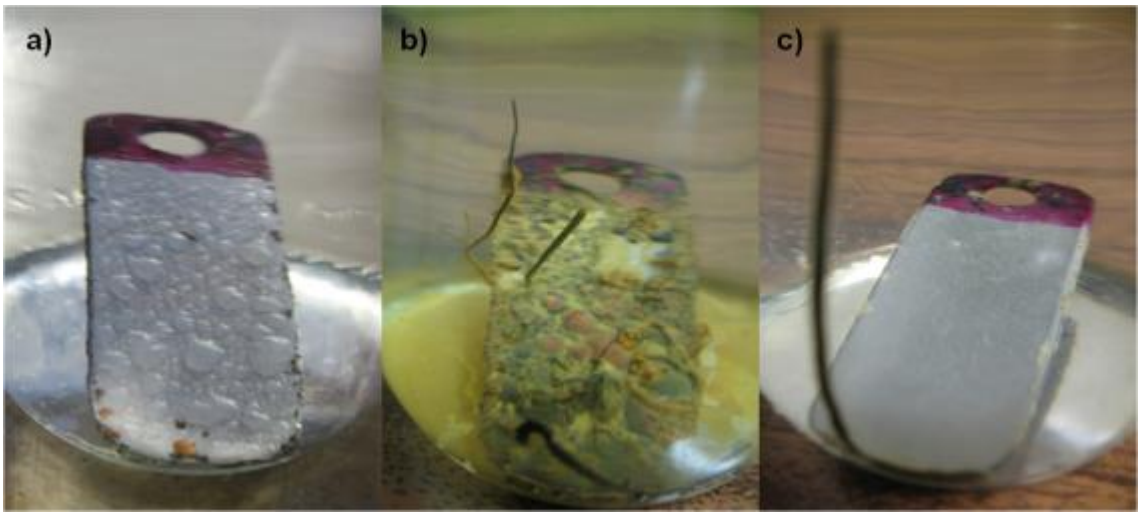

Figure 66: Photographs of coated carbon steel samples: (a) blank aqueous based coating after 8days of immersion, (b) blank aqueous based coating after 4 months of immersion and (c) blank organic based coating after 4 months of immersion.

The differences in coating degradation are mainly due to the barrier properties intrinsically connected to the chemical nature of each coating formulation. The solvent-based coating formulation used in this work was designed to confer long-term anticorrosion protection under aggressive conditions, with a dense matrix and high content of pigments whereas the aqueous coating system herein used is a model polymeric matrix not optimized for any sort of protection under real service life conditions. The fact that the solvent-based coating formulation acts as a more impenetrable layer when compared with the aqueous-based system herein investigated is the same reason why the diffusion of biocides to the coating/solution interface is minimum in the former case and maximum in the latter one.

4. Conclusions

In this work, the encapsulation of DCOIT and MBT in silica nanocapsules was performed successfully. The resulted silica nanocapsules were found to display regular and spherical morphology, with gradual porosity. Both size and textural properties of obtained capsules were influenced by the solvent used in the oil-in-water emulsion and by the molecular size

of the biocide. The release studies performed in solution showed that the release of MBT was affected by the small pores of MBT@SiNC whereas in the case of DCOIT@SiNC pores were large enough and the release of DCOIT was limited only by its solubility.

The biological assays used in this work showed that empty silica nanocapsules have no effect on the cell viability of the tested bacterium, while MBT@SiNC and DCOIT@SiNC, show antibacterial efficacy, as detected by the inactivation of a recombinant bioluminescent strain of E. coli. Identical tests were performed for carbon steel samples coated with two distinct coating systems: an aqueous-based and a solvent-based formulation. The decrease in light emission of the bacterial model, indicative as decrease of metabolic activity, was directly correlated with the level of biocide (MBT or DCOIT) detected in solution after 8 days of immersion. In the presence of aqueous-based coating the level of inactivation increased with the concentration of SiNC with MBT or DCOIT within the coating. Contrastingly, no biocide and no corresponding bacterial inactivation were detected with solvent-based coating loaded with MBT@SiNC or DCOIT@SiNC. These results are consistent with differences in terms of barrier/permeability of the coating matrix to mass transport: the aqueous-based coating displayed higher permeability than the solvent-based coating.

The developed nanomaterials show great potential for application in antifouling coatings and the methodology to assess the inactivation of bacteria is an expedite, real-time screening method to determine biological activity of nanomaterials and new biocidal compounds.

Acknowledgments

FM and JT thank FCT for PhD (SFRH/BD/72663/2010) and for Researcher (IF/00347/2013) grants, respectively. Authors thank Marie Curie IRSES project NANOMAR – Nanocontainer-based active coatings for maritime applications (No. 295145) and the Centre for Environmental and Marine Studies, University of Aveiro (CESAM, project Pest-C/MAR/LA0017/2013). This work was developed in the scope of the project CICECO-Aveiro Institute of Materials (Ref. FCT UID /CTM /50011/2013), financed by national funds through the FCT/MEC and when applicable co-financed by FEDER under the PT2020 Partnership Agreement.

References

[1]. D. M. Yebra, S. Kiil and K. Dam-Johansen, Antifouling technology—past, present and future steps towards efficient and environmentally friendly antifouling coatings, *Prog. Org. Coat.* **50**, 2004, 75-104.

[2]. P. A. Sørensen, S. Kiil, K. Dam-Johansen, C. E. Weinell, Anticorrosive coatings: a review, *J. Coat. Technol. Res*. **6**, 2009, 135–176.

[3]. M.P. Schultz, J.A. Bendick, E.R. Holm, W.M. Hertel, Economic impact of biofouling on a naval surface ship, *Biofouling* **27**, 2011, 87-98.

[4]. M. Lejars, A. Margaillan, Christine Bressy, Fouling Release Coatings: A Nontoxic Alternative to Biocidal Antifouling Coatings, *Chem. Rev*. **112**, 2012, 4347-4390.

[5]. E. Almeida, T.C. Diamantino, O. de Sousa, Marine paints: The particular case of antifouling paints, *Prog. Org. Coat*. **59**, 2007, 2–20.

[6]. I. Banerjee, R.C. Pangule, R.S. Kane, Antifouling Coatings: Recent Developments in the Design of Surfaces That Prevent Fouling by Proteins, Bacteria, and Marine Organisms, *Adv. Mater.* **23**, 2011, 690–718.

[7]. J.E. Gittens, T.J. Smitha, R. Suleiman, R. Akid, Current and emerging environmentally-friendly systems for fouling control in the marine environment, *Biotechnol. Adv*. **31**, 2013, 1738–1753.

[8]. L.D. Chambers, K.R. Stokes, F.C. Walsh, R.J.K. Wood, Modern approaches to marine antifouling coatings, *Surf. Coat. Techol.* **201**, 2006, 3642–3652.

[9]. M. Simões, L.C. Simões, M.J. Vieira, A review of current and emergent biofilm control strategies, *LWT Food Sci. Technol.* **43**, 2010, 573-583.

[10]. M.R. Detty, R. Ciriminna, F.V. Bright, M. Pagliaro, Environmentally Benign Sol–Gel Antifouling and Foul-Releasing Coatings, *Acc. Chem. Res*. **47**, 2014, 678–687.

[11]. D. Carteau, K. Vallée-Réhel, I. Linossier, F. Quiniou, R. Davy, C. Compère, M. Delbury, F. Faÿ, Development of environmentally friendly antifouling paints using biodegradable polymer and lower toxic substances, *Prog. Org. Coat.* **77**, 2014, 485–493.

[12]. S. Krishnan, C.J. Weinman, C.K. Ober, Advances in polymers for anti-biofouling surfaces, *J. Mater. Chem.* **18**, 2008, 3405-3413.

[13]. M. Zhang, E. Cabane, J. Claverie, Transparent antifouling coatings via nanoencapsulation of a biocide, *J. Appl. Polym. Sci*. **105**, 2007, 3824–3833.

[14]. T.N. Borodina, D.O. Grigoriev, M.A. Carillo, J. Hartmann, H. Moehwald, D. G. Shchukin, Preparation of Multifunctional Polysaccharide Microcontainers for Lipophilic Bioactive Agents, *ACS Appl. Mater. Interfaces* **6**, 2014, 6570-6578.

[15]. Z. Zheng, X. Huang, M. Schenderlein, D. Borisova, R. Cao, H. Möhwald, D. Shchukin, Self-Healing and Antifouling Multifunctional Coatings Based on pH and Sulfi de Ion Sensitive Nanocontainers, *Adv. Funct. Mater*. **23**, 2013, 3307–3314.

[16]. C. Franchini, M. Muraglia, F. Corbo, M.A. Florio, A. Di Mola, A. Rosato, R. Matucci, M. Nesi, F. van Bambeke, C. Vitali, Synthesis and Biological Evaluation of 2-Mercapto-1,3-benzothiazole Derivatives with Potential Antimicrobial Activity, *Arch. Pharm. Chem. Life Sci.* **342**, 2009, 605-613.

[17]. M. Pallaske, The late notification of DCOIT for PT 8, an important contribution to the development of full organic wood preservatives for use class 4, Cost Action E37, Poznan, 08-09th May, 2006. Available from [http://www.bfafh.de/inst4/45/ppt/5dcoit.pdf].

[18]. F. Maia, J. Tedim, A.D. Lisenkov, A.N. Salak, M.L. Zheludkevich, M.G.S. Ferreira, Silica nanocontainers for active corrosion protection, *Nanoscale* **4**, 2012, 1287-1298.

[19]. E. Alves, C.M.B. Carvalho, J.P.C. Tomé, M.A.F. Faustino,·M.G.P.M.S. Neves, A.C. Tomé, J.A.S. Cavaleiro, Â. Cunha,·S. Mendo,·A. Almeida, Photodynamic inactivation of recombinant bioluminescent *Escherichia coli* by cationic porphyrins under artificial and solar irradiation, *J. Ind. Microbiol. Biotechnol.* **35**, 2008, 1447-1454.

[20]. W. Burger, M.J. Burge, Digital Image Processing: an Algorithmic Introduction Using Java (Springer, 2010). Available from [http://rsb.info.nih.gov/ij/], accessed and download in 08-09-2014.

[21]. S. Brunauer, P. H. Emmett, E. Teller, Adsorption of Gases in Multimolecular Layers, *J. Am. Chem. Soc*. **60**, 1938, 309–319.

[22]. S.J. Gregg, K.S.W. Sing, Adsorption, Surface Area and Porosity, 1982, Academic Press, London, pp. 209–228.

[23]. J.P. Chesick, J. Donohue, The Molecular and Crystal Structure of 2-Mercaptobenzothiazole, *Acta Cryst.* **B27**, 1971, 1441-1444.

[24]. K.C. Song, S.E. Pratsinis, The Effect of Alcohol Solvents on the Porosity and Phase Composition of Titania, *J. Colloid Interface Sci*. **231**, 2000, 289–298.

[25]. C. Viklund, F. Svec, J.M.J. Fréchet, K. Irgum, Monolithic, "Molded", Porous Materials with High Flow Characteristics for Separations, Catalysis, or Solid-Phase

Chemistry: Control of Porous Properties during Polymerization, *Chem. Mater*. **8**, 1996, 744-750.

[26]. P.D. Brown, S.K. Gill, L.J. Hope-Weeks, Influence of solvent on porosity and microstructure of an yttrium based aerogel, *J. Mater. Chem.* **21**, 2011, 4204–4208.

[27]. B.P. Santora, M.R. Gagne, K.G. Moloy, N.S. Radu, Porogen and Cross-Linking Effects on the Surface Area, Pore Volume Distribution, and Morphology of Macroporous Polymers Obtained by Bulk Polymerization, *Macromol.* **34**, 2001, 658-661.

[28]. M.A. Azam, B. Suresh, Biological activities of 2-mercaptobenzothiazole derivatives: a review, *Sci. Pharm.* **80**, 2012, 789-823.

[29]. H. De Wever, S. Van den Neste, H. Verachtert, Inhibitory effects of 2-mercaptobenzothiazole on microbial growth in a variety of trophic conditions, *Environ. Toxicol. Chem.* **16**, 1997, 843-848.

[30]. M. Moradi, J. Duan, X. Du, Investigation of the effect of 4,5-dichloro-2-n-octyl-4-isothiazolin-3-one inhibition on the corrosion of carbon steel in Bacillus sp. inoculated artificial seawater. *Corros. Sci.* **69**, 2013, 338-345.

[31] M. Shettlemore and K. Bundy, Examination of in vivo influences on bioluminescent microbial assessment of corrosion product toxicity, *Biomaterials* **22**, 2001, 2215–2228.

CHAPTER 8

Final Remarks

Final Remarks

The aim of this work was the development of nanocontainers for incorporation of active compounds in multifunctional coatings aiming the assignment of new functionalities to these coatings. Another interesting feature achieved with nanocontainers is the possibility to control the release of the species encapsulated as result of specific stimulus.

In this work two new types of containers were developed, one in the nanometer range, silica nanocapsules (SiNCs) and other in the micrometer range, polyurea microcapsules (PU-MCs). Both types of capsules allow immobilization of lipophilic compounds, being the capsule formation and the encapsulation performed in a single step. The encapsulation enables the incorporation of functional species in the coatings keeping their intrinsic properties intact and adding new functionalities.

SiNCs were prepared by an oil-in-water (o/w) miniemulsion where the active compound to be encapsulated was dissolved in the dispersed phase. Silica precursor in contact with water and the surfactant (which also act as template) hydrolyses and immediately start their condensation step, until consumption of the precursor. The resulting capsules present a regular and spherical morphology with size diameter between 100 and 150 nm. The shell of SiNCs is porous, being constituted by channels from the core until the external capsule surface. These tubular channels are formed as a result of the co-solvent vaporization, due to the local temperature increase originated from the exothermic reaction that occurred in the condensation step.

PU-MCs were prepared through an interfacial polycondensation in an o/w microemulsion. The reaction occurs at the interface of the emulsion when the two monomers, one lipophilic (diisocyanate) and other hydrophilic (amine), are in contact and the polymerization begins. The resulting microcapsules are uniform and spherical with a broad size distribution, from 100 nm to 2-3 μm. The PU-MCs present a typical core-shell structure, where the walls thickness represents less than 10 % of the capsule diameter. The polymeric shell is continuous and has no porosity.

The incorporation of capsules loaded with active compounds allowed the introduction of new functionalities, such as anticorrosive, sensing and antifouling properties, in coating models. The corrosion inhibitor MBT and the pH indicator phenolphthalein were encapsulated in SiNCs and in PU-MCs, while the biocide DCOIT was only encapsulated in SiNCs. The encapsulation of these compounds causes some modifications in the

morphological and textural properties of the resulting capsules when compared to empty capsules. The encapsulation of MBT in SiNCs resulted in a higher level of aggregation, while the encapsulation of phenolphthalein led to particles with irregular shape and pores with larger diameter. The encapsulation of DCOIT also leads capsules with higher surface area when compared to the empty ones.

Regarding the performance of developed capsules, they were assessed and characterized according to the medium, substrate, coating formulation and functionality.

1. Controlled release studies

The release studies of all the encapsulated compounds were performed in conditions similar to the real application, where parameters like pH, temperature, concentration of NaCl and phosphate-buffered saline (PBS) medium were used as respective stimuli. Thus, the compounds encapsulated in SiNCs are released preferentially at higher concentrations of sodium chloride and in acidic solutions. The mechanism of release is mainly by diffusion and the solubility of the encapsulated compounds also plays an important role in their release. In the specific case of phenolphthalein there is no release under neutral conditions (only adsorbed molecules were released) due to the possible grafting between the silane precursor and phenolphthalein.

The PBS conditions were selected to keep the bacterium viable for the biocidal studies and also due to the high concentration of dissolved salts in the medium. Under these conditions the release of MBT and DCOIT were limited by their solubility in those media and the low amount released occurred by diffusion from the core of SiNCs through the porous channels towards the exterior of the capsules.

In the case of PU-MCs, encapsulated compounds are released preferentially in alkaline conditions and at higher temperatures. The increase of temperature turns the polyurea wall more permeable and allows the diffusion of small molecules, while the alkaline conditions improve the solubility of the compounds under study.

2. Performance in solution

The performance of developed containers (SiNCs and PU-MCs loaded with active compounds) were assessed in solution before their incorporation in the coatings.

Anticorrosion

SiNC-MBT showed corrosion protection activity with increased oxide resistance on AA2024, when dispersed in the electrolyte solution, as a result of the inhibitor release. A prolonged protection effect demonstrated by the absence of visual signs of corrosion and a minimal corrosion activity was observed by EIS even after one month of immersion in the electrolyte solution.

Sensing

SiNC-PhPh and PU_MC-PhPh in suspension showed pH sensitivity, acting as a pH sensor, turning from colorless to pink with the increase of pH values. The pH increase was obtained by adding NaOH to the suspension or in the presence of a galvanic couple. When SiNC-PhPh was added to a NaCl electrolyte in the presence of a Zn–Fe galvanic couple, the corrosion process promotes the formation of hydroxide ions in the cathodic area and consequently a local pH increase. These capsules have pH sensing properties and also allow the identification of the cathodic spots.

Biocidal

The MBT@SiNC and DCOIT@SiNC biocide activity was assessed in the presence of a bioluminescent modified *E. coli*. The bioluminescence of modified *E. coli* decreases in contact with MBT@SiNC and DCOIT@SiNC as result of their biocide activity. However the effect is slower than where there is direct contact with the free biocides.

3. Performance in coatings

The developed containers, when incorporated in model coatings, added extra functionalities to those coatings, namely anticorrosive self-healing properties with the incorporation of SiNC-MBT and MBT@PU-MC, corrosion sensing properties with the incorporation of SiNC-PhPh and PU_MC-PhPh, and biocide (antifouling) properties with the incorporation of MBT@SiNC and DCOIT@SiNC.

Active Corrosion Protection

SiNC-MBT were incorporated in an epoxy-based coating applied to AA2024. The resulting coating was very uniform and no signs of agglomeration were found. The performance of the modified coating was assessed by EIS and visual inspection, showing no negative effects of the addition of MBT encapsulated an also showed active corrosion protection (and self-healing effect) for long immersion times.

MBT@PU-MC were included in sol-gel primer and applied to AA2024, resulting in uniform coating, but in some places, a few agglomerates were identified, due to the presence of bigger capsules in contrast with such a thin film. Nevertheless, the assessment of this coating, by EIS, NSS and adhesion tests, showed that addition of MBT@PU-MC did not promote any negative effect in the barrier properties of sol-gel and also showed that loaded microcapsules suppress corrosion activity and improve the adhesion of sol-gel coatings to the metal substrate when compared with sol-gel without microcapsules.

Sensing

SiNC-PhPh and PU_MC-PhPh were incorporated in an epoxy-based formulation and in an acrylic based polyurethane formulation, respectively, and both systems were applied to aluminum and magnesium alloys. The resulting coatings showed corrosion sensing properties with the beginning of the corrosive process, being more visible for magnesium due to its higher reactivity and consequently more extensive formation of hydroxide ions.

Biocidal

MBT@SiNC and DCOIT@SiNC were incorporated in two different formulation types; an aqueous acrylic based polyurethane formulation and an organic epoxy based formulation, and applied to carbon steel. The samples coated with organic based formulation didn´t show biocide effect, because the coating was very dense due to the high level of solids content, limiting the diffusion of biocides (DCOIT and MBT). In opposite way, samples coated with the aqueous based formulation showed biocide activity due to the diffusion of biocides though the coating.

In conclusion, the developed nanocontainers showed potential to be used as carriers of active compounds for incorporation in a new generation of functional coatings, capable of adding extra functionalities and properties to coatings. They constitute an alternative of actual additives and should be considered in the design of new multifunctional coatings.

My contribution to the work presented (published papers)

The core work and data reported in chapters 3-7 were mainly obtained and analyzed by myself as well as the writing process of the same. Nevertheless, in the papers reported I had the contribution from other people, in particular, regarding the use of some characterization techniques and data obtained using those techniques. In general my work

was focused on capsules preparation, their characterization, incorporation into coating formulations and application to metallic substrates. More specifically: In chapter 3, I prepared all materials and coatings and did the general characterization, except XRD measurements, some SEM images and EIS fittings. In chapter 4, I carried out the core work, namely the microcapsules preparation and their characterization; the sol-gel synthesis, the incorporation of microcapsules into sol-gel, EIS measurements, standard salt spray and adhesion tests were performed by my colleagues and other partners in the frame of NATAL project. In chapters 5 and 6, I performed all the work, except the assays using the Zn-Fe galvanic couple (Chapter 5). In chapter 7, I prepared the capsules and coating and did their characterization, while the experiments with modified *E.coli*, using capsules in suspension and incorporated into coating formulations were performed by our colleagues from Biology Department.

The path…

The synthesis of micro and nanocapsules is very sensitive procedure because the polymerization process occurs in the interface of aqueous-organic phases. Thus, during the execution of this work several attempts to obtain capsules failed. Then, several parameters were tested and adjusted until the desired capsules were achieved. Several times they looked very well in the end of the reactions and after their visualization on SEM, no capsules were found and was necessary to restart and change or adjust another parameter. However, with persistency the procedures for synthesis of silica nanocapsules and polyurea microcapsules were defined.

The following step was also a challenge. The encapsulation of compounds was even more difficult. As active compounds most of the times react with polymer precursors during the encapsulation or were deactivated by the synthesis conditions. Nevertheless, the encapsulation of several compounds in those two types of capsules was successful and their incorporation in coating formulations performed.

Despite the purposed objectives were achieved, many other ideas and approaches to develop multifunctional coatings were not fully explored.

Future activities

As future activities for this work, there are many others capsules and active compounds that could be studied as well as the encapsulation of more than one compound in the same capsule, in order to achieve synergic effect between the encapsulated species.

I started the modification of the synthesis procedure for encapsulation of hydrophilic compounds instead of lipophilic, for both capsules. That is something that I would like to continue and optimize.

Another point that I would like to study is the combination of different nanocontainers with multiple triggers and different release kinetics in order to achieve a prolonged and constant effect in terms of corrosion and biofouling protection.

Although great advances were achieved, there are still a huge challenge to replace the toxic compounds used nowadays, in particular chromium based compounds in the aeronautical industry and the booster biocides in the maritime industry.

From my point of view the scientific community needs to find effective and less toxic solutions (corrosion inhibitors and antifouling agents) to be incorporated in coatings in their free form or immobilized. I think that the search for new and less toxic active compounds together with the combination of different carriers are the two key strategies to find an efficient and more environmental-friendly protective coating in the near future.